

THE KINEMATICS AND DYNAMICS OF THE NEW ENGLAND
CONTINENTAL SHELF AND SHELF/SLOPE FRONT

by

CHARLES NOEL FLAGG

B.S., Cornell University (1969)

M.S., Massachusetts Institute of Technology (1971)

SUBMITTED IN PARTIAL FULFILLMENT OF THE
REQUIREMENTS FOR THE DEGREE OF
DOCTOR OF PHILOSOPHY

at the

MASSACHUSETTS INSTITUTE OF TECHNOLOGY

and the

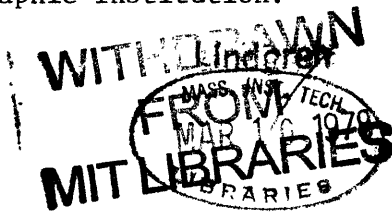
WOODS HOLE OCEANOGRAPHIC INSTITUTION

April, 1977

Signature of Author
Joint Program in Oceanography, Massachusetts Institute of
Technology - Woods Hole Oceanographic Institution, and
Department of Earth and Planetary Sciences, and Department
of Meteorology, Massachusetts Institute of Technology,
April, 1977.

Certified by Thesis Supervisor

Accepted by
Chairman, Joint Oceanography Committee in Earth Sciences,
Massachusetts Institute of Technology - Woods Hole
Oceanographic Institution.



THE KINEMATICS AND DYNAMICS OF THE
NEW ENGLAND CONTINENTAL SHELF AND
SHELF/SLOPE FRONT

by

Charles Noel Flagg

WOODS HOLE OCEANOGRAPHIC INSTITUTION
Woods Hole, Massachusetts 02543

November 1977

DOCTORAL DISSERTATION

*Prepared for the National Science Foundation
under Grants GA-41075 and DES 74-03001.*

*Reproduction in whole or in part is permitted
for any purpose of the United States Government.
In citing this manuscript in a bibliography,
the reference should be followed by the phrase:
UNPUBLISHED MANUSCRIPT.*

Approved for Distribution

Valentine Worthington, Chairman
Department of Physical Oceanography

Robert W. Morse
Dean of Graduate Studies

THE KINEMATICS AND DYNAMICS OF THE NEW ENGLAND
CONTINENTAL SHELF AND SHELF/SLOPE FRONT

by

CHARLES NOEL FLAGG

Submitted to the Massachusetts Institute of
Technology - Woods Hole Oceanographic Institution
Joint Program in Oceanography on April 19, 1977, in
partial fulfillment of the requirements for the
degree of Doctor of Philosophy

ABSTRACT

A 37 day long field program was carried out in March 1974 on the New England continental shelf break to study the current and hydrographic structure and variability on the shelf and in the shelf/slope front. A second experiment was conducted in the shelf break region for one week in January 1975 to study frontal exchange processes.

The mean currents during the March 1974 experiment all had a westward alongshore component, increasing in magnitude progressing offshore from ~ 5 cm/sec to a maximum at the nearshore edge of the shelf/slope front of between 10 and 20 cm/sec, and decreasing in magnitude with depth. The current structure was such that the velocity vector rotated clockwise with depth in the shelf waters inside the front. The mean alongshore transport of shelf water was on the order of 0.4 Sverdrups through a cross-shelf transect south of Block Island. About 30% of the transport occurred in the wedge-shaped region offshore of the 100 m isobath and inshore of the front. Comparison of the observed mean currents with those predicted by the steady frictional boundary layer model of Csanady (1976) indicates that the model captures most of the essential features of the shelf circulation.

The low frequency currents contain approximately 30% of the total current variance. An empirical orthogonal modal analysis indicates that for low frequency alongshore motions the whole shelf together with the water above the front moves as a unit and that the on-offshore currents are characterized by opposing flows at surface and bottom. The alongshore wind stress component is the dominant forcing term for these low frequency motions and for the subsurface pressure field as well. For motion with periods longer than 33 hours, the time derivative term in the cross-shelf momentum balance is comparable with the Coriolis term while the advective terms are 2 to 10 times smaller, on the average.

The semi-diurnal tide is barotropic over the shelf with current magnitudes that increase almost by a factor of two between the shelf break and the inshore mooring 70 km shoreward. At the shelf break one-dimensional continuity gives the correct relation between the surface tide and the semi-diurnal currents. The semi-diurnal tide is clockwise polarized. The diurnal tide is baroclinic, increasing somewhat toward the bottom, is less clockwise polarized than the semi-diurnal, and has

tidal ellipses aligned with the isobaths. The diurnal tidal energy decreases toward shore.

Inertial energy in the frontal zone is equal to the semi-diurnal tidal energy near the surface. The inertial energy decreases with depth and is an order of magnitude smaller further on the shelf. The inertial oscillations are shown to be highly correlated with the wind stress record, arising and decaying on a time scale of 3 to 4 days. The inertial oscillations are shown to be preferentially forced by wind stress events that have a large amount of clockwise energy at near inertial periods.

The frontal zone is shown to be in near geostrophic balance with an anticipated vertical shear across the front of the order of 5 to 8 cm/sec. Thus, there is a wedge-shaped region of velocity deficit that is confined directly under the front and above ~ 200 m. Outside of this region the velocity is alongshore to the west. Low frequency motion of the front is shown to exist on time scales from 3 to 10 days although the complete nature of the motions is not known. An oscillation of the front about its mid-depth position at periods of $3\frac{1}{2}$ to 4 days was caused initially by an eastward wind stress event forcing the front offshore near surface and onshore along the bottom. This was accompanied by large temperature oscillations near the bottom at midshelf and current oscillations confined to those current meters near the front.

The internal wave band is most energetic in the center of the front, is about half as energetic above the front where it is subject to variations associated with the wind stress, and is smaller and nearly constant below the front. The internal wave energy decreases shoreward reflecting the decreasing stratification shoreward of the wintertime hydrography. Linear internal wave theory seems to break down in the conditions of the frontal zone.

A stability analysis of the front to small perturbations is carried out by extending the model of Margules frontal stability of Orlanski (1968) to include the steep bottom topography of the shelf break region. The study covers the parameter range pertinent to the New England continental shelf break region and indicates that the front is indeed unstable; however, the associated growth rates are so slow that baroclinic instability does not seem to be a viable explanation for the observed frontal motions. Application of the theory to the nearly flat topography of the shelf itself shows that the front would be at least 20 times more unstable there suggesting that the front would migrate offshore to the shelf break region until a stable equilibrium was established between frictional dissipation and the instabilities.

Thesis Supervisor: Robert C. Beardsley

Title: Associate Scientist
Woods Hole Oceanographic Institution

4.

To

Barbara

ACKNOWLEDGMENTS

I would like to express my appreciation for the help, guidance, and friendship of my thesis advisor Robert C. Beardsley. Perhaps as important as the scientific advice and help I have received is the awareness of the level of dedication and tenacity required in this or any scientific discipline. I would like to thank the members of my thesis committee, John Bennett and Gabe Csanady, for their many helpful criticisms during the preparation of this thesis. To my wife, Barbara, I owe a large debt of gratitude as she managed to help me through the inevitable periods of despair even though she has been struggling with her own dissertation as well. Lastly, I wish to thank the friends in the MIT/WHOI community who have made my years as a graduate student unusually rewarding.

Funds for the field program and the data analysis of the New England Shelf Dynamics Experiment have been provided by the National Science Foundation through grants GA-41075 and DES 74-03001.

Many people have contributed to the gathering of the data presented in this thesis. John Vermersch has done a lot of work in the preparation of the data and advising me on the use of Buoy Group programs at WHOI. The U.S. Coast Guard graciously provided the use of the USCGC DALLAS and the USCGC HORNBEAM for the hydrographic and current meter array work. The help of Capt. R. Campbell Mate C. Conroy of the tug WHITEFOOT and of Capt. C. Goudey Mate D. Smith of the R/V VERRILL is also appreciated. Dr. W. Red Wright and Brad Butman helped in the hydrographic data gathering; and Dr. Fred Sanders and Mr. Fred Faller collected and analyzed the meteorological data.

The help of Virginia Mills and Cheri Pierce who typed with great dispatch the first and last drafts respectively is appreciated.

TABLE OF CONTENTS

ABSTRACT.....	2
ACKNOWLEDGEMENTS.....	5
TABLE OF CONTENTS.....	6
1. Introduction.....	8
2. Currents on the New England Continental Shelf.....	19
2.1 Introduction.....	19
2.2 Observed Currents.....	23
2.2.1 Mean Currents.....	23
2.2.2 Spectral Characteristics of Variable Currents....	28
2.2.3 Low Frequency Current Structure and Variability..	37
2.3 The Relationships between Wind Stress, Sub-Surface Pressure Gradients, and Low Frequency Currents.....	52
2.3.1 Wind Stress.....	52
2.3.2 Sub-Surface Pressure Gradients.....	63
2.4 Dynamical and Statistical Models of the Shelf Currents..	68
2.4.1 Mean Currents.....	68
2.4.2 Dynamical/Statistical Models of the Low Frequency Currents.....	81
2.5 Discussion.....	87
3. The New England Continental Shelf Frontal Zone.....	92
3.1 Introduction.....	92
3.2 The Thermal Wind Relation and Geostrophic Balance in the Frontal Zone.....	97
3.3 The Alongshore Geostrophic Transport.....	105
3.4 The Variability of the Frontal Zone.....	113
3.4.1 The Internal Wave Band.....	114

3.4.2	The Semi-Diurnal and Diurnal Tides.....	127
3.4.3	The Inertial Band.....	128
3.4.4	Subtidal Frontal Variability.....	133
3.5	Discussion.....	143
4.	Analysis of the Dynamic Stability of the Frontal Zone.....	145
4.1	Introduction.....	145
4.2	Model Development.....	147
4.3	Special Cases.....	160
4.3.1	Shear Waves.....	160
4.3.2	Large Slope and Small Rossby Number.....	165
4.4	The General Case.....	169
4.4.1	Flat Topography.....	169
4.4.2	The Semi-Geostrophic Approximation.....	170
4.4.3	Slope Topography.....	175
4.5	Discussion.....	184
5.	Summary and Conclusions.....	187
	REFERENCES.....	194
	APPENDIX.....	198
	BIOGRAPHICAL NOTE.....	206

1. Introduction

During the past ten years, there has been a surge of interest in the physical oceanography of the U.S. continental shelf. The increasing utilization of the shelves and the need to assess the possible attendant impact have motivated a greater research effort on these areas. Historically, physical oceanographers have been attracted to deep ocean problems, partly because the shelves were felt to be too complex due to strong interaction with the topography and poorly understood coupling with the open ocean. However, recent exploratory studies have indicated that at least in some respects the dynamics of the continental shelf margins seem to be simpler than originally supposed. With studies of the shelf and the ocean/shelf interaction establishing the needed observational evidence, it is now reasonable to hope that a unified conceptual shelf model can be formulated. Toward this goal, this thesis seeks to increase our understanding of the kinematics and dynamics of the currents on the broad continental shelf south of New England.

Prior to 1970 direct measurements of the currents and circulation on the shelf for the Mid Atlantic Bight by moored current meters were practically non-existent. What little that was known (see Bumpus, 1973) was derived from drifter measurements and a vast but largely intermittent collection of temperature and salinity measurements. These measurements served to outline features of the continental shelf circulation in very general terms for motion with seasonal or longer time scales and with space scales of several hundred km. In 1972 Stommel and Leetmaa made a pioneering attempt to model the wintertime shelf circulation based upon the then existing knowledge. The results suggested that the shelf was

in a dynamic regime where wind stress was the most important forcing term. Therefore, the effects of the high wind stress events of winter storms, many times the mean stress, might well dominate the steady flow associated with the weak mean stress, basic offshore density gradient, and a possible mean alongshore pressure gradient. In order to test this hypothesis and others and to add to the sparse amount of data available, the M.I.T. Meteorology Department began, in 1973, a series of observational experiments on the continental shelf combining moored current meter arrays of at least a month duration with concurrent hydrographic surveys.

The initial experiment was a pilot study to test the feasibility of the mooring design and to monitor the current variability during a few strong wind events. A single mooring was deployed at mid-shelf (see Figure 1.1). The results of the experiment are summarized by Beardsley and Butman (1974) and generally, indicate that the attempt was a success; the mooring design proved practical, and the single current meter record demonstrated large variability of the alongshore component of the current. Further, it was clear that the variations of current were associated with wind stress events and that a coupling existed between wind stress, currents, and sea level gradients.

Encouraged by the success of this effort, a more ambitious field program was conducted the following winter. The goals of this experiment were to: 1) monitor the variability of the storm forced currents to verify the previous results; 2) examine the vertical diffusion of horizontal momentum during wind events; 3) document the vertical and horizontal structure of the mean and variable currents; 4) begin to examine the relationship between the shelf currents and the shelf/slope front;

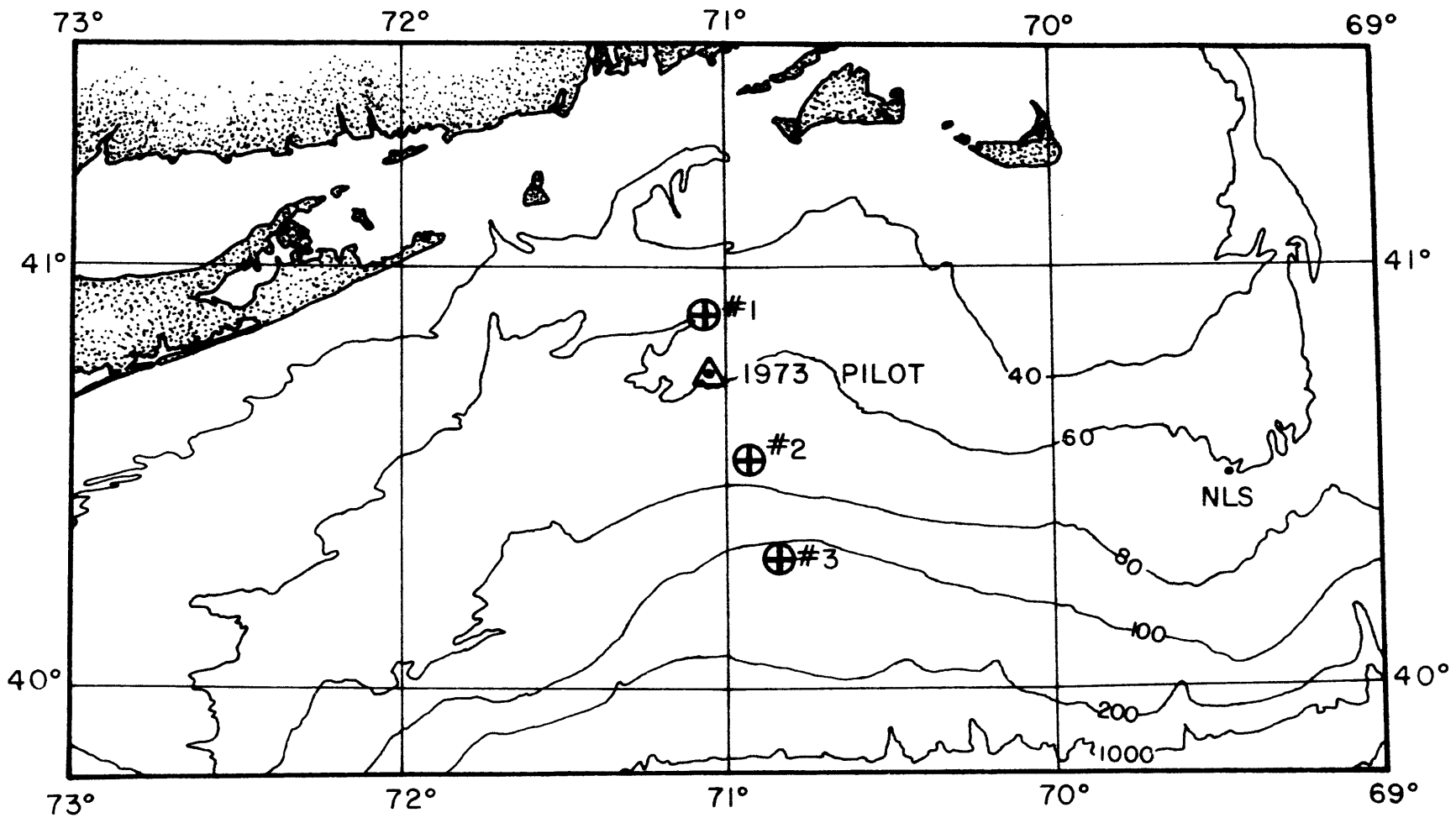


Figure 1.1 Chart of the mooring arrays for the 1973 MIT Pilot Experiment and the 1974 MIT New England Shelf Dynamics Experiment. The depth contours are in meters and NLS is the position of the Nantucket Lightship.

and 5) monitor the behavior of the bottom boundary layer. The field experiment lasted 37 days, from February 27 to April 4, 1974, and contained three basic components: 1) a three-element moored array of current meters and bottom mounted pressure recorders set across the shelf south of New England near the 70° W meridian; 2) a series of four hydrographic surveys carried out at approximately equal intervals around the moored array; and 3) the collection of detailed synoptic meteorological and coastal tide data.

Figure 1.1 shows the mooring positions and Figure 1.2 shows the cruise track of the USCG DALLAS, the most extensive of the four hydrographic cruises. A total of 69 STD casts and 110 XBT launches were made during this cruise. The remaining three cruises employed the R/V VERRILL of the Woods Hole Marine Biological Laboratory, and an average of 14 Nansen casts and 40 BT stations were made on each survey. A total of 14 instruments were deployed: 12 current meters consisting of 5 VACM's from WHOI, 4 EG&G 102 CM's from MIT, 2 EG&G 101 CM's from Nova University, 1 electromagnetic CM loaned by EG&G, and 2 pressure/temperature recorders borrowed from Draper Laboratory. Figure 1.3 shows the distribution of these instruments across the shelf. Instrument designation is a two digit number; the first digit indicates the mooring with #1 the closest to shore, and the second digit gives the relative position in the vertical with #1 the shallowest instrument on the mooring. The data return from the instruments was about 80% with irretrievable time base errors occurring in instruments 12, 24, and 34. The data from this experiment are contained in two reports, one on the hydrography (Flagg and Beardsley, 1975) and another on the current, sub surface pressure, and meteorological measurements (Flagg, Vermersch, and Beardsley, 1976).

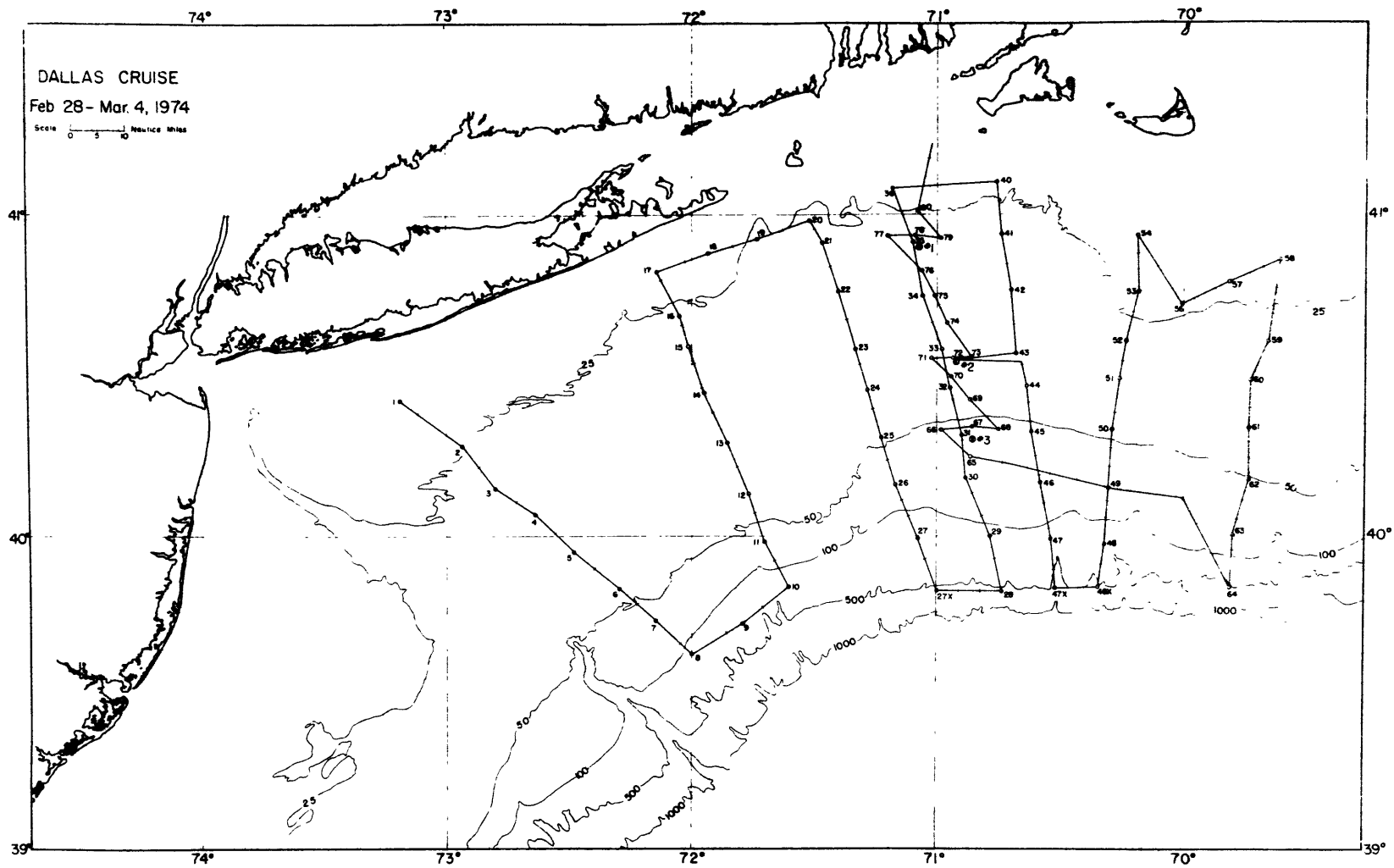


Figure 1.2 Cruise track of the USCGC DALLAS, February 28 to March 4. The numbered stations are STD casts and the tic marks between these stations are XBT launches.

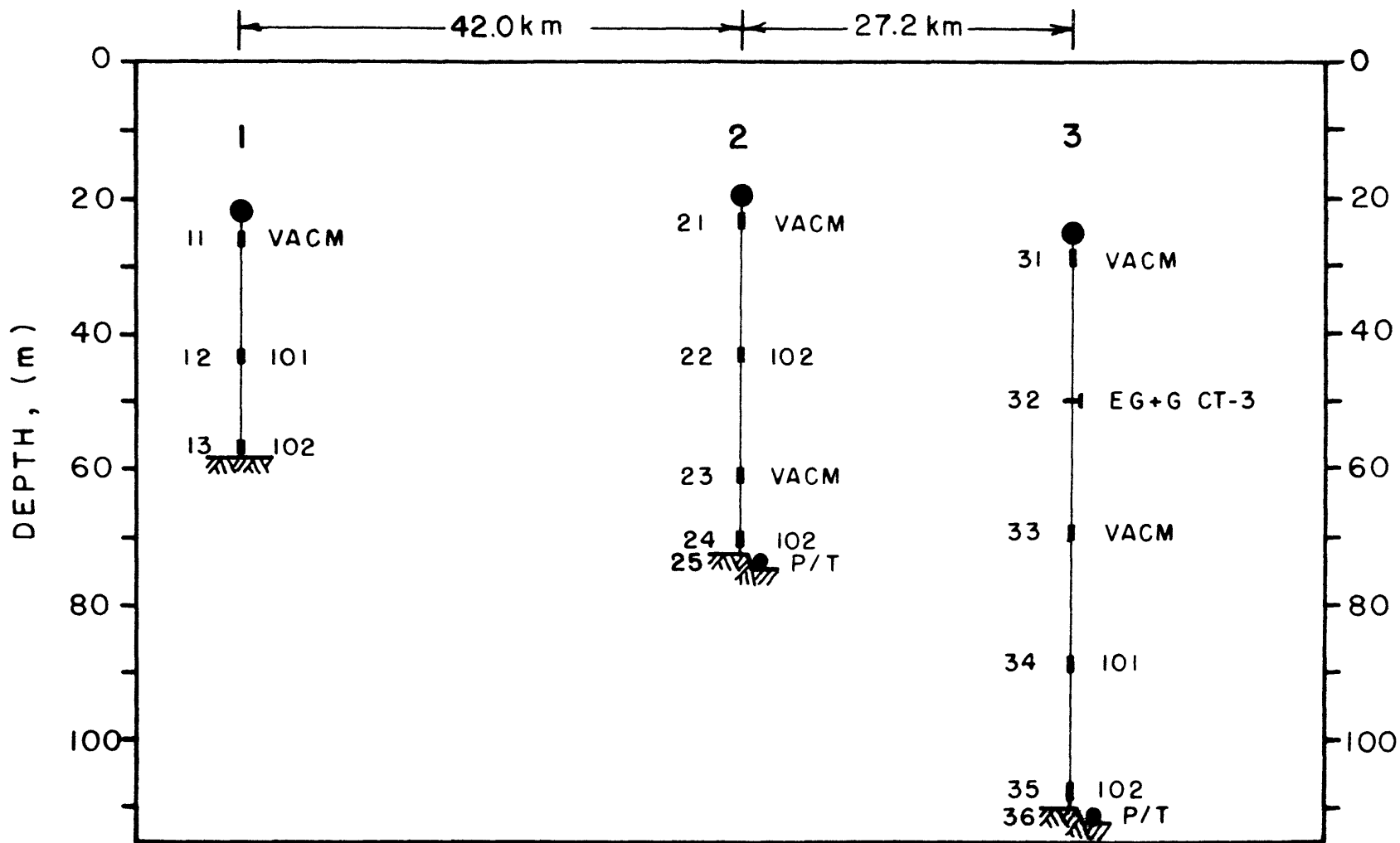


Figure 1.3 Diagram of the relative positions, types of instruments, and designations for the moorings of the 1974 MIT New England Shelf Dynamics Experiment.

The results of the hydrographic portion are described by Beardsley and Flagg (1975). The principal features of the winter hydrography of the New England shelf included the vertically well-mixed character of the shelf water, the abrupt transition zone of the shelf/slope front, and a tight T-S correlation. The experiment occurred during the period of winter extreme in the water properties so that there was little change over the month. Beardsley et al. (1976) give the results of the bottom pressure measurements together with three MESA pressure measurements by the NOAA Atlantic Oceanographic and Meteorological Laboratory taken near Hudson Canyon where there were overlapping data series. The tides dominate the subsurface pressure (SSP) records containing 85% to 98% of the variance with the relative amount increasing offshore. The amount of subtidal variance decreased offshore from ~13% near shore to ~1% at the shelf edge. The SSP records were coherent over distances large compared to the shelf width for periods of more than 4 days. The variable part of the SSP gradients were 5 to 10 times larger in the cross-shelf direction than in the along-shelf direction. In addition, the standard deviation of the alongshore slope off New Jersey was 40% larger than estimates of the mean for March 1975 made by EG&G (1976) with a maximum value more than four times as large. The pressure records also showed a single short duration pulse of edge waves which seemed to be meteorologically forced, lasting about 18 hours with approximately 6 hour periods.

In January 1975 Beardsley and Flagg were asked to participate in a short, one week long, experiment aboard the R/V KNORR sponsored by the Brookhaven National Laboratory Coastal Shelf Productivity Program. The goal was to define the distribution of nutrients near the shelf edge and along a cross-shelf transect near the 72°W meridian. We deployed a

single mooring in the center of the shelf/slope front (see Figure 1.4) consisting of three EG&G 102 CM's set to continuously record data at 5 second intervals and four temperature recorders of extremely primitive design borrowed from WHOI. A diagram of the mooring is shown in Figure 1.5. The deployment lasted 77.2 hours and the time series of speed, direction, east and north currents, and temperature are shown in the Appendix. The usefulness of this data set lies with our ability to set the depth and position of the instruments precisely relative to the front and to monitor the frontal position throughout the deployment with Nansen casts and XBT launches. In addition, we were lucky enough to be hit by a storm right in the middle of the cruise so that we could observe more precisely and immediately the effect of a wind stress event on frontal behavior. In this respect the January 1975 experiment complements the March 1974 observations.

The goal of this thesis is to describe and understand the water movements on the New England continental shelf with respect to their structure and variability and to explore the interaction between the shelf and slope in the shelf/slope frontal zone. The thesis falls into three logical sections. Chapter 2 investigates the mean and variable shelf currents and defines the structure of these currents, their frequency constituents, and their response to wind stress and SSP gradient forcing. Csanady (1976) has developed a model for the mean shelf currents using frictional dynamics. The degree to which it is applicable to the New England shelf is examined. For the low frequency currents the relative magnitude of the terms in the horizontal momentum equations are calculated.

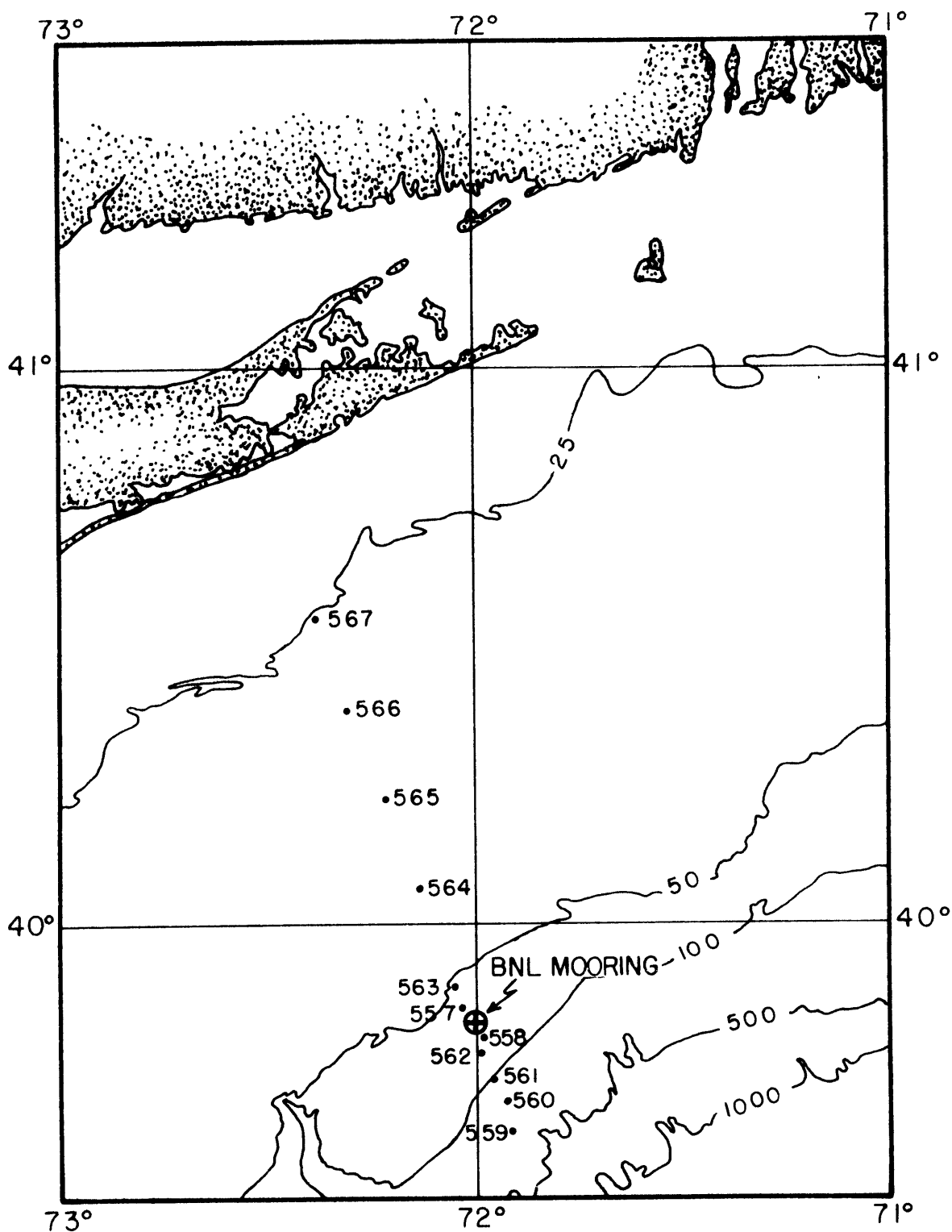


Figure 1.4 Chart of the mooring position and the Nansen cast locations for the Brookhaven National Laboratory Coastal Productivity program aboard the R/V KNORR, cruise 46, from 24 to 30 January 1975. Depths of the isobaths are in fathoms.

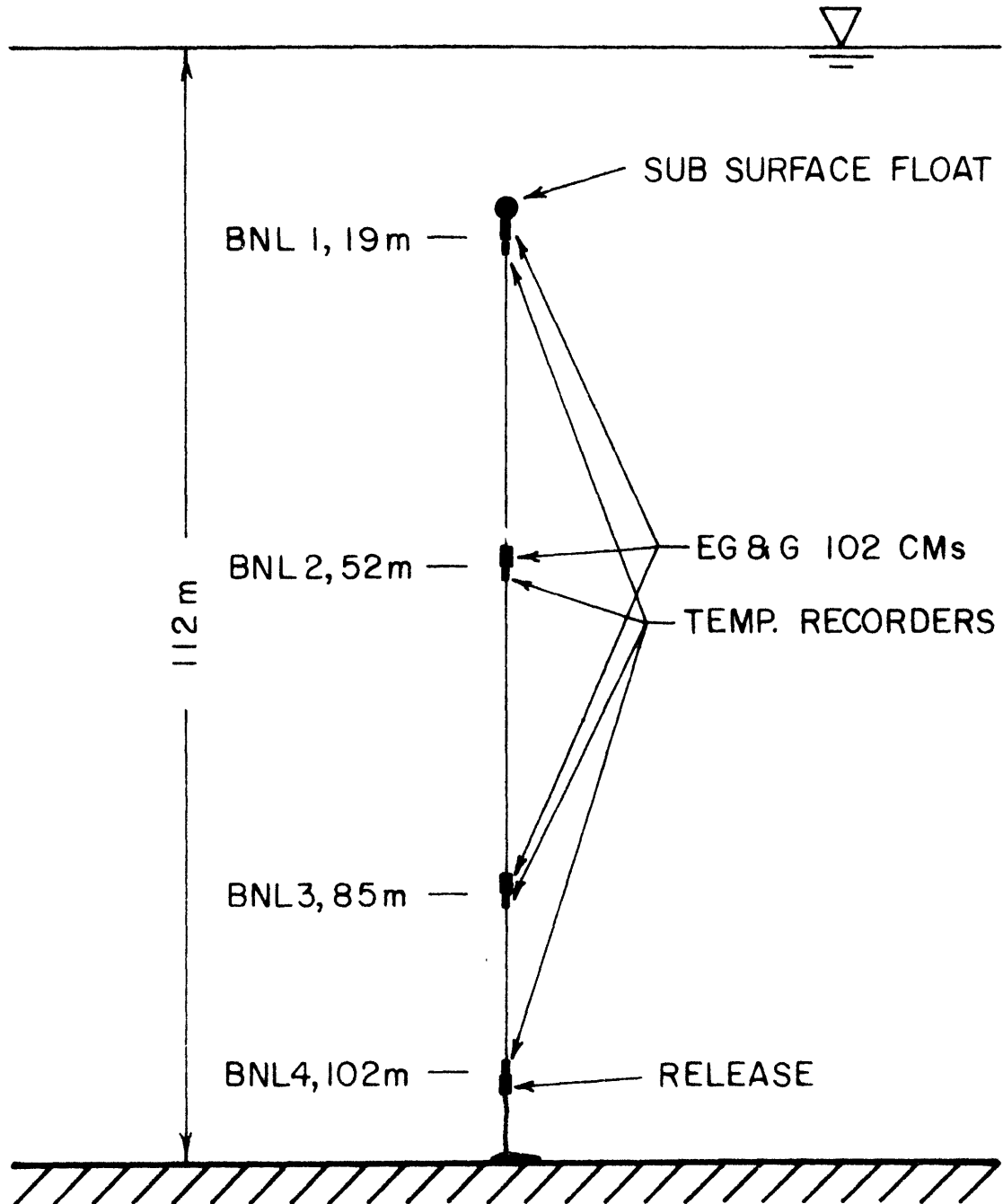


Figure 1.5 Diagram of the mooring showing the distribution and designation of the current meters and temperature recorders for the Brookhaven National Laboratory Coastal Productivity Program experiment in January 1975.

Chapter 3 investigates the structure and variability of the shelf/slope front for motions ranging from internal waves to those with periods of 7-10 days. We determine the degree to which the front actually exhibited the geostrophic shear implied by the sloping frontal surface. Using geostrophic shears and measured currents, an estimate is made of the role of the frontal zone in transporting shelf water to the west. We also look at the low frequency and alongshore variability of the front shown by the hydrographic surveys and low frequency currents.

Chapter 4 explores the possibility that the observed alongshore undulations of the front might be caused by baroclinic instabilities. A numerical model is developed for the stability of a Margules front similar to that of Orlanski (1968) but with the inclusion of steep topography. Stability diagrams are investigated for several parameter ranges that might apply to the New England shelf.

2. Currents on the New England Continental Shelf

2.1 Introduction

The earliest significant study of the physical oceanography of the continental shelf of the Mid-Atlantic Bight was that of Bigelow (1933) and Bigelow and Sears (1935) on the mean distribution and seasonal variation of temperature and salinity. This remains today the most complete survey of the shelf hydrography and is the basis of many modern concepts about shelf current structure. The general observed features are: 1) an increase in salinity in the offshore direction with an abrupt transition to slope water salinities near the 100 m isobath; 2) temperature slowly increases offshore over the whole shelf in winter and over the outer half of the shelf and below the seasonal thermocline during summer with an abrupt increase at the shelf/slope front in winter and at the offshore edge of the "cold band" during summer; and 3) at mid-shelf during winter, temperature and salinity increase slightly with depth by 2°C and $0.5^{\circ}/\text{oo}$ respectively. On the basis of this structure, Iselin (1939, 1955) postulated a cross-shelf circulation pattern of offshore flow near the surface and inshore flow along the bottom and an intensification of the alongshore mean flow to the southwest near the 200 m isobath. Bumpus (1973) gives a review of the literature on the non-tidal currents on the shelf previous to recent investigations using moored current meters. Most of the results were based upon mean hydrography, surface and bottom drifters, and occasional drift pole measurements. The studies showed that there is generally a westward to southwestward flow south of New England of 5 to 10 cm/sec which might be strongest outside the 100 m contour. During low runoff periods in late

summer, the drifters showed occasional reversals of the nearshore flow. Bottom drifters indicate the possibility of a line of divergence near the 60 to 70 m isobaths with drifters released inshore of this line having a shoreward velocity component while those released further out had an offshore component.

In the past 5 to 10 years an effort has been made to obtain observational information on current motions with shorter space and time scales than previously available. Results from experiments combining hydrographic surveys with current meter deployments lasting a month or more for the Mid-Atlantic Bight region are given by: Boicourt (1973), Beardsley and Butman (1974), Beardsley and Flagg (1975), Boicourt and Hacker (1975), Beardsley et al. (1977), Scott and Csanady (1976) and EG&G (1974, 1975). As a result it appears that the alongshore transport to the west and southwest inside the 100 m isobath is roughly constant from south of New England to the Chesapeake. It is clear that the shelf responds to wind forcing with resultant alongshore currents coherent over large alongshore distance relative to the shelf width and with magnitudes considerably larger than the mean. Beardsley and Butman (1975) showed a possible asymmetry in current response on the shelf to eastward versus westward wind stress. One of the major benefits of these exploratory studies is that at least in some respects the dynamics of wide continental shelves seem to be simpler than originally supposed.

The paper by Stommel and Leetmaa (1972) was the first attempt at modeling the important dynamical inputs to the continental shelf mean motion. They included explicitly fresh water input from shore, mean wind stress, and vertical mixing on a semi-infinite, constant depth shelf with the hope of examining winter conditions in the Mid-Atlantic

Bight. The model indicated that the shelf was in a wind driven regime and that an alongshore pressure gradient was necessary to account for the observed gross flow features. Perhaps the most significant result of the model was that it pointed out the major influences, stimulated interest in the shelf, and gave a conceptual departure point for the design of experiments to study the relative importance of the forcing terms.

The experiments that followed showed that fluctuations of sources and sinks of momentum were large but that at least qualitatively much of the resulting flows could be explained by simple frictional coastal boundary layer theory. Csanady (1976) expanded upon the Stommel and Leetmaa model demonstrating that in terms of the mean flow it was possible to parameterize the effects of large fluctuations in wind stress and turbulent diffusion and to decouple the cross-shelf transport of salt from the mean circulation. He also had to resort to a sea level gradient to drive a westward flow with sufficient intensity. Two particularly noteworthy features of the model are that with an alongshore gradient of the magnitude found by Scott and Csanady (1976) the alongshore velocities are toward the west with the right order of magnitude and increase offshore, and that there is a line of bottom flow divergence. The cause of the surface gradient remains unknown and the role of the deep ocean on the shelf dynamics has not been defined although it is probable that these two points are connected.

In this section we discuss the structure and variability of wintertime shelf currents based upon observations from the March 1974 experiment. Using this data we examine the major assumptions of the Csanady mean flow model and explore how well the model predicts observed flow

features. The suitability of dynamical/statistical models for describing the low frequency currents is also examined. Lastly, several periods of intense storm activity are studied with a view toward understanding the mechanisms of these important events,

2.2 Observed Shelf Currents

2.2.1 Mean Currents

Figure 2.1 and Table 2.1 give the mean currents obtained from the current meter array of the March 1974 experiment. East and north are approximately the alongshore and onshore directions respectively. All the CM's showed a mean westward current ranging in magnitude from nearly zero to 8 cm/sec. There was a consistent increase by a factor of 3 to 4 in the westward flow at mid-depth progressing from the 50 to 110 m isobaths. Vertically the mean westward flow decreased monotonically with depth to less than 1 cm/sec 1 m above the bottom. The northward component of the mean currents increased with depth by a factor of 2 to 3 from ~ 25 m to the bottom or the top of the shelf/slope front at mooring 3. The magnitude of the mean maximum northward currents increased offshore by a factor of 3 between moorings 1 and 3. Anomalous behavior in this respect is shown by instrument 24 which had an offshore component. This instrument was 1 m off the bottom and somewhat further offshore than mid-shelf. The net result of the mean along and onshore current components is that the mean current vectors rotate clockwise with depth, from being directed alongshore to pointing more onshore while decreasing in magnitude. The westward component of instrument 22 seems small and does not quite fit the above pattern and is probably caused by a sticky rotor. Instruments 34 and 35 were below the mean position of the shelf/slope front and would not be expected to exhibit the same shelf related behavior. The mean currents below mid-depth at mooring 1 are directed toward the entrances to Long Island Sound and Narragansett Bay and are suggestive of a mean flow pattern required to maintain the salt balance in these areas. The low salinity water from these bays as shown by the

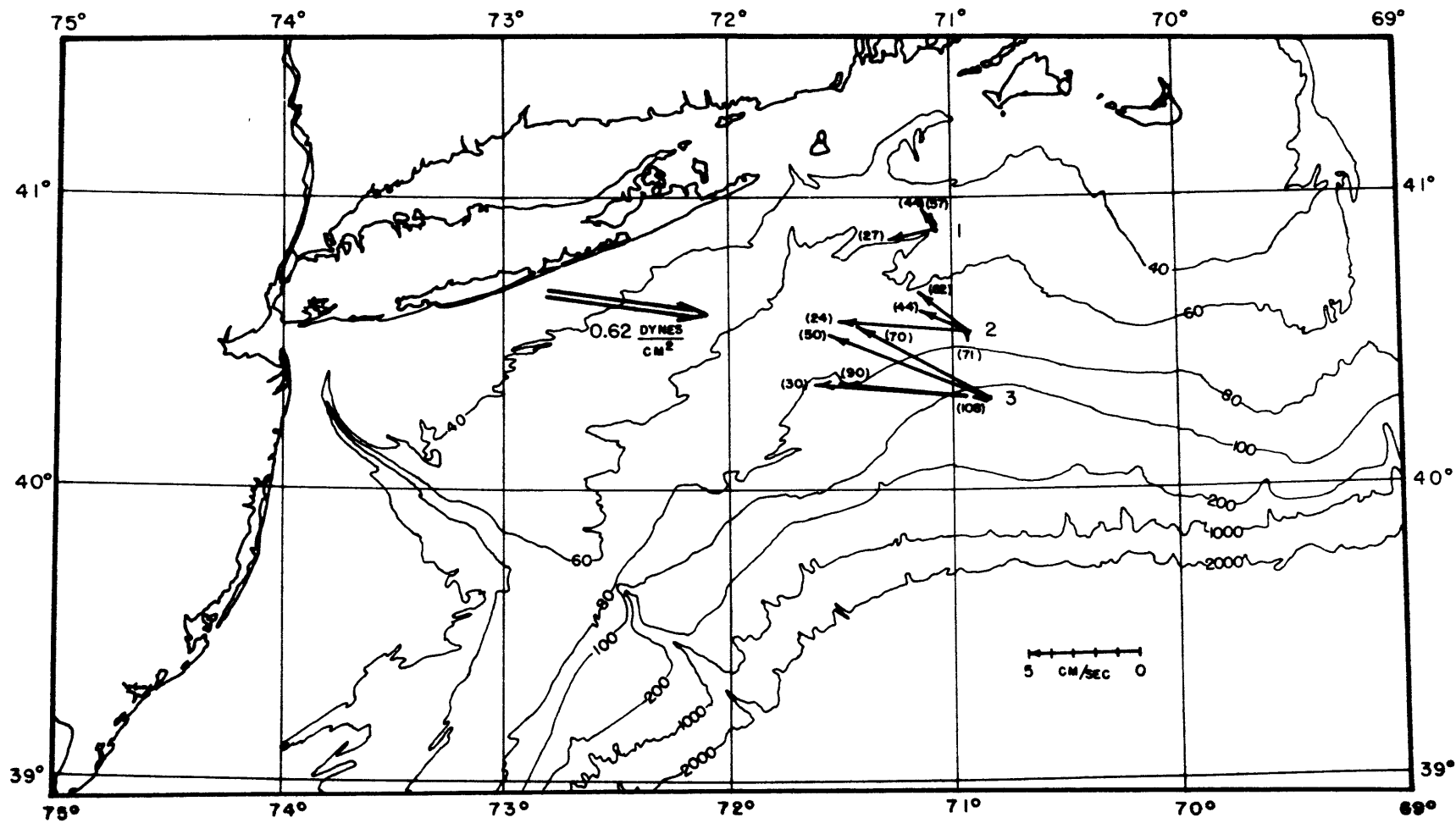


Figure 2.1 Mean currents and wind stress during the 1974 MIT New England Shelf Dynamics Experiment; February 27 - April 3 1974. Numbers in parenthesis are the instrument depths in meters. Isobaths are in meters.

TABLE 2.1

INSTRUMENT	DEPTH (m)	EAST			NORTH		
		$\overline{\text{EAST}}$ (cm/sec)	σ_E	ϵ_E	$\overline{\text{NORTH}}$ (cm/sec)	σ_N	ϵ_N
11	27	-2.10	11.94	2.48	-0.45	7.87	0.62
12	44	-0.62	9.47	—	0.93	5.67	—
13	57	-0.23	5.80	1.09	0.78	4.33	0.43
21	24	-5.72	12.81	2.76	0.51	8.61	1.03
22	44	-2.16	8.57	1.69	0.96	4.97	0.56
23	62	-2.21	11.56	2.15	1.78	8.94	1.19
24	71	-0.01	5.01	—	-0.48	4.36	—
31	30	-7.81	11.34	3.45	0.71	8.99	1.54
32	50	-7.18	9.41	2.66	2.88	7.85	1.36
33	70	-5.91	11.51	3.06	3.32	8.95	1.20
34	90	-6.71	20.36	—	0.68	16.53	—
35	108	-0.75	5.27	1.55	0.04	4.13	0.54

Table 2.1 Tabulation of the mean east and north currents for the March 1974 experiment. Also shown are the standard deviations of the one hour averaged currents, $\sigma_{E,N}$. An estimate of the statistical error, $\epsilon_{E,N}$, based upon a method used by Kundu and Allen (1975) is discussed in the text. Bottom depths at the mooring sites are 58, 72, and 109 - 112 m for moorings 1, 2, and 3 respectively.

DALLAS cruise (Flagg and Beardsley, 1975) leaves in a plume close to the Long Island shore perhaps explaining why the surface current at mooring 1 is not directed more offshore. The low salinity water in the area of the moorings primarily comes from the Gulf of Maine around Nantucket Shoals (Bigelow and Sears, 1935).

Also shown in Figure 2.1 is an estimate of the mean wind stress for the New England shelf region during the March 1974 experiment. The estimate is 0.62 dynes/cm^2 directed toward 98°T . This figure was derived from mesoscale weather maps compiled for the New England shelf region from 6 hourly ship and shore observations. The wind speed and direction were subjectively determined from these maps for the mooring region and the stress computed using the quadratic drag law with a drag coefficient of 1.22×10^{-3} . The value of 0.62 dynes/cm^2 is lower than the 31 year climatological mean winter wind stress of almost 1 dyne/cm^2 calculated by Saunders (1977). The value of the drag coefficient used is on the low side of the range of values used by Saunders; however, the winter of 1974 was a particularly mild one and our wind stress value seems reasonable. The mean wind stress is opposed to the currents indicating that the source of momentum for the currents is something other than the wind.

Table 2.1 also contains the standard deviations of the currents and an estimate of the statistical error given by

$$\epsilon_{E,N} = \sigma_{E,N} \sqrt{\frac{2\Gamma}{T}}$$

where T is the length of the record, $\sigma_{E,N}$ the standard deviation, and Γ is the correlation time scale. Following Kundu and Allen (1975), an estimate of Γ is given by the first zero crossing of the auto-covariance

function. For shelf records, tides represent a large but constant source of variance so that a more appropriate estimate for Γ and $\sigma_{E,N}$ is obtained from the detided record. 2Γ was approximately 2.5 days for mooring 1 and 2 for both east and north and 5.0 days for the east and 3.0 days for the north components at mooring 3. The total record length for instrument 13 was 16 days while for all the rest the record length was ~ 35 days. These errors do not include instrumental errors which would be much smaller. The statistical errors are often nearly as large or larger than the means suggesting that in some cases the signs of the means may vary over the years. An analysis of the stability of the means with increasing record length indicates that the sample mean is within 10% of the total variance of a true mean for the 1974 winter after approximately 25-30 days.

2.2.2 Spectral Characteristics of the Variable Currents

Figures 2.2, 2.3, and 2.4 show half of the two sided horizontal kinetic energy spectra for moorings 1, 2, and 3 respectively. Table 2.2 gives the distribution of the total variance divided into three frequency bands: 1) low frequency for periods greater than 33 hours; 2) the tidal-inertial band for periods between 10 and 33 hours; and 3) the internal wave band at periods less than 10 hours. In this section we discuss the variable currents as they apply to the shelf as a whole; the vertical structure at mooring 3 associated with the shelf/slope front is covered in chapter 3.

The energy in the internal wave band decreases progressing onshore from the shelf edge, a reflection of the decreasing vertical density gradient. The exception to this is the growth of the tidal harmonic peaks at periods of 6.21 and 4.06 hours, absent at mooring 3 and quite striking at mooring 1. This amplification of the semi-diurnal tidal harmonics was also observed on the Scotian shelf by Petrie (1974). The spectral decay except for the tidal harmonics goes approximately as $f^{-5/3}$ at all three moorings. The contribution to the total variance of the internal wave band is small, generally less than 10%.

The semidiurnal energy peak is dominant in all spectra and becomes relatively more so shoreward. The semidiurnal tidal energy level is essentially constant vertically except within the bottom boundary layer. (The anomalous behavior of instrument 22 again may have been caused by a sticky rotor.) Between moorings 2 and 3 the semidiurnal current amplitude exhibits very closely an h^{-1} depth dependence while between moorings 1 and 2 the cross-shelf dependence is close to $h^{-1/5}$. The semidiurnal energy is almost completely clockwise polarized implying near

TABLE 2.2

INSTRUMENT	TYPE	DEPTH (m)	Percentage of Total Variance in Frequency Band			TOTAL VARIANCE (cm ² /sec ²)
			Low Freq. 3.1×10^{-3} - 3.0×10^{-2}	Tidal-Inert. 3.0×10^{-2} - 0.10	Internal Wave 0.10 - 0.50	
11	VACM	27	25	67	8	204
12	101	44	—	—	—	122
13	102	57	9	86	5	52
21	VACM	24	34	63	3	238
22	102	44	31	62	7	98
23	VACM	62	31	66	2	213
24	102	71	—	—	—	44
31	VACM	30	27	69	4	209
32	CT-3	50	27	67	6	150
33	VACM	70	27	67	6	212
34	101	90	—	—	—	688
35	102	108	26	52	13	45

Table 2.2 For the March 1974 experiment, a tabulation of the horizontal current variance and the percentage of the variance in three frequency bands: 1) low frequency for $3.1 \times 10^{-3} \text{ hr}^{-1} \leq f \leq 3.0 \times 10^{-2} \text{ hr}^{-1}$; 2) tidal-inertial bands for $3.0 \times 10^{-2} \text{ hr}^{-1} \leq f \leq 0.10 \text{ hr}^{-1}$; and 3) internal wave band for $0.10 \text{ hr}^{-1} \leq f \leq 0.50 \text{ hr}^{-1}$.

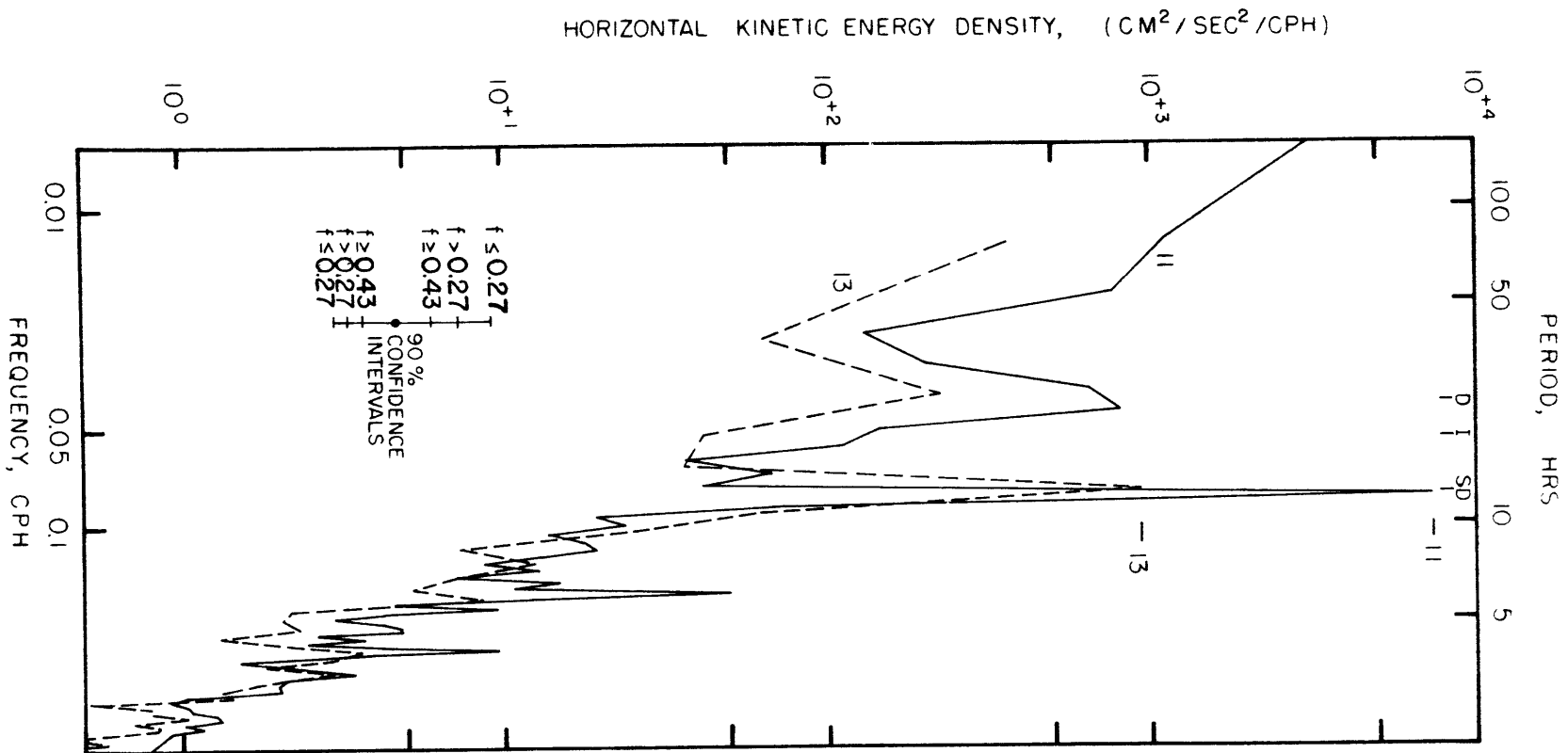


Figure 2.2 Auto spectra of east and north current components for instruments 11 and 13 from the March 1974 experiment. Spectra for 11 computed with 400 estimates and 13 computed with 192 estimates and both were averaged over 5 adjacent frequency bands. Spectra are normalized such that a unit sine wave has energy of $1/2$.

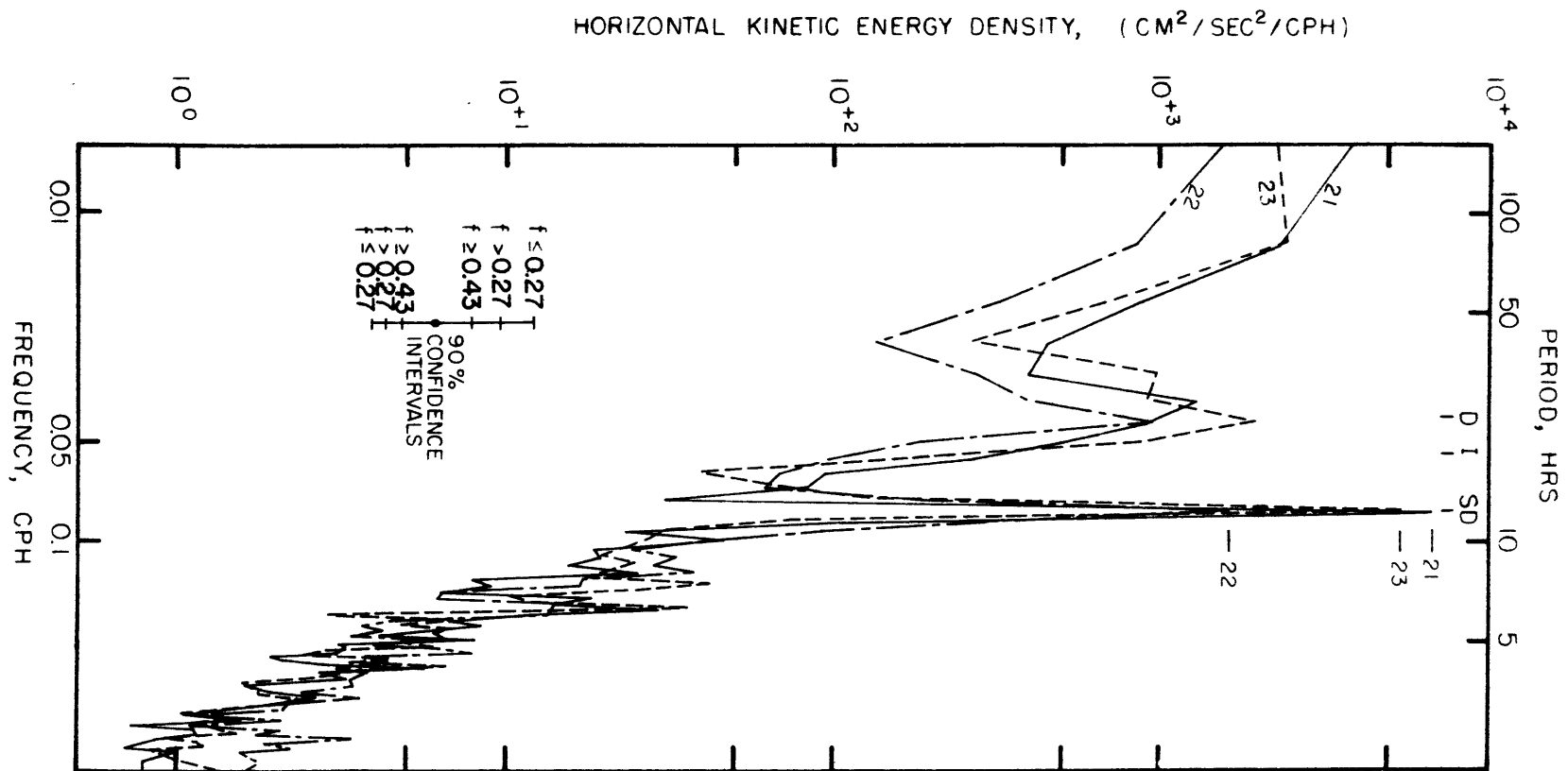


Figure 2.3 Auto spectra of east and north current components for instruments 21, 22, and 23 from the March 1974 experiment. Spectra are computed with 400 estimates averaged over 5 adjacent frequency bands. Spectra are normalized such that a unit sine wave has energy of 1/2.

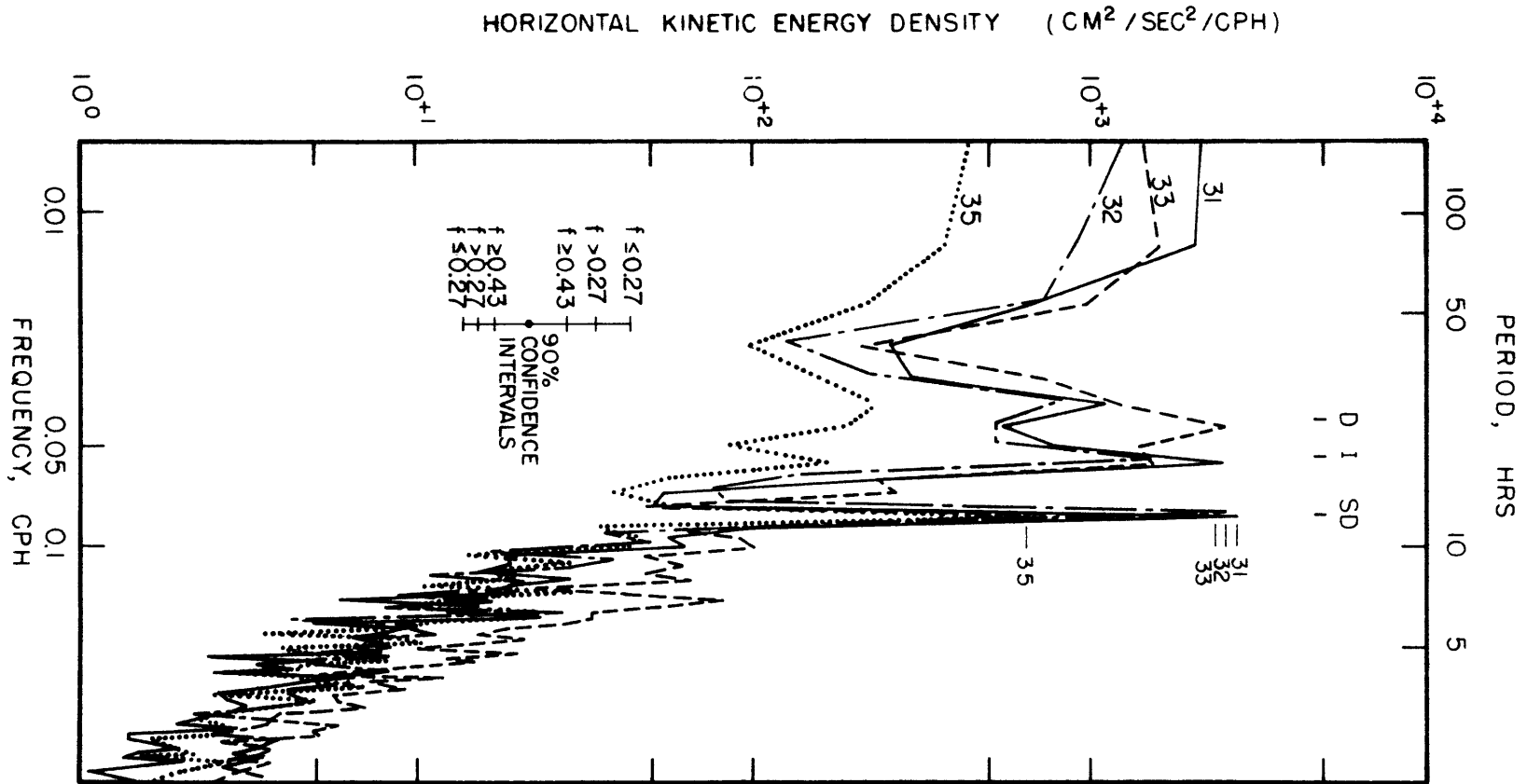


Figure 2.4 Auto spectra of east and north current components for instruments 31, 32, 33, and 35 from the March 1974 experiment. Spectra are computed with 400 estimates averaged over 5 adjacent frequency bands. Spectra are normalized such that a unit sine wave has energy of 1/2.

circular tidal eclipses. The peak to peak amplitude of the semidiurnal surface tide at both moorings 2 and 3 is approximately 86 cm. Simple one dimensional continuity of the form

$$u = \frac{\pi \zeta L}{h T_{sd}}$$

where ζ is the surface tide, L is the distance from shore, h is the water depth, and T_{sd} is the semidiurnal tidal period, comes very close to predicting the semidiurnal tidal velocity at mooring 3 but not at mooring 2. This suggests that the lines of constant tidal phase are parallel to the isobaths at 110 m but become progressively more convoluted between moorings 2 and 3. Onshore conservation of tidal energy requires

$$E \cdot C_g = \frac{1}{2} \rho_w u^2 h \sqrt{gh} = \text{constant}$$

indicating that, without friction, u should be proportional to $h^{-3/4}$.

That u increases slower than this between moorings 3 and 2 is mostly due to bottom friction. There is a relative concentration of tidal energy at mooring 1 possibly due to the funneling effect of the entrances to the nearby sounds combined with some changes in phase in these areas.

The diurnal tidal kinetic energy differs from the semidiurnal in that there is a shoreward energy decrease by as much as a factor of 2 between moorings 1 and 3. In addition the diurnal energy exhibits a greater vertical dependence with generally an increase toward the bottom until within the bottom boundary layer. In contrast to the semidiurnal tide, the diurnal has a significant amount of clounter-clockwise energy so that the tidal ellipses are more elliptical with the major axes generally aligned with the isobaths.

Inertial currents assume a significant position because of the importance of transient wind stress in forcing the low frequency currents. Figure 2.4 shows an inertial peak at instrument 31 which is nearly as large as the semidiurnal peak while 32 and 33 have somewhat smaller peaks. The records for mooring 1 and 2 do not indicate the presence of the inertial peaks at all! In order to be somewhat more definite about the cross-shelf behavior of the near inertial energy, the current records for the 5 VACM's (see Figure 1.2) were demodulated by least square fitting a sine wave of inertial period (18.6 hours) to successive 37 hour long data segments. The inertial amplitudes as a function of time are shown in Figure 2.5. Note first, that the average amplitude decreases toward shore, consistent with the spectra. The maximum amplitude decreases from 16 cm/sec at instrument 31 to 6 cm/sec at 11, a factor of 7 in peak energy. At least part of the amplitude at 11 may be considered as a measure of the noise inherent in the demodulation method. It is possible that the decrease in amplitude shoreward is due to a short circuiting of the wind stress directly to the bottom by the large vertical eddy viscosity associated with storms. This effect would be most prominent in shallow water and least effective over the front where the shelf/slope front acts as a slippery bottom. Secondly, note the large variability of amplitude of the inertial motion with peaks arising and decaying generally on the order of 3 days. Most of these oscillations are associated with wind stress fluctuations.

Low frequency current variations with periods greater than 1.5 days are of primary interest on the shelf because the lower frequency motions are responsible for large displacements of the shelf water. Our short record lengths prohibit spectral analysis at periods greater than about a

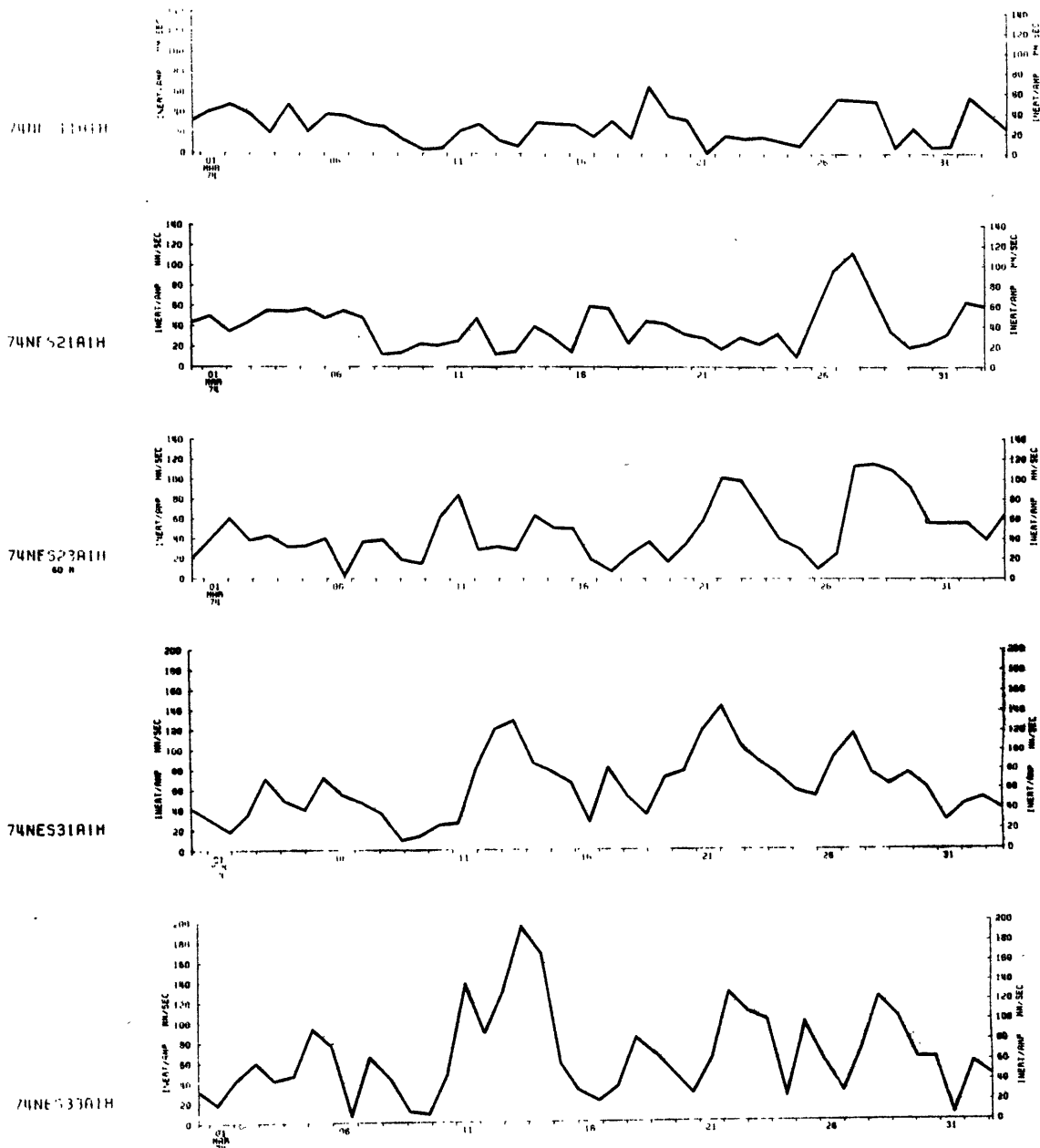


Figure 2.5 Amplitudes of the inertial oscillations for the 5 VACM's computed by least square fitting a sine wave with 18.6 hour periods to 50% overlapping successive 37 hour segments for the March 1974 experiment.

week. The low frequency energy level for periods between 1.5 and 7 days is somewhat less than the energy level of the tidal-inertial band and contains about 1/3 the total variance. However, about 70% of the total displacement variance is contained in the low frequency motions.

2.2.3 Low Frequency Current Structure and Variability

Figures 2.6, 2.7, and 2.8 are vector plots of the low frequency currents observed at moorings 1, 2, and 3, respectively. Due to the predominance of the alongshore flows, eastward (alongshore) currents are plotted in the up direction and northward (onshore) currents are plotted toward the left. The low frequency currents are calculated from the records by using a phase preserving, sharp cutoff, low pass filter with its half amplitude at 33 hours (Flagg et al., 1976).

These vector plots show considerable visual vertical and horizontal coherence. Currents at moorings 1 and 2 are highly coherent while somewhat less vertical coherence is seen at mooring 3. The large westward event at moorings 1 and 2 on March 29-30 is nearly absent at mooring 3. There is considerable variability in current magnitudes with east-west currents ranging from 8 cm/sec near the bottom to more than 30 cm/sec near surface, north-south currents range from 3 to 15 cm/sec from bottom to surface. Characteristic periods seem to range between 3 and 6 days as expected from the spectra. The stack plots clearly demonstrate a counter-clockwise rotation of the current vector with depth consistent with simple frictional coastal boundary layer dynamics. Comparison of these current plots with the local wind stress (shown in Figure 2.14) clearly indicate an association between major wind and current levels. We will explore the nature of the wind/current relation after looking at the structure of the currents themselves.

The spectra for the low frequency currents at mooring 3 and for instrument 23 show a possible peak at periods of ~ 3.5 days while the rest of the records peak at the lowest spectral estimate which is at 6.7 days. We will show later that the peak at 3.5 days is probably

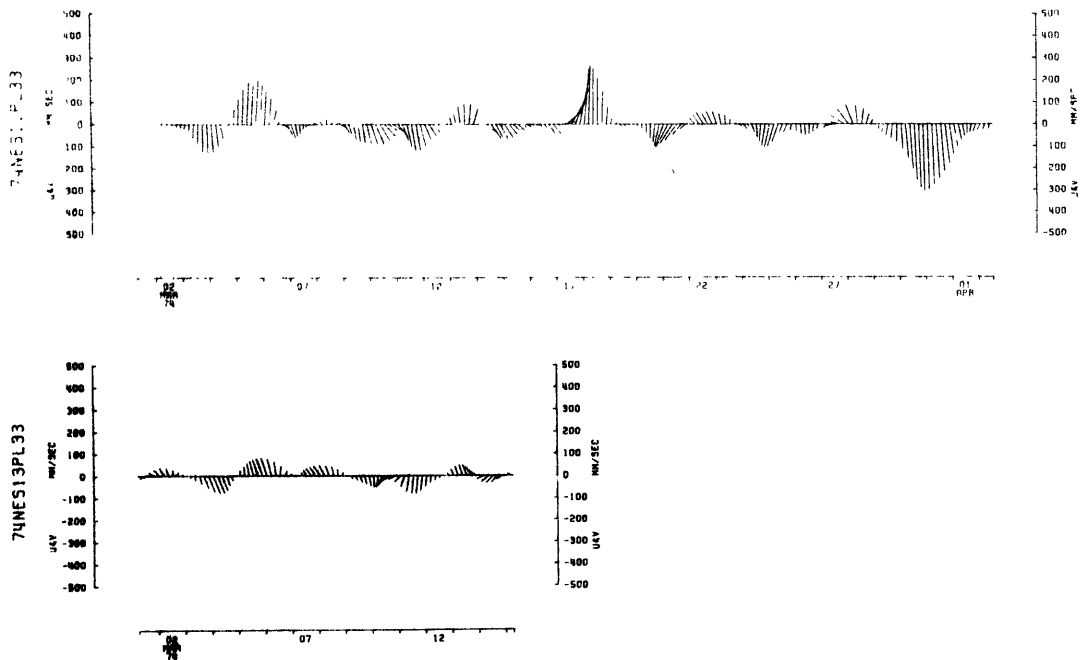


Figure 2.6 Vector plot of the low passed currents from mooring 1 of the March 1974 experiment. East is upward and north is to the left. Instrument depths are: 11, 27m; 13, 57m; with a bottom depth of 58m.

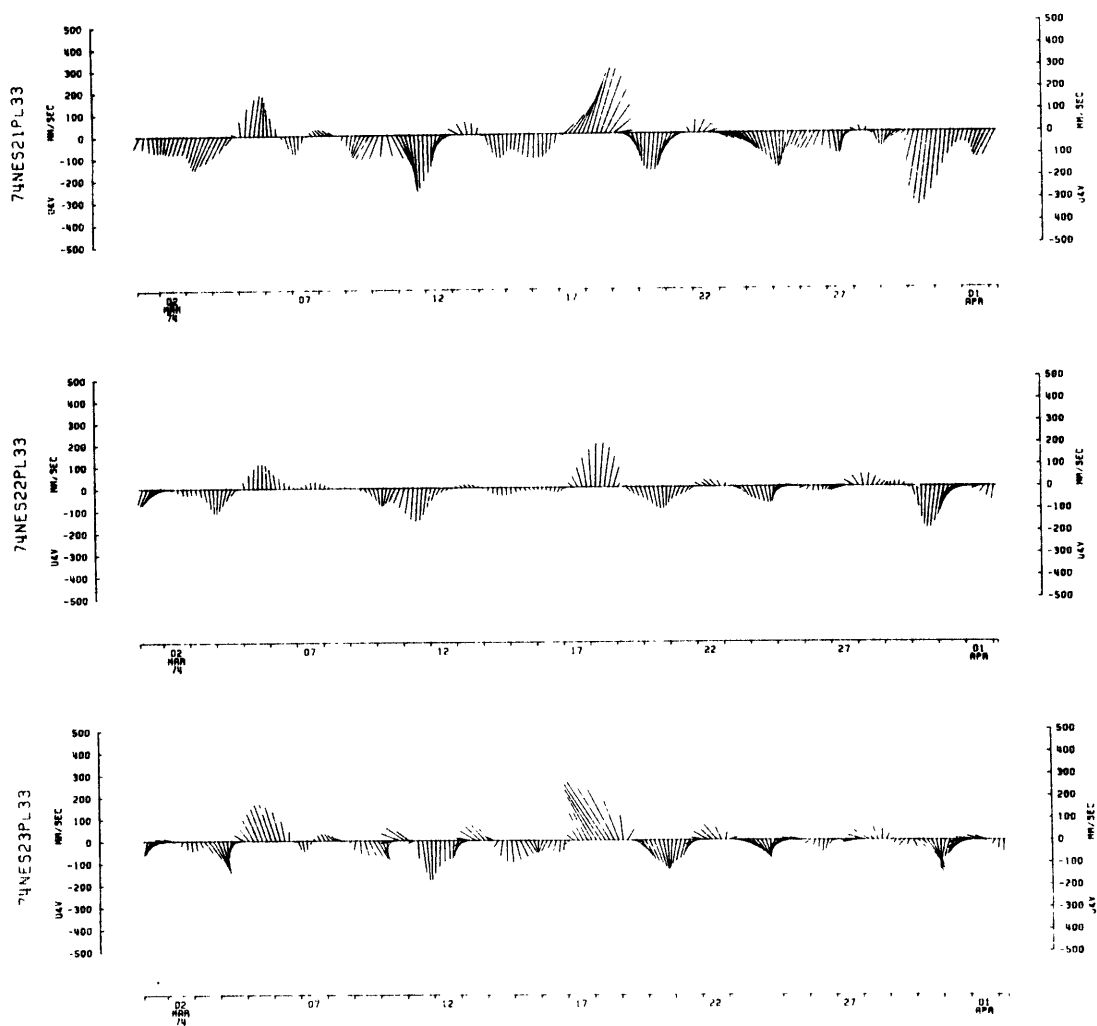


Figure 2.7 Vector plot of the low passed currents from mooring 2 of the March 1974 experiment. East is upward and north is to the left. Instrument depths are: 21, 24m; 22, 44m; 23, 62m; with a bottom depth of 72m.

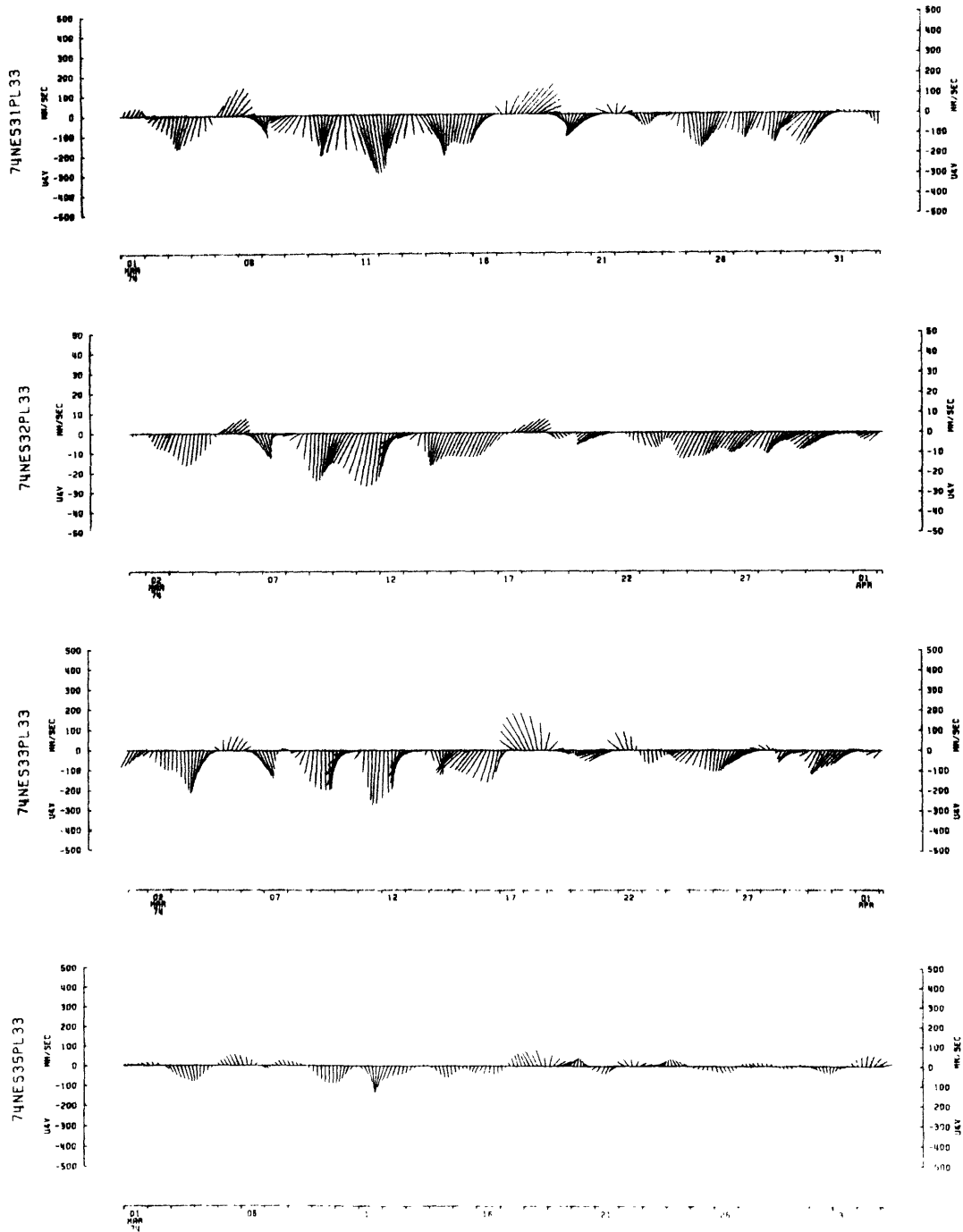


Figure 2.8 Vector plot of the low passed currents from mooring 3 of the March 1974 experiment. East is upward and north is to the left. Instrument depths are: 31, 30m; 32, 50m; 33, 70m; 35, 108m; with a bottom depth of 112m.

associated with movement of the shelf/slope front. The spectra on the outer half of the shelf exhibit a definite flattening which is in marked contrast to the red spectra at site D (Webster, 1969) or on the continental slope (Schmitz, 1974). There is a suggestion that the low frequency energy is greatest at mooring 2, decreasing slightly in both the on- and off-shore directions.

We next describe the observed low frequency currents in terms of vertical and cross-shelf empirical orthogonal models (EOM's). This is a purely statistical procedure which has been recently used by Kundu, Allen, and Smith (1975) to describe the vertical current structure on the Oregon shelf. We will outline the development of the procedure here and refer the reader to Kundu et al. (1975) and Busch and Peterson (1971) for more discussion.

Let $u_k(\underline{x}_j)$ be a discretely sampled current component at time t_k , $k = 1, 2, \dots, K$, at position \underline{x}_j , $j = 1, 2, \dots, N$. The covariance matrix of the currents can then be written as

$$C(\underline{x}_i, \underline{x}_j) = \frac{1}{K} \sum_{k=1}^K u_k(\underline{x}_i) u_k(\underline{x}_j).$$

This is a real $N \times N$ symmetric matrix with the diagonal elements equal to the variance of each current component. The N eigenvectors of this matrix are given by the equation

$$(C + \lambda_n I) \phi_n = 0,$$

where I is the identity matrix, λ_n the eigenvalues, and ϕ_n the eigenvectors. The eigenvectors form a set of orthogonal axes, such that

$$\sum_{i=1}^N \phi_n(\underline{x}_i) \phi_m(\underline{x}_i) = \delta_{nm}.$$

The projection of the observed currents onto this new set of axes defines a new set of variables

$$E_{kn} = \sum_{i=1}^N u_k(\underline{x}_i) \phi_n(\underline{x}_i)$$

such that the covariance matrix of the new variables has no off diagonal terms, i.e.,

$$\frac{1}{K} \sum_{k=1}^K E_{kn} E_{km} = \lambda_n \delta_{nm}.$$

Thus, the eigenvalues are the variances of the observed currents along each of the new set of axes with the total variance conserved through the transformation, i.e.,

$$\sum_{i=1}^N C(\underline{x}_i, \underline{x}_i) = \frac{1}{K} \sum_{k=1}^K \sum_{i=1}^N u_k^2(\underline{x}_i) = \frac{1}{K} \sum_{k=1}^K \sum_{n=1}^N E_{kn}^2 = \sum_{n=1}^N \lambda_n.$$

The eigenvectors are structure functions or "modes" weighting the contribution of each of the velocity components with the eigenvalues giving the amount of variance in each mode. There are two methods of ranking the modes, the first being the amount of variance in each mode and the second being by the structural complexity represented by the ϕ_n 's. The structural ranking for a vertical array of velocity measurements progresses from a barotropic-like model to a first baroclinic-like mode, and so forth, with generally an additional zero crossing mode added for each added element in the vertical.

A two-dimensional example serves to illustrate the results obtained. Consider a set of perpendicular velocity components, (u_k, v_k) . The EOM's of these two velocities form new velocities where one velocity has a maximum variance and the other a minimum. The two new velocities or modes

are oriented along the principal axes of the current. However, at any given time the original current components are given in terms of the EOM's by

$$u_k(\underline{x}_i) = \sum_{n=1}^N E_{kn} \phi_n(\underline{x}_i).$$

Thus, time series of the amplitudes of the EOM's tell us what combinations of the different eigenvectors are required to make up the instantaneous current pattern. The description of the current data in terms of the EOM's becomes particularly useful when most of the current variance is contained in a small number of modes (like 1 or 2). Then those few modes describe the primary response of the current field and the EOM amplitude time series can be compared to other data to study what drives the current field.

We have computed the EOM's for the vertical structure at each mooring and the cross-shelf model structure at nominal 25 and 65 m depths. Current meters 12, 24, and 34 had uncorrectable time based errors, so that those records were not used. Current meter 13 worked only for the first half of the experiment so the EOM structure at mooring 1 is valid only for this initial period. Instruments 13 and 35 were in the bottom boundary layer; thus their amplitudes are generally smaller than those above and this effect is visible in the results. Lastly, instrument 22 seems to read low because of the possible sticky rotor and again this is reflected in the results.

Table 2.3 gives the percentage of the total vertical and cross-shelf variance contained in each mode for the east and north currents. The terminology has been modified to refer to the mode with no zero crossings as the 0th mode, etc. Figures 2.9-2.13 show the vertical

TABLE 2.3

Percentage of Variance in Vertical Modes

MOORING	EAST			NORTH		
	1	2	3	1	2	3
ϕ_0	96.6	94.2	88.5	31.7	34.6	68.0
ϕ_1	3.4	3.9	8.4	68.3	59.6	20.2
ϕ_2		2.0	2.1		5.9	8.5
ϕ_3			1.0			3.3

Percentage of Variance in Cross-Shelf Modes

Nominal Depths (m)	EAST		NORTH	
	25	65	25	65
ϕ_0	83.0	89.5	78.1	69.4
ϕ_1	14.6	10.5	12.3	30.6
ϕ_2	2.5		9.6	

A tabulation of the percentage of total variance in each of the vertical and cross-shelf east and north empirical orthogonal modes from the low passed currents of the March 1974 experiment.

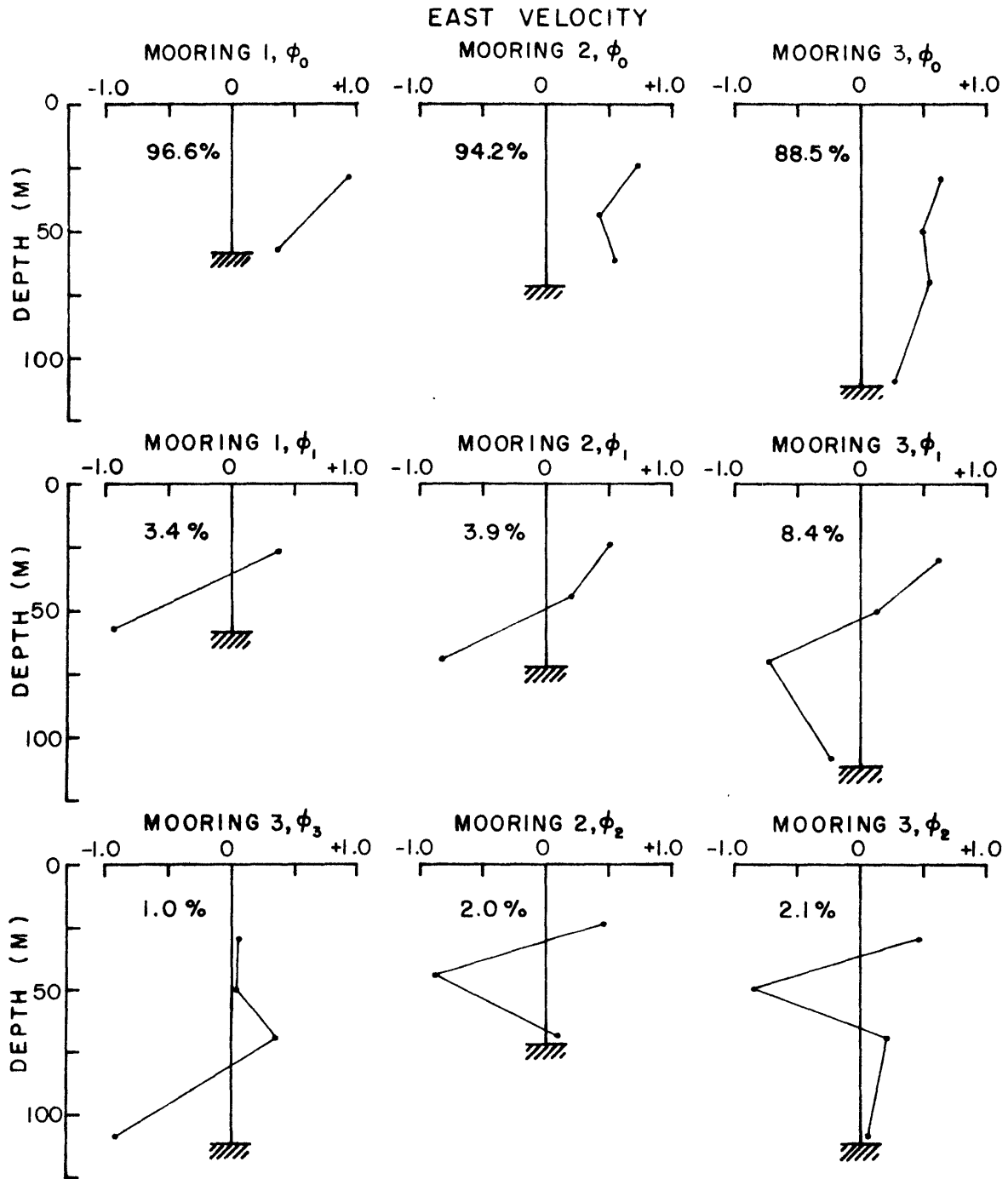


Figure 2.9 Vertical eigenvectors and percentages of total variance in each mode from the empirical orthogonal modal analysis of the eastward currents at each mooring.

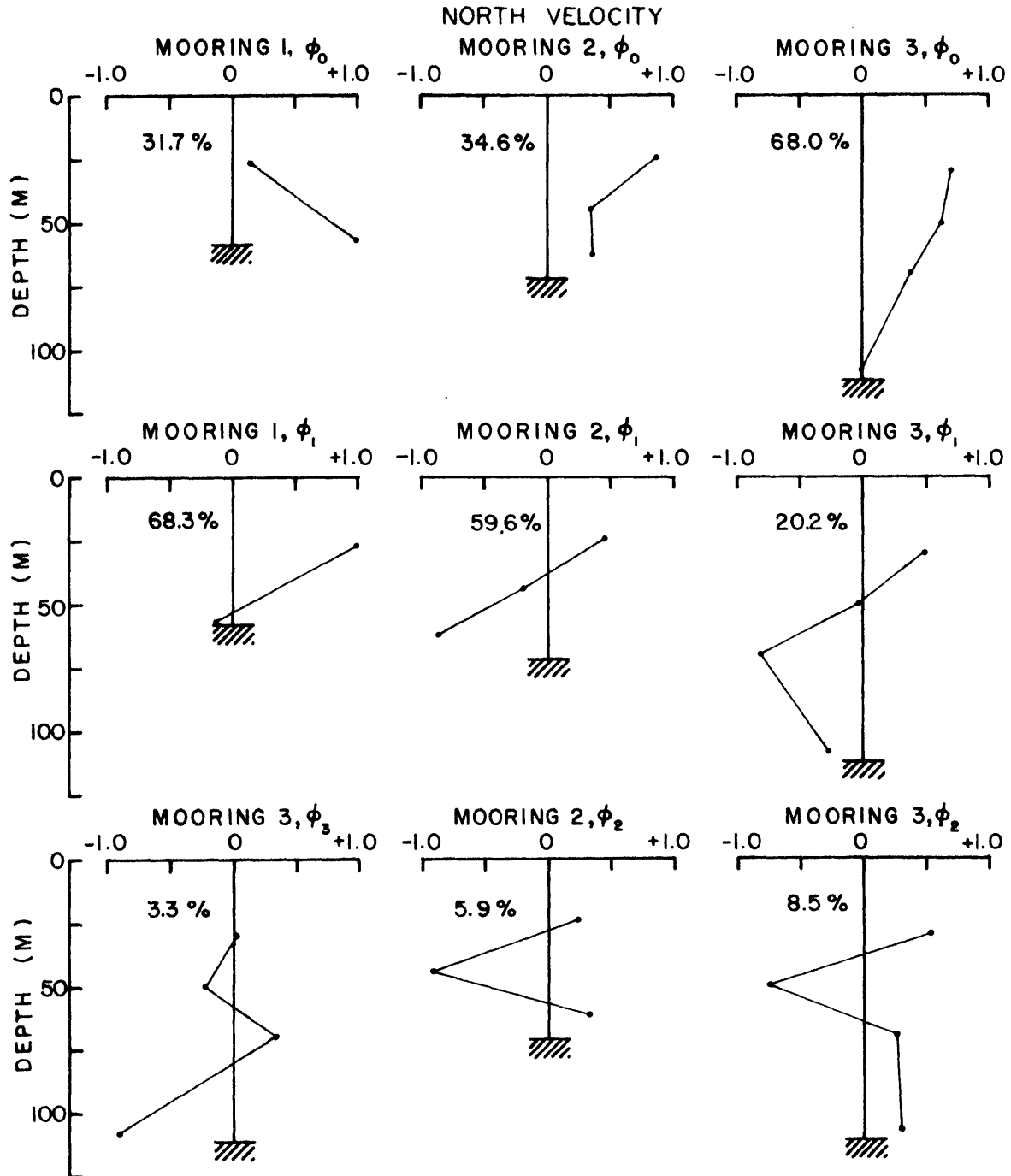


Figure 2.10 Vertical eigenvectors and percentages of the total variance in each mode from the empirical orthogonal modal analysis of the northward currents at each mooring.

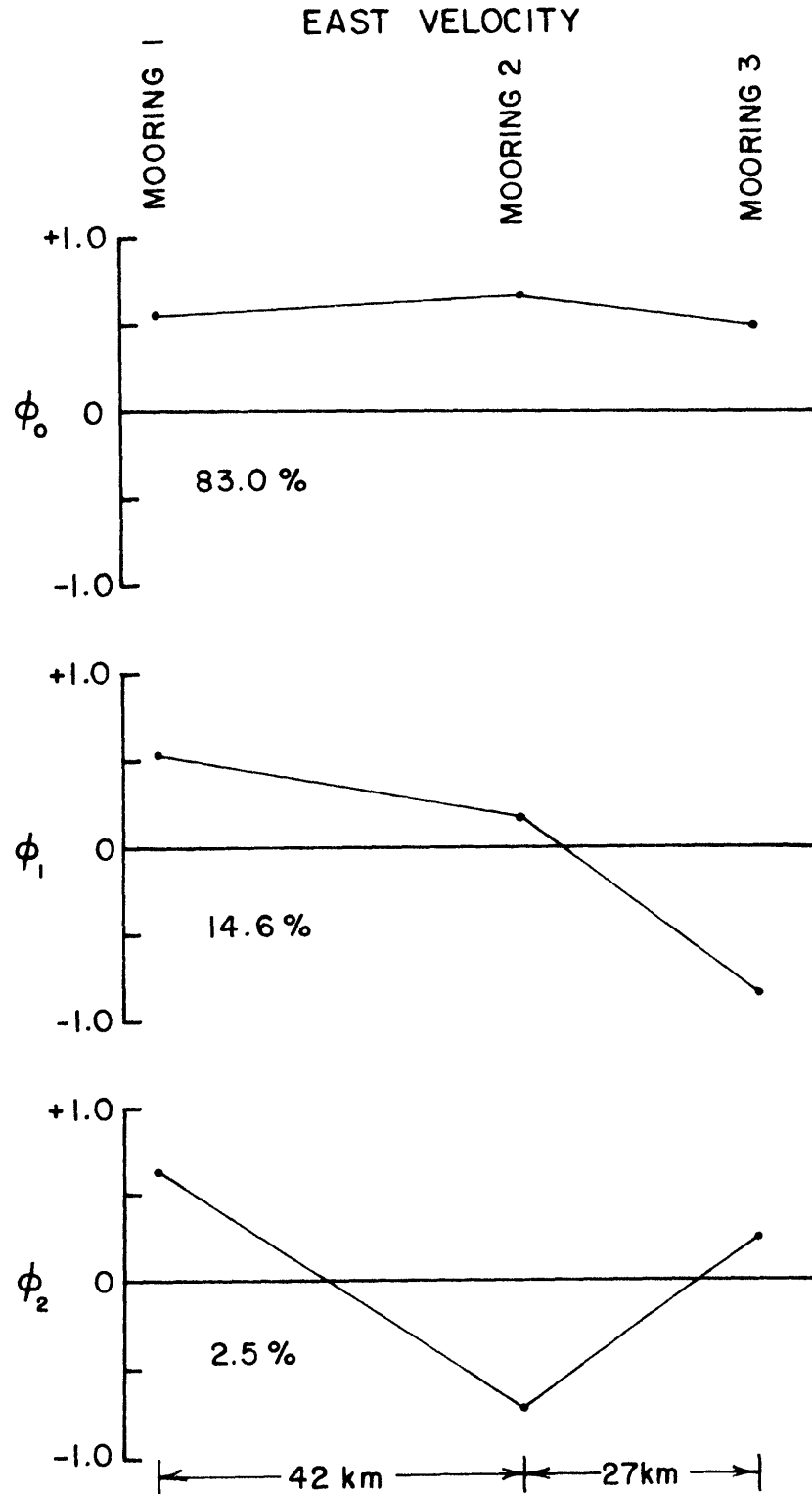


Figure 2.11 Cross-shelf eigenvectors and percentages of total variance in each mode from the empirical orthogonal modal analysis of the eastward components at a nominal depth of 30 meters.

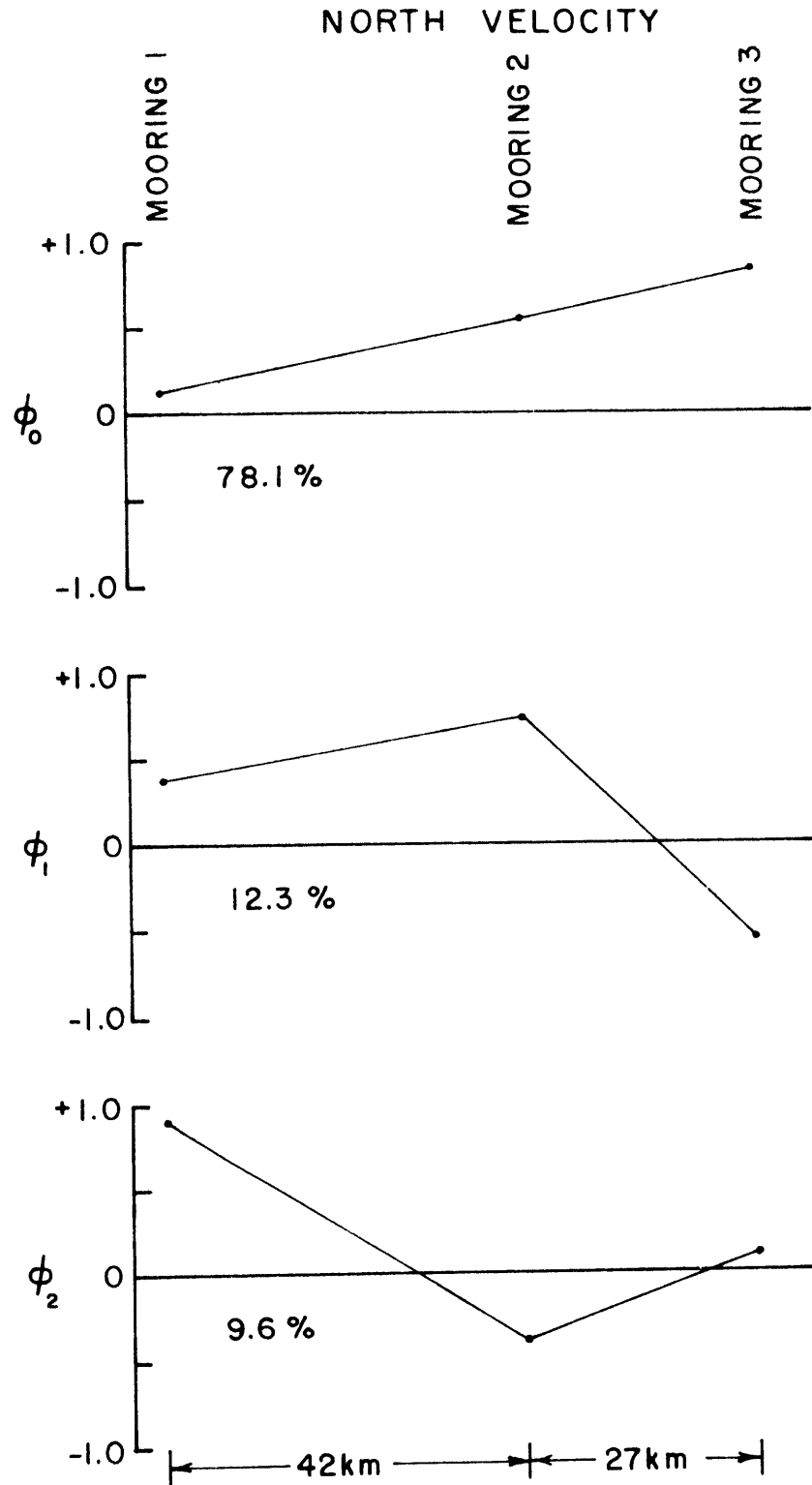


Figure 2.12 Cross-shelf eigenvectors and percentages of the total variance in each mode from the empirical orthogonal modal analysis of the northward components at a nominal depth of 30 meters.

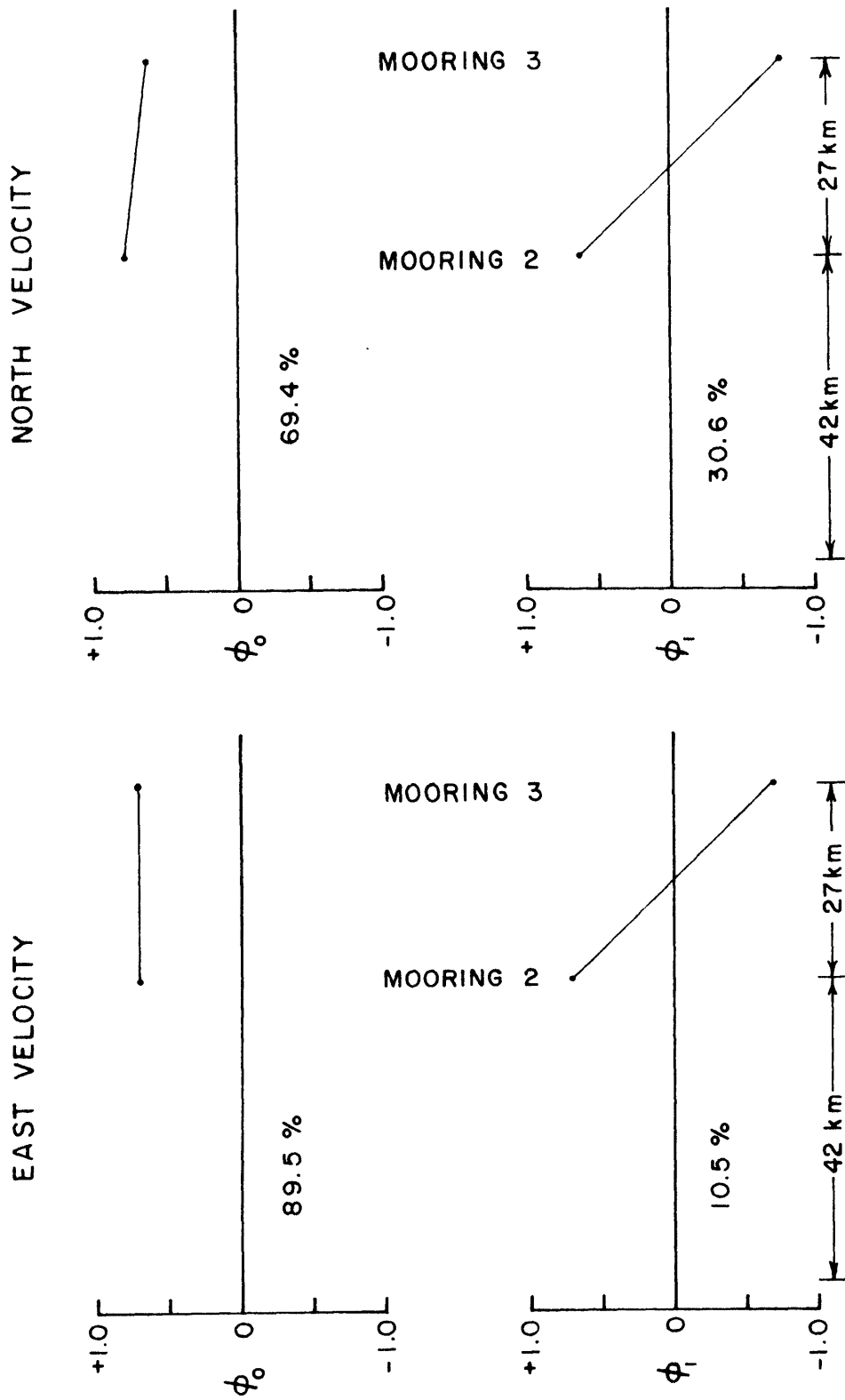


Figure 2.13 Cross-shelf eigenvectors and percentages of the total variance in each mode from the empirical orthogonal modal analysis of the east and north currents at a nominal depth of 70 meters.

and cross-shelf eigenvectors. For east (alongshore) currents the zeroth vertical mode contains by far the major portion of variance, almost 90% or better, with the relative amount increasing toward shore slightly. Thus the water column predominantly moves east-west as a unit with the near surface currents being somewhat larger. The cross-shelf modes for the eastward currents also show a predominance of energy in the zeroth cross-shelf mode with 83-90% of the variance. Figure 2.11 for the zeroth mode indicates that mooring 2 has slightly higher velocities in agreement with the cross-shelf low frequency energy distribution mentioned earlier. The results are much different for the northward, nearly on-shore component where for moorings 1 and 2 about 60% of the variance is contained in the first mode as compared to 30% in the zeroth vertical mode. Thus, there is a tendency for offshore flow near the surface to be accompanied by onshore motion along the bottom. The cross-shelf structure of the northward current is predominantly zeroth mode with about 70% of the variance with the implication that the on-offshore movement tends to be a coherent function of depth. That the vertical structure of the north current at mooring 3 is mostly zeroth mode is because instruments 31, 32, and 33 are generally above the shelf-slope front and act together with the upper currents at mid-shelf. The cross-shelf modal structure indicates that the largest on-offshore coherent currents are at moorings 2 and 3.

Some preliminary dynamical observations can be drawn from the EOM analysis. The east-west alongshelf flow tends to be very coherent both in the vertical and across shelf. When plots of zeroth modal amplitudes for the east components are compared with the wind stress of Figure 2.14, the currents are visually highly coherent with the eastward wind stress

with little or no discernable phase lag. The on-offshore flow is mainly concentrated in the first mode and this is too highly coherent with the eastward stress. This picture is again consistent with coastal boundary layer dynamics.

2.3 The Relationships Between Wind Stress, Sub-Surface Pressure Gradients, and Low Frequency Currents

2.3.1 Wind Stress

The time series of the wind stress for the March 1974 experiment determined from the 6 hourly mesoscale weather maps is shown in Figure 2.14. For the period of the experiment, from February 27 to April 4, 1974, the average wind velocity was 5.8 kts (301 cm/sec) directed toward 92°T and the average wind stress vector, computed using the quadratic drag law with $C_D = 1.22 \times 10^{-3}$, was 0.62 dynes/cm^2 directed toward 98°T . The average magnitudes of the wind velocity and wind stress were respectively 16.5 kts (848 cm/sec) and 1.62 dynes/cm^2 . Thus, the average magnitude of the stress is on the order of three times the vector averaged stress. A study of the mesoscale charts indicates that the higher average magnitude will very often come from one quadrant for 24 to 48 hours at a time. During major storms the wind speeds reached 40 to 50 kts corresponding to wind stresses of 8 to 12 dynes/cm^2 . These stresses are an order of magnitude greater than the means calculated above and one clearly expects them to have a large effect on transport of shelf water.

The storms which occurred during the March 1974 experiment were typical in their general character of the types of storms that take place during the winter along the New England coast and their evolution is important in understanding the currents during the period. If storms can be generalized, there seem to be two dominant types of winter storms. The first type involves the generation of a low in the great plains and mid-west which then intensifies and moves northeastward through the St. Lawrence river valley. These storms with their associated cyclonic wind

74NESWSTRS

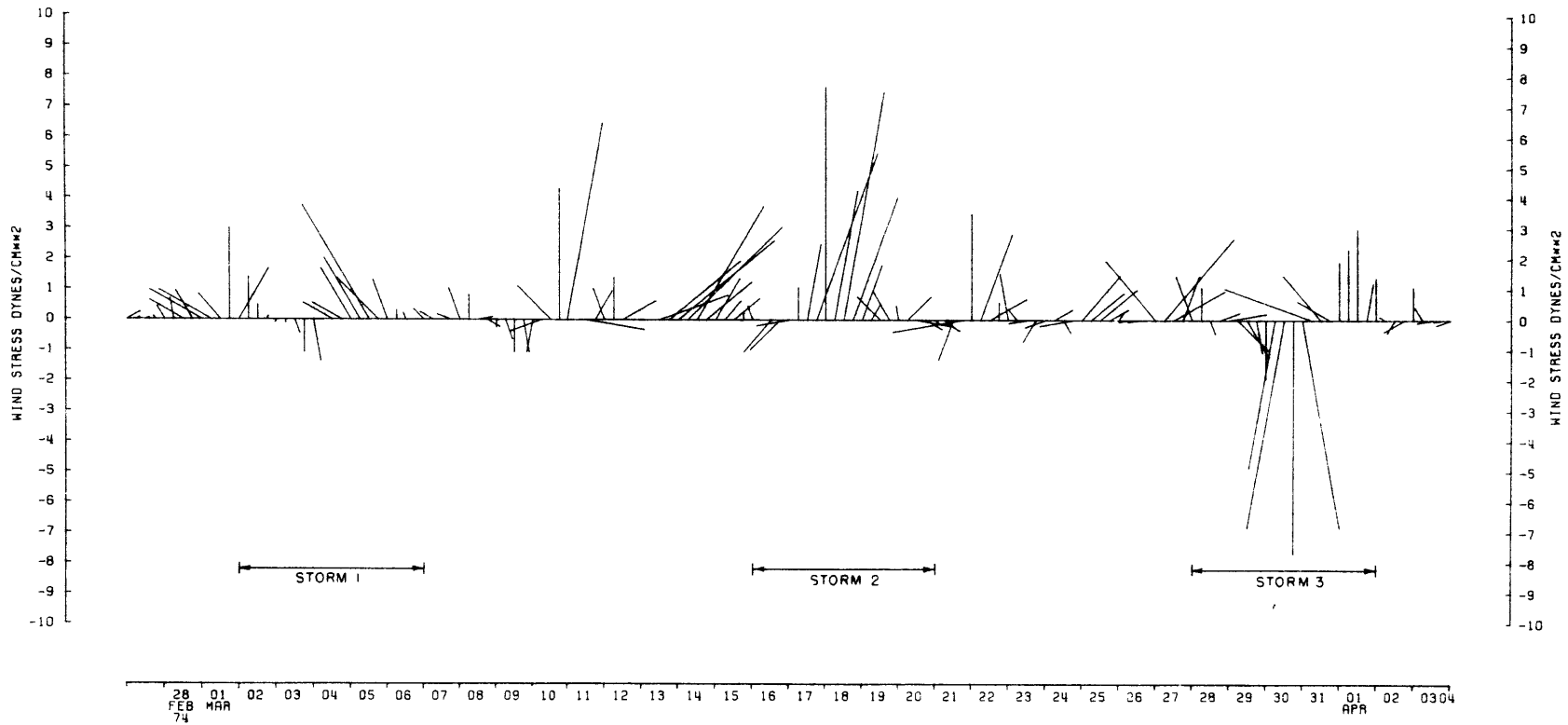


Figure 2.14 Vector plot of the quadratic wind stress during the March 1974 experiment computed using a drag coefficient of 1.22×10^{-3} . Eastward stress is upward and northward is toward the left.

patterns generate a strong flow of air from the west and southwest over the New England shelf. In addition, the wind stress vector rotates clockwise as the storm moves by. The storms marked 1 and 2 in Figure 2.14 are of this general type. The second kind of storm generally originates over the southeastern United States and moves northeastward leaving the coast in the vicinity of Cape Hatteras. The centers of these storms tend to pass south of the New England shelf, thus the winds are from the southeast and east and there is a counter clockwise rotation of the wind stress vector. The third major storm during the March 1974 experiment was more or less of this general type.

Figure 2.15 is the spectrum of the wind stress series for the March 1974 experiment. Since wind speed and direction were subjectively determined from the mesoscale weather maps the error bars may be somewhat larger than normal. The spectrum shows a peak in the wind stress at periods of ~ 3.6 days and another much smaller peak at the diurnal period. The decrease in wind stress energy at longer periods is consistent with the composite wind velocity spectrum from buoy measurements given by Millard (1971). Of major interest with regard to the stress spectrum is its striking similarity to the spectra of horizontal currents at mooring 3 and for instrument 23 (see Figures 2.3 and 2.4). That these instruments might be expected to be influenced by shelf/slope frontal motions implies a connection between the wind and the front.

The high visual correlation between the wind stress record and the low frequency currents and the similarity in the low frequency portions of the wind stress and current spectra indicate that the wind stress is the greatest single source of momentum for the variable currents. To increase our understanding of the structure of the wind/current inter-

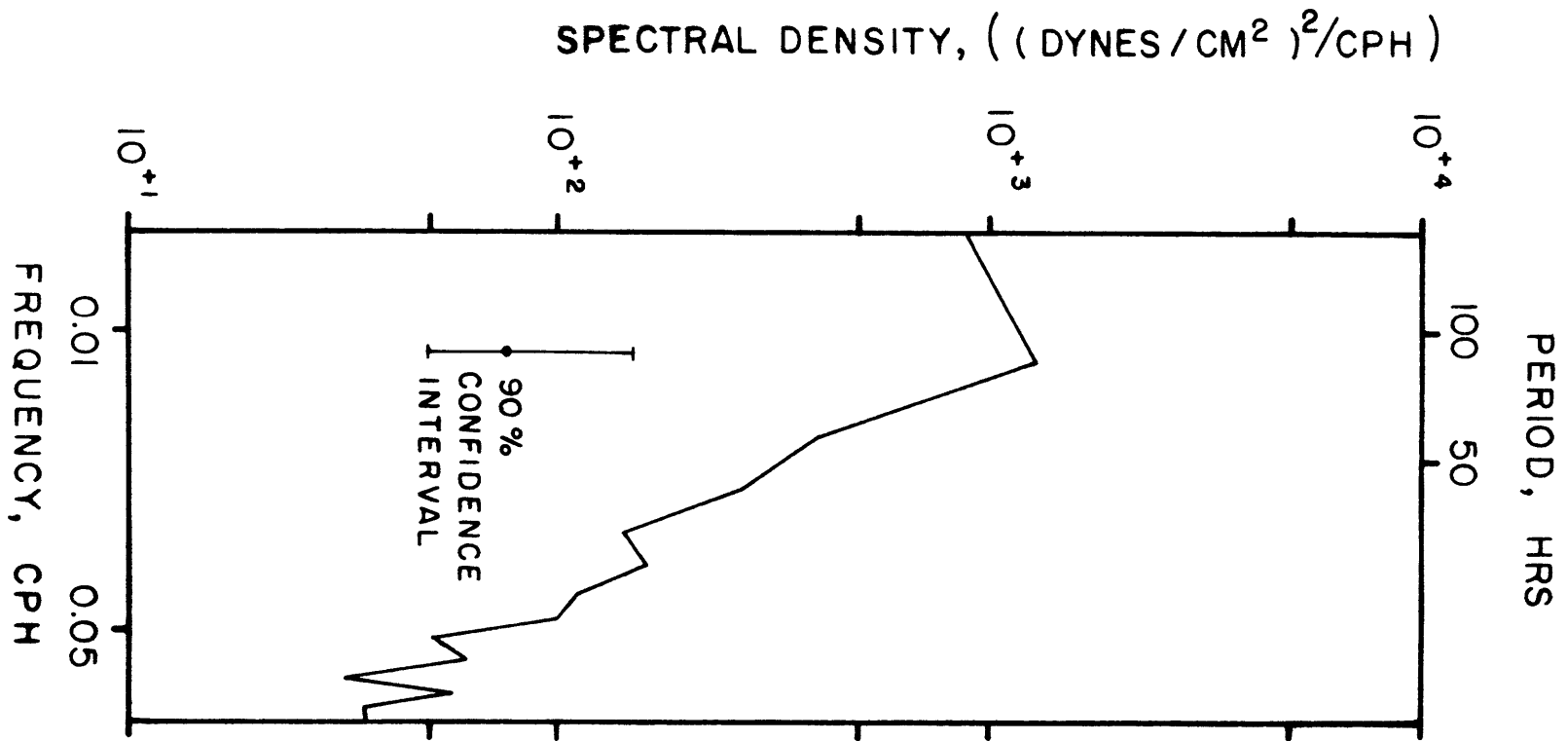


Figure 2.15 Auto spectrum of the east and north wind stress components from the March 1974 experiment. The spectrum was computed with 72 estimates averaged over 5 adjacent frequency bands.

action we examine the coherence and phase relationships. Table 2.4 gives the coherence and phases for the four lowest frequency bands between the east and north components of stress and the east and north currents. For periods centered at 2, 3, and 6 days, each estimate has approximately 5 degrees of freedom with a 95% significance level for non-zero coherence of 0.72. For the lowest band for periods greater than 12 days there are approximately 3 degrees of freedom with a 95% significance level of 0.88. Those estimates significantly non-zero by these standards are underlined in Table 2.4.

Although the coherence levels are not all significant in the lowest band, a consistent relationship between eastward stress and eastward current is evident on moorings 1 and 2. In this band the eastward current is nearly in phase as one would expect, with perhaps current leading the stress by a small amount. The north currents at 25 to 30 meters are approximately 180° out of phase while those at 60 meters on mooring 2 are in phase yielding a cross-shelf circulation consistent with coastal dynamics. On mooring 3 the lowest frequency coherences are not significant except for north at 31 which is $\sim 180^\circ$ out of phase in agreement with instruments 11 and 21.

For the shorter periods of 2 to 6 days, the level of coherence with eastward stress is generally higher with a particular exception being the north-south current at 11. The phases are generally consistent with alongshore current lagging behind alongshore stress by 2 to 6 hours at all depths. The on-offshore currents exhibit the same cross-shelf circulation pattern noted before and generally, but not always, lag the wind by a few hours.

The general level of coherence between the north component of the

TABLE 2.4

EASTWARD WIND STRESS

PERIODS (hrs)	288 - ∞	144	72	48
Instr/Direct				
11 EAST	0.82 4°	<u>0.87</u> -14°	0.67 -24°	<u>0.82</u> -14°
NORTH	<u>0.92</u> -121°	0.20 -118°	0.08 -45°	0.54 -74°
21 EAST	0.72 7°	0.68 -8°	<u>0.79</u> -28°	0.63 -3°
NORTH	<u>0.98</u> 151°	0.62 165°	0.69 162°	0.56 180°
23 EAST	0.54 4°	<u>0.74</u> -4°	<u>0.78</u> -24°	<u>0.94</u> -15°
NORTH	0.79 -4°	<u>0.77</u> 32°	<u>0.83</u> 6°	<u>0.88</u> -24°
31 EAST	0.28 -62°	0.57 22°	0.67 5°	0.54 44°
NORTH	<u>0.96</u> -156°	<u>0.84</u> 178°	0.69 149°	0.62 167°
33 EAST	0.67 -66°	0.58 -39°	<u>0.73</u> -12°	0.63 -3°
NORTH	0.36 -87°	0.70 131°	0.46 43°	0.62 17

NORTHWARD WIND STRESS

PERIODS (hrs)	288 - ∞	144	72	48
Instr/Direct				
11 EAST	0.20 46°	0.42 -130°	0.39 -121°	0.43 -155°
NORTH	0.53 25°	0.52 175°	0.35 -41°	<u>0.75</u> 131°
21 EAST	0.35 32°	0.38 -131°	0.41 -152°	0.29 -99°
NORTH	0.38 -47°	0.45 90°	0.61 -21°	0.51 20°
23 EAST	0.56 38°	0.43 -103°	0.58 -162°	<u>0.72</u> -155°
NORTH	0.81 152°	0.63 -87°	0.59 -151°	0.71 -174°
31 EAST	<u>0.88</u> 40°	0.48 94°	0.52 -101°	0.59 -70°
NORTH	0.36 70°	0.46 62°	<u>0.77</u> -24°	<u>0.73</u> -1°
33 EAST	0.76 60°	0.43 -140°	0.50 -143°	0.67 -127°
NORTH	<u>0.95</u> 144°	0.56 16°	0.23 -71°	<u>0.82</u> -144°

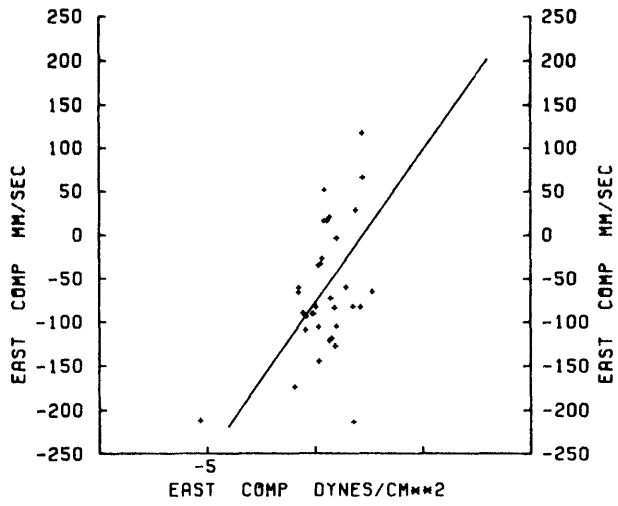
Table 2.4 Coherence and phase between eastward and northward wind stress and east and north currents at the four lowest frequency bands. Those coherences significantly non-zero at the 95% confidence level are underlined. Positive phase angles correspond to currents leading wind stress.

wind stress and the currents is less than for the east component although the level of coherence rises for shorter periods. The expected pattern of northward flow at the surface and southward flow below for a northward stress seems to hold at moorings 2 and 3 at 2 day periods but is not visible at longer periods. The relation of north stress with alongshore currents is less evident although there is a suggestion of northward stress being associated with westward current. This seems likely to be the result of the negative correlation between east and north stress and the greater effectiveness of the east stress in driving the currents.

A somewhat clearer presentation of some of these same results can be obtained by examining scatterplots of one day averaged wind stress components versus one day averaged currents. Figures 2.16a, b, and c show the scatterplots of τ_E versus u , τ_N versus v , and τ_E versus v for instruments 21, 22, and 23 respectively. The lines through the points are linear regressions for current regressed onto the stress. The general behavior illustrated by these figures and the amount of data scatter are representative of the data from moorings 1 and 3 as well. Ignoring for the moment the quality of the curve fit, the behavior with depth of the slope of the lines presents a picture consistent with frictional coastal boundary layer dynamics. Eastward wind stress is positively correlated with eastward current at all depths. Northward wind stress is correlated with northward current at 25 m, is almost independent of current at mid-depth, and is correlated with southward currents near the bottom. This is a clear picture of wind setup and setdown against a coast. The correlation of eastward (alongshore) wind stress with northward (onshore) current shows the upwelling type circulation noted before

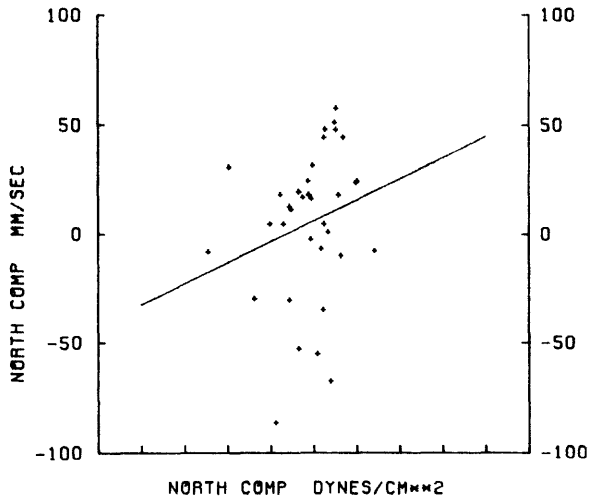
X AXIS
74NESWSTRS1D

Y AXIS
74NES21A1D



X AXIS
74NESWSTRS1D

Y AXIS
74NES21A1D



X AXIS
74NESWSTRS1D

Y AXIS
74NES21A1D

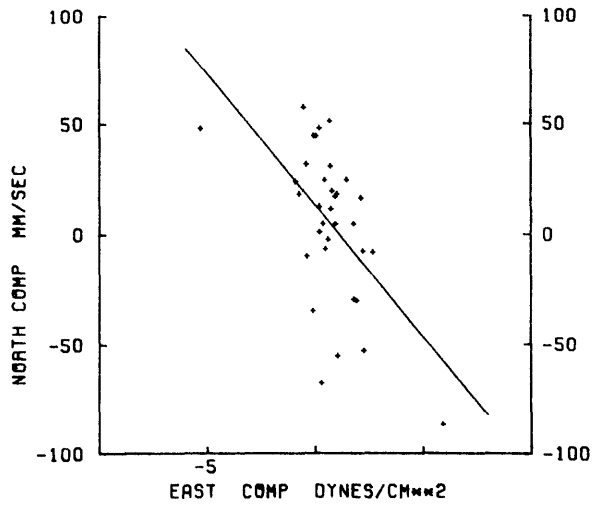
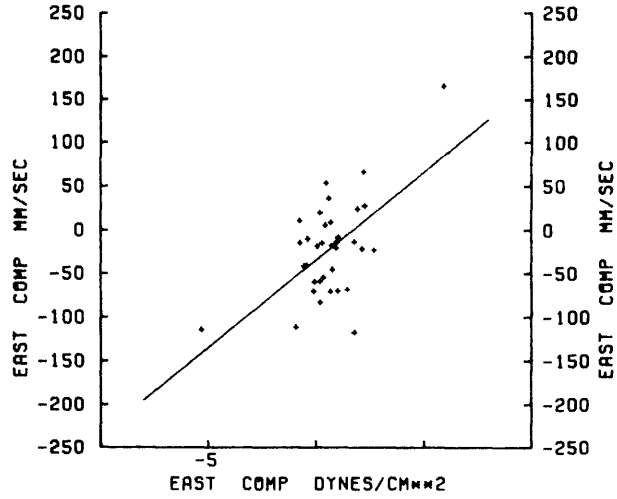


Figure 2.16a Scatter plots of daily averaged wind stress versus daily averaged currents at mooring 2. Lines are linear regressions of current regressed onto wind stress.

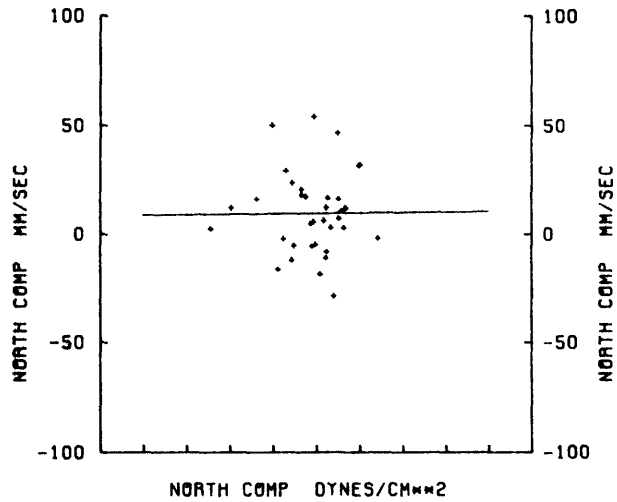
X AXIS
74NESWSTRS1D

Y AXIS
74NES22A1D



X AXIS
74NESWSTRS1D

Y AXIS
74NES22A1D



X AXIS
74NESWSTRS1D

Y AXIS
74NES22A1D

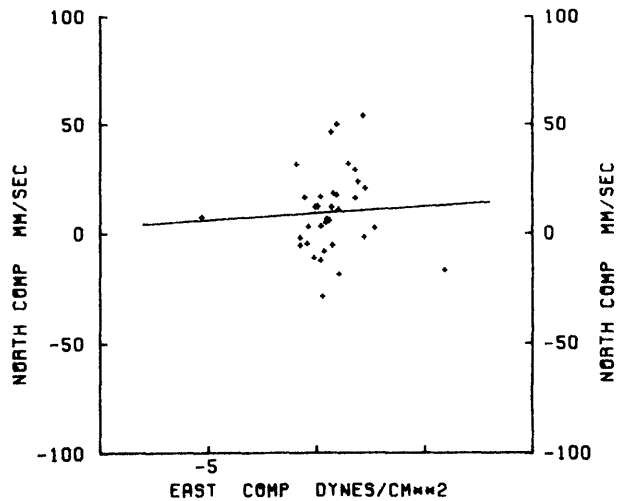
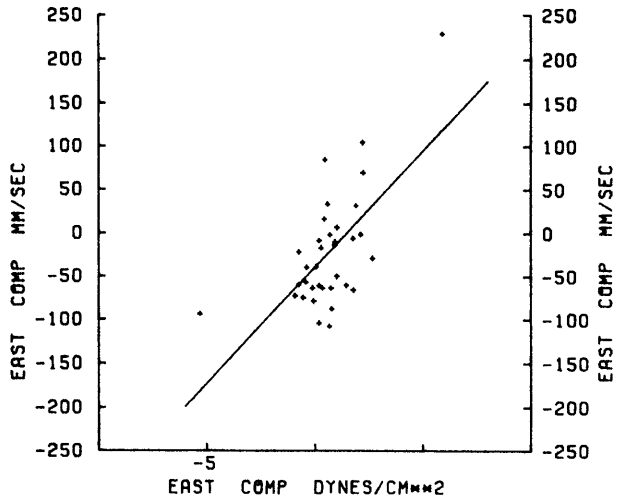


Figure 2.16b

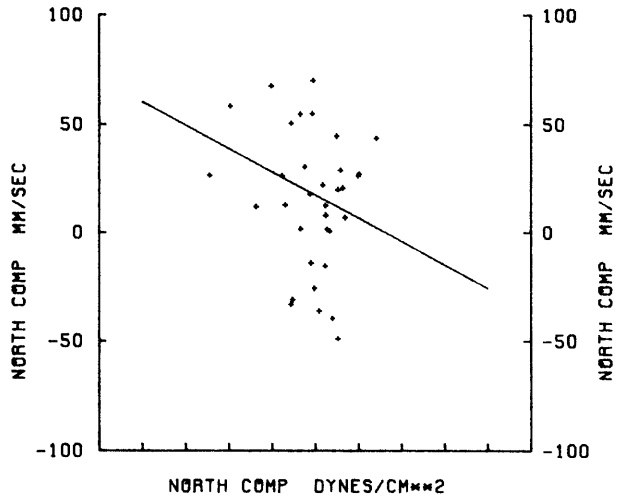
X AXIS
74NESWSTRS1D

Y AXIS
74NES23A1D



X AXIS
74NESWSTRS1D

Y AXIS
74NES23A1D



X AXIS
74NESWSTRS1D

Y AXIS
74NES23A1D

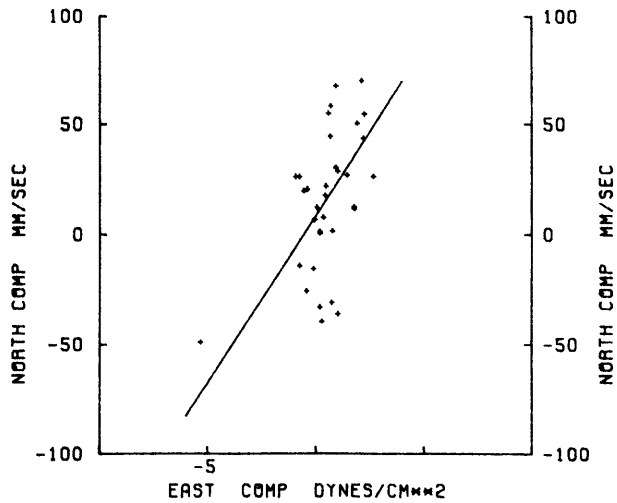


Figure 2.16c

with a component of the surface flow to the right of the wind progressing with depth to a return flow in the opposite direction near bottom.

The scatter of points about the regression lines is large with the slope of the line mainly determined by a few extreme points. That currents during low wind stress periods are randomly distributed is what one should expect in the presence of phase differences between wind and currents, of other types of forcing, and of possible free or forced inertio/topographic waves on the shelf. With the possible sources of error, the scatterplots show a surprisingly unified description of the forced wind response of the shelf currents.

2.3.2 Sub-Surface Pressure Gradients

Beardsley et. al. (1977) have shown that during the March 1974 experiment the rms amplitude of the variable portion of the alongshore sea surface slope is 3 to 4 times larger than mean alongshore slopes deduced by Stommel and Leetmaa (1972) or measured by Scott and Csanady (1976). The rms amplitude of the cross-shelf gradients was 5 to 8 times the rms alongshore gradients, primarily due to the great amplitude reduction of the sub-surface pressure (SSP) fluctuations toward the shelf break. The variable portion of the cross-shelf SSP gradient decreases to about 1/10th its value on the shelf out past the shelf break. The eastward (alongshore) component of the wind stress seems to be the primary cause of low frequency SSP fluctuations on the shelf as it is significantly correlated at all low frequency coherence estimates. However, SSP gradients may have a greater significance than as simply the passive manifestation of wind stress events since pressure gradients would be the probable mechanism for ocean/shelf interaction.

Bottom pressure was measured during the March 1974 experiment at moorings 2 and 3 by bottom mounted pressure gauges with the intention of calculating the cross-shelf SSP gradient fluctuations. Unfortunately, the instrument at mooring 3 drifted making this difference calculation impossible. The SSP fluctuations observed at mooring 3 were sufficiently small in comparison to those at mooring 2 that we can assume that the local SSP gradient near 2 is proportional to the SSP signal at 2. Calculating the gradient between a shore station and mooring 2 is not possible because of the very evident effects of coastal topography upon near shore SSP data. With the measurements available it is not possible to directly measure the SSP gradients in the alongshore direction on the shelf

itself. However, we might expect them to be 1/3 to 1/10th the value of the cross-shelf gradients.

A detailed description of the energy distribution of the SSP fluctuations is contained in Beardsley et al. (1977). Figure 2.17 shows the low passed SSP record from mooring 2 and Figure 2.18 is the spectrum of this record. The visual correlation between the pressure record and the wind and current records is quite high and the spectrum is also very similar at the low frequencies to the wind stress spectrum and those current records near the shelf/slope front. The coherence and phase relationships between the SSP at mooring 2 and the currents is shown in Table 2.5. Again the 95% confidence levels for non-zero coherence is 0.88 at the lowest frequency estimate and 0.75 for the rest. Those estimates that are significant by these criteria are underlined in the table. Generally, eastward currents seem to be more coherent with the pressure than northward currents except at the lowest frequency for moorings 1 and 2. For periods longer than 13.5 days only eastward currents at mooring 3 were significantly coherent. At the higher frequencies westward currents at nominal 30 m depth lead the SSP at mooring 3 by approximately 5 hours progressing to lagging by approximately 1 hour at mooring 1. At depths of 60 to 70 m westward currents lag the SSP by generally 4 to 5 hours. Evidence about the northward currents shows no consistent pattern although there is significant coherence between southward flow and SSP at instrument 23. At moorings 2 and 3 the behavior of the eastward currents is consistent with an initially wind driven alongshore surface current which veers to the right, either setting up or down the sea surface a quarter to one half inertial period later which in turn initiates a geostrophically balanced interior flow.

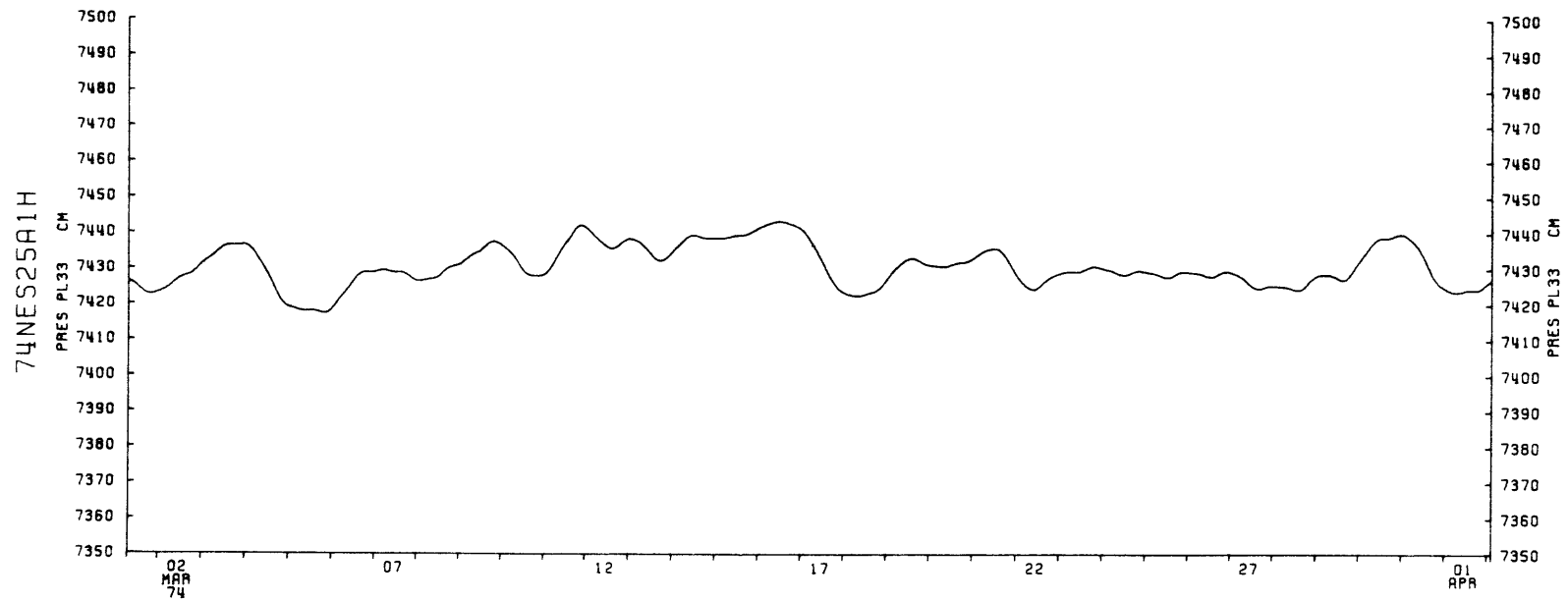


Figure 2.17 Low passed bottom pressure from mooring 2 of the March 1974 experiment.

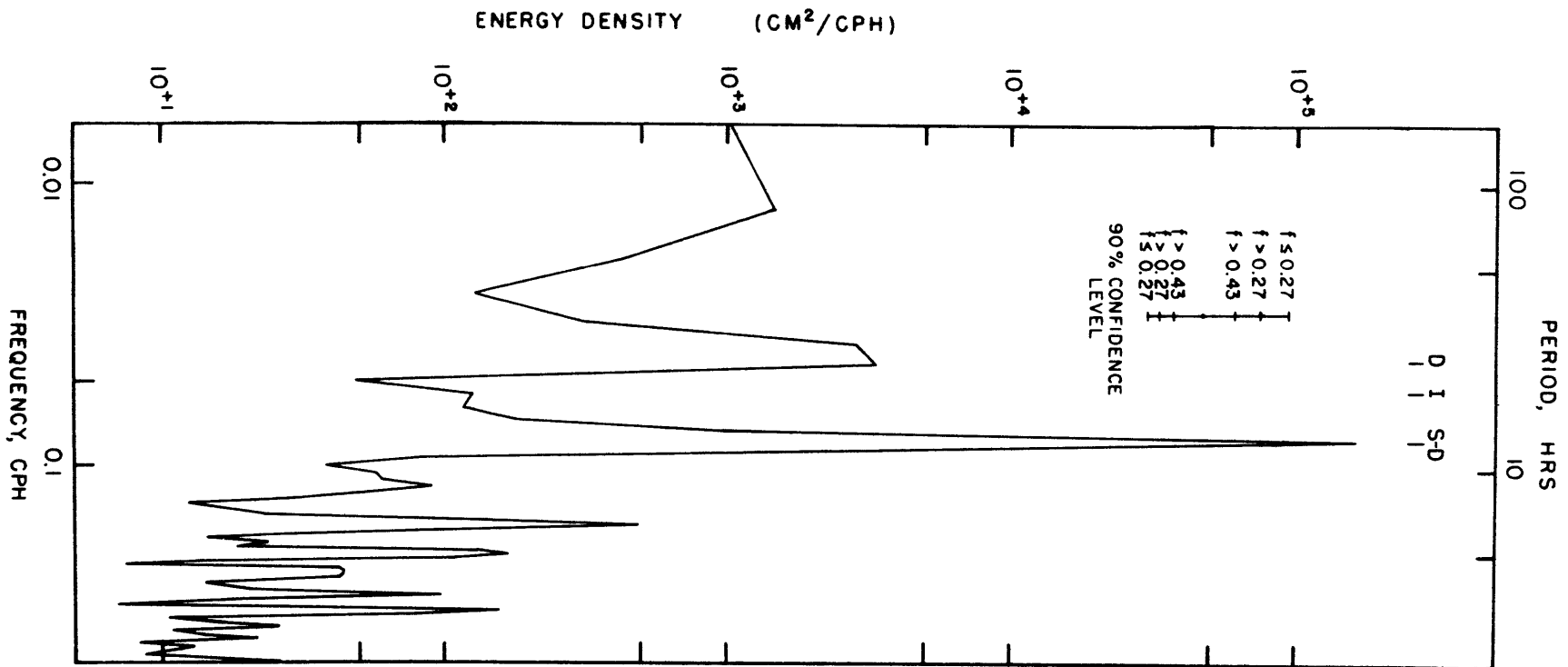


Figure 2.18 Auto spectrum of bottom pressure at mooring 2 from the March 1974 experiment. The spectrum was computed with 405 estimates averaged over 5 adjacent frequency bands.

TABLE 2.5

BOTTOM PRESSURE AT MOORING 2

PERIODS (hrs)	324 - ∞	162	81	54
Instr/Direct				
11 EAST	0.24 -83°	<u>0.85</u> -175°	<u>0.89</u> 162°	<u>0.87</u> 166°
NORTH	0.86 -159°	0.39 90°	0.12 -70°	0.52 97°
21 EAST	0.32 -89°	<u>0.84</u> -172°	<u>0.81</u> 180°	<u>0.74</u> -174°
NORTH	0.57 -125°	0.62 15°	0.70 -31°	0.40 -82°
23 EAST	0.36 -101°	<u>0.86</u> -163°	<u>0.87</u> 167°	<u>0.84</u> 150°
NORTH	0.82 -48°	<u>0.86</u> -146°	<u>0.81</u> -159°	<u>0.72</u> 161°
31 EAST	0.90 -128°	0.70 -166°	<u>0.88</u> -161°	0.67 -149°
NORTH	0.27 177°	<u>0.82</u> 13°	0.66 -21°	0.53 -69°
33 EAST	<u>0.95</u> -110°	<u>0.82</u> 163°	<u>0.88</u> 170°	<u>0.92</u> 168°
NORTH	0.69 -36°	<u>0.77</u> -36°	0.66 -122°	<u>0.83</u> 175°

Table 2.5 Coherence and phase between bottom pressure at mooring 2 and east and north currents at the four lowest frequency bands. Those coherences significantly non-zero at the 95% confidence level are underlined. Positive phase angles correspond to currents leading bottom pressure.

2.4 Dynamical and Statistical Models of the Shelf Currents

2.4.1 Mean Currents

It is of primary interest to compare the mean flows observed with the dynamical model of the mean continental shelf circulation proposed by Csanady (1976). First we will examine some of the basic assumptions of the model, then look at a qualitative comparison of the predicted and observed behavior, and finally see whether values for some important dynamical parameters may be obtained. The model equations are the steady state, linear, frictional momentum equations:

$$-fv = -g(\zeta + D)_x + A_z u_{zz},$$

and

$$fu = -g(\zeta + D)_y + A_z v_{zz},$$

2.1

where v is alongshore to the east, u is offshore, ζ is the surface elevation, A_z is the vertical eddy diffusivity, and D is the dynamic height given by:

$$D = \int_z^0 \frac{\rho - \rho_0}{\rho_0} dz.$$

It is assumed that the shelf is straight and uniform in cross section so that all gradients in the alongshore direction are zero except for ζ_y . Because the model is meant to duplicate winter shelf conditions the density is taken only as a function of x , the offshore direction, so that

$$D_y \equiv 0 \quad \text{and} \quad D_x = -z/L, \quad 2.2$$

where $L \equiv \rho_0 / (\partial \rho / \partial x)$ and is the appropriate density length scale. The boundary conditions are:

$$A_z \frac{\partial u}{\partial z} = \frac{T^x}{\rho} \quad ; \quad A_z \frac{\partial v}{\partial z} = \frac{T^y}{\rho} \quad \text{at } z=0$$

and

2.3

$$A_z \frac{\partial u}{\partial z} = r u \quad ; \quad A_z \frac{\partial v}{\partial z} = r v \quad \text{at } z=-h.$$

A simplified condition is put on the oceanic open boundary such that the net onshore transport is zero and the transport along an isobath is constant, i.e.,

$$\int_{-h}^0 u \, dz = 0, \quad \text{and} \quad \int_{-h}^0 v \, dz = -V(x). \quad 2.4$$

An important assumption which makes this model less complex mathematically than that of Stommel and Leetmaa (1972) is that the salt balance is decoupled from the mean flow. The decoupling depends primarily upon the condition that

$$\int_{-h}^0 \bar{u} \bar{S} \, dz \ll \int_{-h}^0 \overline{u' S'} \, dz.$$

This inequality will hold if the mean salinity is constant with depth and the vertical integral of the onshore velocity is zero for some suitable orientation of the coordinate system. However, the March 1974 experiment showed that there was approximately a 0.5% increase in salinity from a depth of 25 m to the bottom at mooring 2, away from direct influence of the shelf/slope front. An order of magnitude estimate of the salt transport by the mean using the appropriate cross-shelf model velocities and the observed mean salinities gives a flux of $0.2 \text{ gm cm}^{-1} \text{ sec}^{-1}$ toward shore. This says that the ratio of the two

integrals is one half, which taking into account the extremely crude estimations, means that the two terms may be actually of the same order.

Another important approximation is that the means of the advective terms are negligible in comparison to the means of the other terms. Because shelf motion is coherent across the shelf it is possible to approximate the advective terms $\frac{\partial(uv)}{\partial x}$ and $\frac{\partial(u^2)}{\partial x}$ by finite differences. The first part of Table 2.6 shows ratios of the mean advective terms to the mean Coriolis terms using velocity measurements at nearly equal depths on the three moorings. It is apparent that over the outer half of the shelf the advective terms are small but proportionally larger in the alongshore momentum balance. The advective terms appear to be important on the inner half of the shelf. An estimate of the role of the other horizontal advective terms, $\frac{\partial(v^2)}{\partial y}$ and $\frac{\partial(uv)}{\partial y}$, is possible by estimating the alongshore scale length required to make these terms, say 10%, of the Coriolis term and compare this length with the known characteristics of the shelf. These distances are all, except for 11, less than half the shelf width so that it seems likely that the alongshore advective terms are at least as small as the cross-shelf terms. The length scale for 11 for the alongshore velocity is large because of the small mean cross-shelf flow and how representative this is considering the error bars of the means from Table 2.1 is unknown.

The approximation that the alongshelf change in density can be neglected is probably justified as Bigelow (1973) indicates there is less than 2°C systematic difference between the waters off Nantucket and those off New Jersey. That density is independent of the vertical is a less well justified assumption. An idealized concept of the winter shelf hydrography progresses from vertically homogeneous near shore to the

TABLE 2.6

INSTRUMENTS	AVERAGE DEPTH (m)	DISTANCE APART (km)	$\frac{\overline{\partial(uv)}}{\partial x}$	$\overline{\frac{\partial(u^2)}{\partial x}}$
			\overline{fu}	\overline{fv}
11 - 21	25	42	2.876	0.866
21 - 31	27	27	0.025	0.004
23 - 33	66	27	0.049	0.008

INSTRUMENT	DEPTH (m)	$L_{0.1} =$	$\frac{10 \cdot \overline{v^2}}{\overline{fu}}$	$\frac{10 \cdot \overline{vu}}{\overline{fv}}$
11	27		340 km	2 km
21	24		31	37
23	62		64	15
31	30		18	18
33	70		24	2

Table 2.6 Estimates of the relative importance of the advective terms in the 35 day long averaged momentum equations. x is directed offshore and y alongshore toward the west. The lower box is an estimate of the length scale to make the alongshore advective terms one tenth of the Coriolis term.

offshore sloping interface of the shelf/slope front. Thus isopycnals start out vertical and slope increasingly as the shelf edge is approached. A better approximation of the dynamic height gradient then is of the form

$$D_x = \frac{1}{\rho_0} \left\{ -\overline{\frac{\partial \rho}{\partial x}} z - \frac{1}{2} \overline{\frac{\partial^2 \rho}{\partial x \partial z}} z^2 \right\}. \quad 2.5$$

Using mean temperature data recorded at the three moorings and taking advantage of the tight and nearly linear T-S correlation, estimates for these gradient terms are

$$\overline{\frac{\partial \rho}{\partial x}} = 3.8 \times 10^{-11} \text{ gm cm}^{-4},$$

and

$$\overline{\frac{\partial^2 \rho}{\partial x \partial z}} = -6.3 \times 10^{-15} \text{ gm cm}^{-5}.$$

The effect then is for the density scale length to decrease with depth so that at 100 meters it is $\sim 1/2$ that at the surface. The effect is to increase the geostrophically balanced shear, by a factor of two at 100 meters.

Csanady uses a linear bottom drag in his mean circulation model. To test whether this linearization is valid on the shelf, we compared the directional difference between the low passed bottom current and the low passed quadratic drag law stress based upon the bottom current. Kundu's (1975) method was used to measure the mean veering between two vector series, giving for the mean angular difference

$$\phi = \tan^{-1} \left\{ \frac{(\tau_1^x \tau_2^y - \tau_2^x \tau_1^y)}{(\tau_1^x \tau_2^x + \tau_1^y \tau_2^y)} \right\},$$

where $\underline{\tau}_1 \propto \mathcal{I}(|\underline{u}_b| u_b)$ and $\underline{\tau}_2 \propto \mathcal{I}(\underline{u}_b)$ and the linear operator

is the low pass filter. The correlation between the two vector series is given by

$$\rho = \frac{\left(\overline{(\tau_1^x \tau_2^x + \tau_1^y \tau_2^y)^2} + \overline{(\tau_1^x \tau_2^y - \tau_2^x \tau_1^y)^2} \right)^{1/2}}{\left(\overline{\tau_1^{x^2} + \tau_1^{y^2}} \right)^{1/2} + \left(\overline{\tau_2^{x^2} + \tau_2^{y^2}} \right)^{1/2}}.$$

The method weights those angular differences occurring at times of high bottom stress, that is, at times of greatest momentum loss to the bottom. The results shown in Table 2.7 for the lowest current meter on each of the three moorings indicate that the angular differences are small, decreasing closer to the bottom, and that the correlations between the series are high. Clearly then, with the appropriate drag coefficients, linearizing the bottom drag is justified.

The final justification of the model lies in its ability to predict the important observed features of the shelf circulation. In this respect the model seems extremely good. Csanady's (1976) solution to equations (2.1) yields mean horizontal velocities given values for the eddy viscosity, A_z , the bottom friction coefficient, r , the cross-shelf density length scale, L , and the imposed alongshelf surface elevation gradient, ζ_y , as well as the mean wind stress and the water depth. The solution is basically local, related to the shelf geometry only through the requirement of no net onshore flow. The alongshore transport toward the west, V , is determined once the alongshelf pressure gradient is imposed.

Neglecting the vertical variation, the average density scale length, L , was $\sim 2.7 \times 10^{10}$ cm during the 1974 experiment. Csanady (1976) suggests a value for A_z of $115 \text{ cm}^2/\text{sec}$ based upon mean velocities which are almost three times the rms velocity observed at mid-shelf.

TABLE 2.7

INSTRUMENT	HEIGHT ABOVE BOTTOM (m)	ϕ	ρ
13	1.2	-0.41°	0.98
23	10.0	3.24°	0.97
35	1.2	-0.18°	0.93

Table 2.7 The average veering angle and correlation between the low passed quadratic bottom stress and the bottom currents at instruments 13, 23, and 35 using a method outlined by Kundu (1975).

Butman (1975) tried to determine values of A_z during periods of calm and storm at mid-shelf with the result that A_z ranged from 20 to 50 cm^2/sec during calm periods and 100 to 200 cm^2/sec during storm periods. Because of the importance of storms in imparting momentum to the water, the observation that the water tends to move as a vertical unit, and because the effects of a storm decay within a day or so, a relatively large value of A_z seems likely. Somewhat arbitrarily then, we assume a value for A_z of 110 cm^2/sec . During the fall of 1975 Scott and Csanady (1975) empirically determined the bottom stress coefficient, r , to be 0.16 cm/sec in the very near shore waters south of Long Island, N.Y. This seems to be a large value with an implied roughness length of ~ 2 cm for rms velocities of 20 cm/sec . We measured near bottom rms velocities $\sim 1/3$ these values and have taken $r = 0.08 \text{ cm sec}^{-1}$. It turns out that the mean flow is not particularly sensitive to the values of A_z and r for mid-shelf depths.

The surface elevation gradient, ζ_y , on the other hand has quite a large effect on the qualitative features of the model. In the surface layer if the gradient is small enough the mean eastward wind stress becomes relatively larger and drives the surface current eastward. In the middle of the water column the effect of decreasing ζ_y is to decrease the geographically balanced onshore flow and at the same time through a coupling with the cross-shelf gradient allow the vertical shear due to the dynamic height gradient to send the alongshore flow toward the east. The alongshore flow at the bottom is a balance between down pressure gradient flow and wind stress so that decreasing ζ_y tends toward an eastward bottom flow. The cross-shelf flow at the bottom is a slightly more complicated balance and includes integrated cross-shelf Coriolis force

and a down the dynamic height gradient flow. The effect of decreasing ζ_y is principally to decrease ζ_x to the point where the integrated Coriolis force and dynamic height gradient drive the bottom flow onshore. Scott and Csanady (1975) determined one month mean for ζ_y of 1.4×10^{-7} , a value which is of the same order as coastal leveling estimates (Emery and Uchupi, 1972). Since this was determined very near shore and because it may vary slowly with time we will try a range of ζ_y to compare with the observed behavior.

Table 2.8 lists the model velocities and cross-shelf elevation gradients for three values of ζ_y , 1.0, 1.4, and 2.0×10^{-7} , for depths corresponding to mooring locations 1 and 2 together with the observed flows and surface gradients. Our shallowest instruments were at 25 meters so that we have no comparison with the predicted surface currents. The model indicates that there is an offshore Ekman flow at the surface which is constant across the shelf while the alongshore flow increases by a factor of 1.5 to 3 toward the west. At mid-depth the model predicts a relatively slow onshore flow constant with cross-shelf position and a relatively slow onshore flow constant with cross-shelf position and an alongshore flow which increases by a factor of two between moorings 1 and 2. The observed alongshore flow would suggest that the correct value for ζ_y is slightly greater than 10^{-7} . The onshore flow at mid-depth for mooring 2 is close to and of the same sign as that predicted while at 1 the observed flow is small but offshore. Given the uncertainty in the "alongshore" orientation this is a minor discrepancy. The on-offshore flow at the bottom again suggests a value for ζ_y of slightly greater than 10^{-7} . The predicted westward flow at the bottom is much greater than that observed at mooring 2 while being

TABLE 2.8

	Depth = 58 m				Depth = 72 m			
	Model			Observed	Model			Observed
$\zeta_y \times 10^7$	1.00	1.40	2.00	0.74	1.00	1.40	2.00	1.05
$\zeta_x \times 10^7$	-0.86	-5.50	-12.44	-2.74	-4.26	-10.05	-18.73	-5.55
u_s	4.00	3.58	2.96	?	4.00	3.58	2.96	?
v_s	2.92	-1.92	-9.19	?	-0.63	-6.68	-15.76	?
$u_{1/2}$	-1.05	-1.46	-2.09	0.45	-1.05	-1.46	-2.09	-0.85
$v_{1/2}$	0.22	-4.62	-11.89	-2.10	-3.06	-9.12	-18.19	-3.05
u_b	-0.98	-0.23	0.89	-0.78	-0.36	0.63	2.12	0.48
v_b	0.32	-2.52	-6.79	-0.23	-1.39	-4.92	-10.22	-0.01

Table 2.8 Comparison between the observed mean currents and surface height gradients at moorings 1 and 2 with those predicted by the coastal boundary layer model of Csanady (1976) for several values of the along-shore surface height gradient, ζ_y .

about right at 1.

The "observed" gradients, ζ_x , ζ_y , were determined by using the depth integrated forms of equations 2.1 applied to mooring 1 and 2:

$$-fv = -g(\zeta_x + D'_x/H) + T^x/\rho H - ru_b/H,$$

and

$$fu = -g(\zeta_y + D'_y/H) + T^y/\rho H - rv_b/H,$$

where $D'_{x,y} = \int_{-H}^0 D_{x,y} dz$, and u , v are depth averaged velocities.

For the integrated dynamic height explicit account is taken of the non-uniform behavior of L with depth by integrating the full form of D given by (2.5). In addition the approximate orientation of ∇D relative to south and east is included. Estimates of u and v are relatively crude as there were no instruments near the surface. Bottom velocity measurements gave (u_b, v_b) and a value for r of 0.08 cm/sec was used to obtain bottom stress. Under these assumptions we then solved for ζ_x and ζ_y with the results shown in Table 2.8. The alongshore gradients, ζ_y , are less than observed by Scott and Csanady (1975) but of the same order. The cross-shelf gradients are close to predicted values and exhibit the characteristic increase in amplitude progressing offshore.

It is more than can be reasonably expected for so simple a model to duplicate nature in all details yet the results are amazingly accurate. Of more importance is that general features of the shelf circulation be correctly predicted by the model. Several features that the model predicts and which are observed are: 1) an increase in westward transport progressing offshore; 2) a return onshore flow at mid-depth; 3) a divergence of the bottom on-offshore flow; and 4) an

increase in the magnitude of the cross-shelf surface elevation gradient in the offshore direction. The model does not seem significantly affected by the inadequacies in modeling the salt flux and the cross-shelf density structure.

The model gives as an expression for the bottom depth at which the onshore bottom velocity goes to zero of:

$$h = \left(\frac{2A_E}{f} \right)^{1/2} + \frac{T^y}{\rho g h_y} + \frac{A_E}{f L h_y} .$$

This expression is most sensitive to the gradient ζ_y so that if we have an idea of what h might be we can look at the inverse problem of determining ζ_y . Interpolating between the onshore flow at mooring 1 and the offshore flow at 2 gives a value for h of 67 meter which in turn gives a value of 1.3×10^{-7} for ζ_y with our parameters. This is just a bit higher than that deduced from the current profiles. The net result is that the linear viscous model of the mean circulation seems to capture all the major features. It seems so accurate in a qualitative sense that inverting the problem using observed behavior to obtain values for crucial parameters is clearly indicated. Present efforts are directed toward this goal and results will be presented in the future.

An important element which has been somewhat glossed over is the existence of the alongshore surface height gradient, ζ_y , and its necessity in the model to drive the westward flow. There seems to be only three candidates which will either drive a westward flow or maintain the surface height gradient. The first is the freshwater runoff from shore yielding the offshore dynamic height gradient. The most

that this gradient can support is 2-3 cm/sec to the west and in addition would suggest that the greatest currents should occur along the edges of river plumes. This is not supported by observation. The second candidate is the mean wind stress which has its major component toward the east and which would support a setup. There are two arguments against this: 1) there does not seem to be a large enough barrier to the along-shore flow (Nantucket Shoals does not appear to be sufficient as it does not seem to effect the variable currents, thus, there is no reason to suppose that would effect the mean currents); and 2) the surface flow would be eastward contrary to the observed behavior. The most likely candidate seems to involve the dynamics of the near shore edge of the Gulf Stream. Oceanic models of the Gulf Stream (Stommel, 1966) show a decrease in surface elevation northward along the western edge of the Atlantic. However, if because of sidewall and bottom friction there were a nearshore ageostrophic region, the centripetal acceleration associated with the turning of the Gulf Stream might support an along-shore gradient of the type needed.

2.4.2 Dynamical/Statistical Shelf Models

The sum of the evidence on the structure of the shelf currents and the relationships between wind stress, sea surface gradients, and current overwhelmingly indicates that coastal boundary layer dynamics, at least qualitatively similar to those describing the mean flow, should also describe the low frequency currents. We can test the extent to which the steady state model can describe the low frequency currents by applying the depth dependent solution of equations (1) to the measured currents and forcing. The solutions for the horizontal velocities can be written in the form:

$$u = A + B \eta_x + C \eta_y + D T^x + E T^y,$$

and

$$v = A' + B' \eta_x + C' \eta_y + D' T^x + E' T^y,$$

where the coefficients are complicated functions of depth, the cross-shelf density length scale, L , and the friction parameters A_z and r . The absolute value of cross-shelf sea level gradient, ζ_x , is not known but an estimate can be obtained of the varying portion, ζ_x' , from the sub-surface pressure at mooring 2. The mean part of ζ_x can be absorbed into the constants A and A' . There is no direct measure of either the mean or the variable part of the alongshore gradient. However, it can be eliminated from the two equations leaving a single equation of the form:

$$u = a_1 + b_1 v + c_1 \eta_x' + d_1 T^x + e_1 T^y,$$

or alternatively:

$$v = a_2 + b_2 u + c_2 \eta_x' + d_2 T^x + e_2 T^y,$$

where: $a_2 = \frac{-a_1}{b_1}$, $b_2 = \frac{1}{b}$, $c_2 = \frac{-c_1}{b_1}$, $d_2 = \frac{-d_1}{b_1}$, and $e_2 = \frac{-e_1}{b_1}$.

For ζ'_x is substituted p' , the bottom pressure at mooring 2 with the pressure length scale incorporated in the c'_i 's. From the time series of low passed u , v , p' , τ^x , and τ^y , a least squares fit can determine the coefficients as an inverse problem.

The results of the fits are given in Table 2.9 together with the rms errors. The quality of the results can be judged on several levels. The rms errors are large and the percentage of variance accounted for generally small, giving a rather poor impression of the adequacy of the model. The goodness of the fit in these terms improves with depth at moorings 1 and 2 and is better in predicting the alongshelf as compared to the cross-shelf currents. The signs of the coefficients are all, except in a few instances, consistent with qualitative features of an upwelling shelf model. However, in only the b_i and d_i coefficients is the expected coefficient symmetry between u and v evident and then only in their signs. In comparing the actual time series with the predicted series, the predicted currents generally have the character of being out of phase (usually leading by 6 to 12 hours) and of underestimating the high values, sometimes severely. Also in quiet periods the predicted values rarely settle back far enough.

It seems then that assuming a series of near steady state conditions is inadequate to describe oscillations of periods from 2 days to a week. How complex a model and how many added refinements will be needed to account for the behavior? Going back to the horizontal momentum equations an estimation of the role of the time derivative and advective terms can be obtained using finite space and time derivatives. Table 2.10 gives the average ratio of these terms to the Coriolis term

TABLE 2.9

$u = a_1 + b_1 v + c_1 p' + d_1 \tau^x + e_1 \tau^y$							
INSTRUMENT	a_1	b_1	c_1	d_1	e_1	σ_u	rms error
11	0.370	0.017	-0.233	-0.538	0.527	2.32	2.064
13*	-0.009	-0.209	0.114	0.033	-1.014	1.61	0.819
21	-0.507	0.066	-0.034	0.180	0.924	3.86	3.103
23	-0.290	0.179	-0.112	-0.013	-0.408	4.47	1.881
31	-1.866	0.005	0.117	0.884	1.618	5.27	3.588
33	-4.170	-0.145	0.270	0.391	-0.291	4.10	3.978
35	-0.104	0.028	0.022	0.362	-0.411	1.86	1.765

$v = a_2 + b_2 u + c_2 p' + d_2 \tau^x + e_2 \tau^y$							
INSTRUMENT	a_2	b_2	c_2	d_2	e_2	σ_v	rms error
11	-3.560	0.169	-0.570	0.871	2.176	9.27	6.421
13*	0.244	-1.524	-0.658	1.649	-2.206	4.02	2.212
21	-6.710	0.357	-0.570	-0.446	2.207	10.32	7.226
23	-1.942	0.925	-0.417	0.306	1.489	8.06	4.270
31	-8.137	0.015	-0.697	-3.603	1.398	9.14	6.312
33	-7.196	-0.280	-0.912	1.501	0.488	8.09	5.523
35	-0.902	0.069	-0.467	0.277	0.312	4.09	2.751

Table 2.9 A tabulation of the coefficients for equations of the indicated forms determined by least squares and the rms error of using these equations to predict the observed low passed currents. The record for 13 is only 14 days long, while all the rest are approximately 32 days long.

TABLE 2.10

INSTRUMENT	DEPTH (m)	$\left \frac{\partial u}{\partial t} \right $	$\left \frac{\partial v}{\partial t} \right $
		$f v$	$f u$
11	27	0.43	17.57
13	57	0.30	1.78
21	24	0.14	2.19
23	62	0.40	1.89
31	30	0.19	1.12
33	70	0.52	1.30

INSTRUMENTS	DEPTH (m)	$\frac{\partial(u^2)}{\partial x}$	$\frac{\partial(uv)}{\partial x}$
		$f v$	$f u$
11 - 21	25	0.04	0.13
21 - 31	27	0.07	0.21
23 - 33	66	0.08	0.29

Table 2.10 Estimates of the relative importance of the time derivatives and the cross-shelf advective terms in the momentum equations for motions with periods longer than 33 hours. Tabulated is the average magnitude of the ratio of the time derivative and the advective terms to the Coriolis terms.

over the record period for the low frequency currents. For the cross-shelf balance the time derivative term is between 0.1 and 0.4 times the Coriolis term with the advective terms being almost an order of magnitude less. In the alongshelf direction the time derivative is everywhere larger than the Coriolis term and at instrument 11 it is ~ 18 times as large. The cross-shelf advection of the alongshore flow is more significant than that of the cross-shelf flow, but it is still smaller than the Coriolis term. The advective terms requiring alongshore differences cannot be estimated directly. Order of magnitude calculations indicate that for motions with alongshore length scales of 100 km these terms will be less than 1/2 of the Coriolis term for the alongshelf balance and an order of magnitude smaller in the cross-shelf balance. Alongshore length scales estimated from tide gauge records for this period can be as large as 1000 km (Beardsley et al., 1977) for periods of 2 to 7 days. It seems then that alongshore advection effects are negligible even though the alongshore flow is much stronger than the cross-shelf flow. The net result is that time derivative terms should be included especially in the alongshore balance and that cross-shelf advection also could be important in the alongshore balance as well.

Since the nonlinear terms are less important in the cross-shelf momentum equation and because it is possible to approximate the cross-shelf gradient with the bottom pressure measurement we attempted to balance the cross-shelf accelerations. The depth averaged cross-shelf equation of the form:

$$u_t - fv = -g \eta_x + \frac{T^x}{\rho H} - \frac{\tau}{H} u_b, \quad 2.6$$

where the left hand side and the variables on the right were treated as

known, was fit to the data by least squares to determine the coefficients on the right. The coefficients obtained for τ^x and u_b did not give the expected results and in fact r often came out negative. It was clear that the primary balance was between v and ζ_x , with the lack of precision in the vertical averaged velocities almost certainly a major source of error. Using the equation to determine the alongshore velocity, v , with the coefficients obtained gave results only marginally better than obtained with the quasi-steady state model.

2.5 Discussion

We have shown that the mean circulation pattern is extremely well described by the linear dynamics of the Csanady (1976) model. In addition, analysis of motion with periods from 1 1/2 to 7 days indicates that these motions are also in qualitative agreement with a frictional coastal boundary layer model. However, when attempts are made to be more precise and to use these dynamics to actually predict the observed flow, they do not appear to be adequate. What are the causes for the difficulty? For shelf-wide models the complication of a non-rectilinear coastline make the choice of coordinate systems difficult, if not altogether invalidating the straight coast hypothesis. Previously mentioned studies (Butman, 1975; Csanady, 1976; EG&G, 1975) have pointed out that the vertical eddy diffusivity varies by perhaps a factor of 10 between storm and non-storm periods. That the bottom drag parameter, r , also varies by this order is also probable, however the bottom drag term in equation 2.6 is much smaller than the other terms. In addition, equation 2.6 is a local force balance, and provided that one can measure the terms precisely enough, it should be independent of any of the shelf-wide boundary conditions of a complete model. That it is not able to predict the flow adequately does not seem to be entirely the fault of the measurement quality. The answer to the dilemma seems to be that the shelf dynamics contain more subtle influences. The discussion below outlines two such effects which are visible in the 1974 data and, while they are not the total answer, indicate some of the added complexities required for a complete understanding of shelf motions.

An examination of the low passed current records in Figures 2.6, 2.7, and 2.8 together with the wind stress record in Figure 2.14 show a

few periods of anomalous behavior. One is centered around the 10th of March when the wind stress is to the east, and for a short while, nearly as strong as at any other period. However, the current response is generally small, especially as compared to the response to the wind during the time marked "storm 1" when the magnitude of the stress is generally less. A possible explanation is that the vertical eddy viscosity was abnormally low during this storm such that the wind stress was balanced by Ekman layer transport rather than largely by bottom stress. Thus the lower layer exhibited only inertial oscillations rather than a transport in the direction of the wind, and the oscillations persisted because the vertical diffusion to the bottom friction was particularly small. The wind stress was of short duration and showed the characteristic clockwise rotation of lows passing to the north of the shelf. Pollard (1970) suggests that the wind stress will be especially effective in initiating inertial oscillations if the wind stress vector has a large clockwise component at near inertial frequencies. This seems to be the cause for the observed behavior. The same general effect, but to a lesser extent, can be seen as a result of the high stress occurring on March 13 and 14. The wind events which do not stimulate much inertial motion such as the storm periods marked in Figure 2.14, produce large alongshore currents. At these times the effective vertical eddy viscosity is large, the Ekman layer is deep enough to be evident at the upper instruments, the inertial oscillations are damped out, and the wind stress is predominantly balanced by bottom friction. The inertial oscillations disappear abruptly during "storm 3" because the wind stress vector had a large counter-clockwise component, typical of lows passing offshore of the shelf region. It

thus seems that the vertical eddy viscosity is a crucial parameter in understanding the response of the shelf to wind forcing and a major problem will be understanding the causes for the variation. Apparently, the viscosity is not solely related to either the wind stress magnitude or duration. Beardsley and Butman (1974) described the response of the New England shelf to wind stress during the pilot experiment and noted that an eastward stress event resulted in inertial oscillations rather than an alongshore transport. They attributed this as being due to a possible natural asymmetry of the shelf to wind forcing. The March 1974 experiment, however, showed that eastward flow is equally as possible as westward flow so that the oscillations observed were most likely caused by the process described here.

The temperature record from the bottom mounted pressure/temperature recorder at mooring 2 is the key to an event which gives credence to early fears about the complexity of the shelf dynamics. Specifically, this shows that the shelf/slope boundary will need to be included if we intend to understand shelf motions with periods from 1 1/2 days to 10 days. Figure 2.19 shows the temperature from the bottom of mooring 2 and the low passed east and north current components for instruments 23 and 31. The later half of the temperature record is dominated by four large temperature oscillations with a maximum amplitude of 4°C and a time between peaks of 3 1/2 to 4 days. The oscillations die out in 11 days ending abruptly due to "storm 3". The e-folding decay time is between 7 and 10 days. The initial cause for the oscillations was the wind stress of "storm 2" driving an offshore Ekman surface flow forcing the upper part of the shelf/slope front offshore while the near bottom return flow brought the lower part of the front shoreward. This shore-

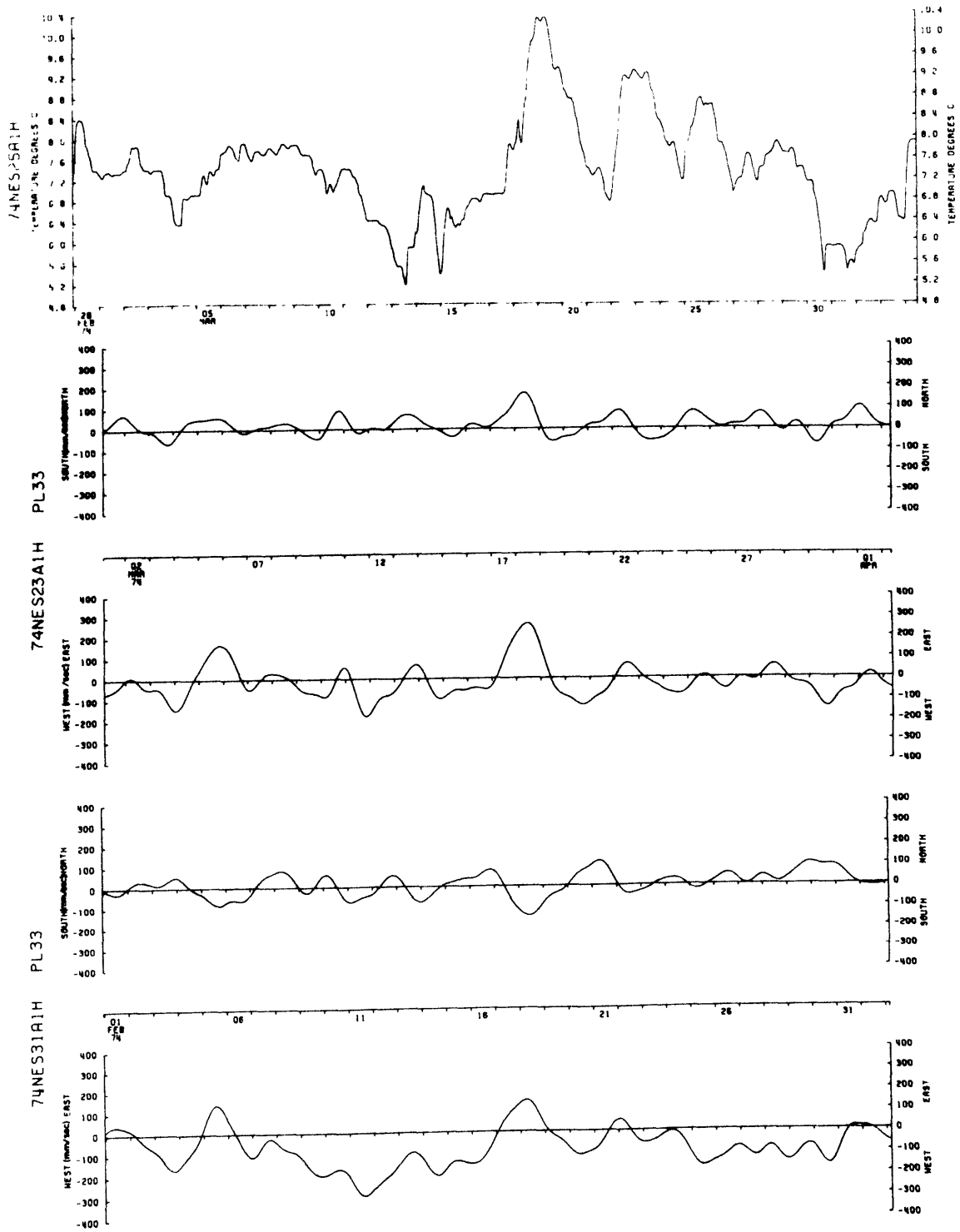


Figure 2.19 Stack plot of temperature from instrument 25 on the bottom at mooring 2 and the low passed east and north current components for instruments 23 and 31 from the March 1974 experiment.

ward movement along the bottom of the warm slope water caused the temperature rise at mooring 2. Subsequent to the initial forced disturbance, the front apparently oscillated about its mean position. The wind stress record of Figure 2.14 shows an oscillation during this period which also has periods of about 3 to 4 days more or less in phase with the frontal motion. It does not seem however, that the wind is the cause for the subsequent frontal oscillations, although it might minimize the decay, since the same type of oscillation in the wind stress was observed before "storm 2" without similar frontal motions. The north current record of instrument 23 leads the temperature oscillations by approximately 90° which is expected for an on-offshore oscillation of the front. The north component at 31 is $\sim 180^\circ$ out of phase with 23 during this period showing that the water farther off the bottom is moving offshore at the time that the near bottom water is moving onshore. This behavior becomes harder to discern farther from the frontal zone indicating that perhaps it is confined close to the area of frontal movement. The record at 35 shows much smaller north-south oscillations. Neither of the bottom pressure records at moorings 2 or 3 show evidence of these oscillations. With the slope of the front varying in this manner one expects that eastward velocity above the front would oscillate and be in phase with the temperature. Although the alongshore current oscillates with approximately the correct period, it does not seem to have the right phase relation. The mechanism for these motions is clearly the shelf/slope front oscillating about its mean position, but the dynamics behind the ~ 4 day period and the possible alongshore structure is not understood yet.

3 The New England Continental Shelf Frontal Zone

3.1 Introduction

In this chapter we discuss the behavior of the frontal zone south of New England during the periods of the March 1974 and January 1975 experiments. The frontal zone is the region of significant transition between the continental shelf and continental slope water masses. The early work of Bigelow (1933), Bigelow and Sears (1935), the more recent studies of Cresswell (1967), Boicourt (1973), Beardsley and Flagg (1975), Wright (1976), and Voorbis, Webb, and Millard (1976), among others, describe various general features of the frontal zone. For completeness, a brief description of the winter time front and the basic seasonal changes is given next.

The front has a conceptually simple structure during the winter when the front marks the interface between the cooler, fresher shelf water and the warmer, more saline slope water (see Figure 3.1 for a typical cross-shelf hydrographic section). The water in the shelf is fairly homogeneous in the vertical, with temperatures and salinity increasing from about 4°C and 32.5⁰/∞ near shore to about 8°C and 33.5⁰/∞ just shoreward of the front. Salinity is the dominant influence on density so that density increases in the offshore direction with σ_t varying from about 25.5 near shore to 26.1 just inside the front. Slope water just offshore of the frontal zone has surface temperatures of 14 to 16°C and surface salinities of 35.5 to 36.0⁰/∞. Both temperature and salinity generally decrease with depth over the continental slope with water at 1000 meters typical of North Atlantic Central waters at 4.0°C and 34.94⁰/∞. Therefore across the front, temperature, salinity, and σ_t change by approximately 5°C, 2⁰/∞ and 0.5 respectively. These

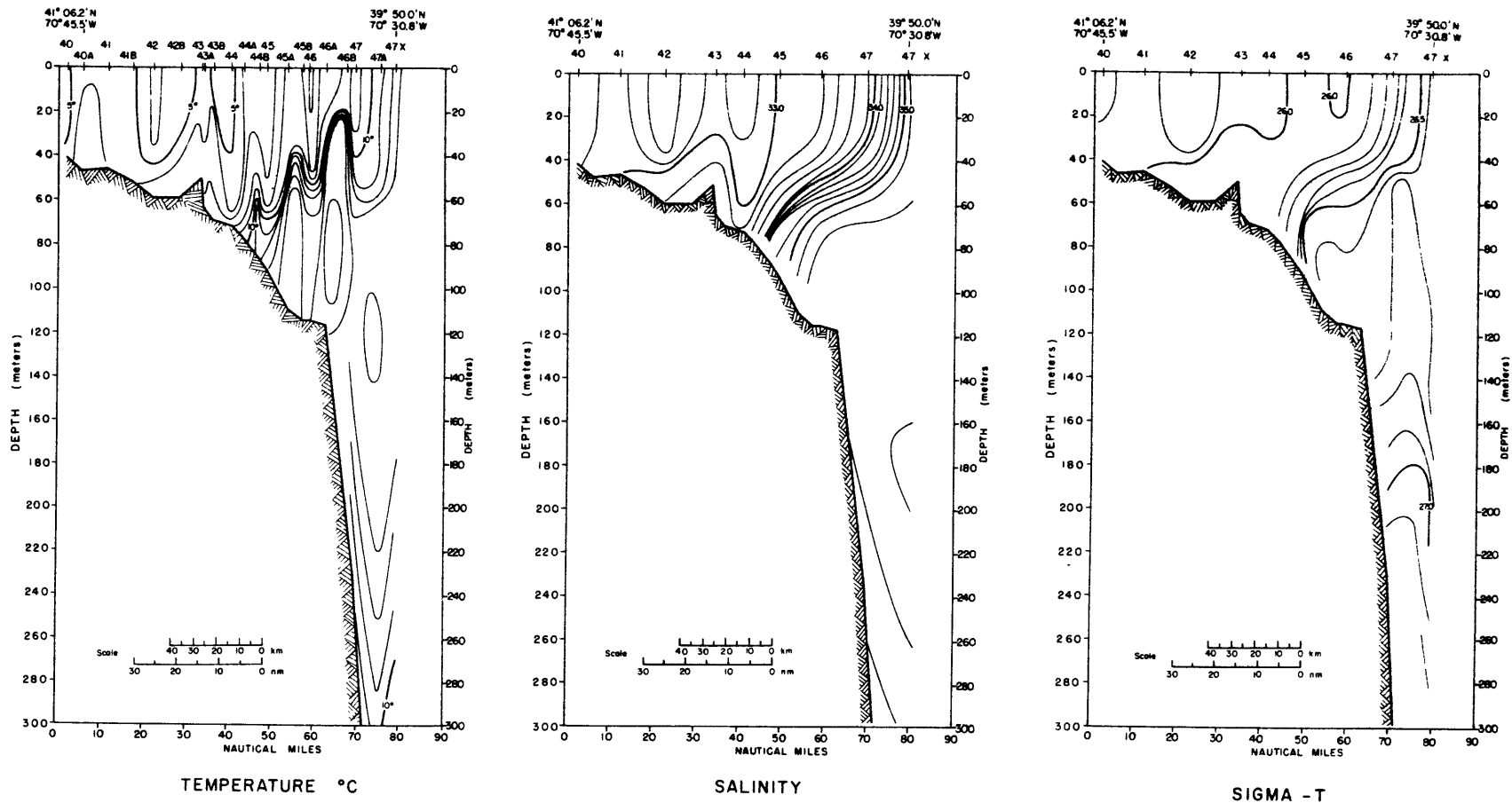


Figure 3.1 Temperature, salinity and sigma-t profiles across the continental shelf south of New England from the cruise of the USCGC DALLAS, February 23 - March 4, 1974. Contour intervals are: 1.0°C, 0.2 ‰, and 0.1 respectively.

changes occur in a horizontal distance ranging from 7 to 40 km and a vertical distance ranging from 15 to 60 m. The center of the front is generally characterized by the 10°C isotherm, the 34.5‰ isohaline, and the 26.5 σ_t contour.

The front always straddles the shelf break, the zone of abrupt increase in bottom slope marking the transition between the continental shelf and upper slope. South of New England, the shelf break occurs at about 120 m, is somewhat deeper off Nantucket Shoals by ~20 m and somewhat shallower near Hudson Canyon by ~30 m. During the March 1974 experiment, the center of the front contacted the bottom on the average along the 80 m (\pm 20 m) isobath south of Block Island. The front slopes up from the bottom and offshore over the shelf break for an offshore distance ranging from 20 to 50 km. The mean slope of the front during the March 1974 experiment was approximately 2×10^{-3} , a value which is about twice the average shelf bottom slope and about one-tenth the average bottom slope of the underlying continental slope. The surface expression of the center of the front seems to be generally confined shoreward of the 500 m isobath. The front is a continuous feature located along the shelf break from at least as far east as 65°W, westward almost to Cape Hatteras. Thus the winter front is simply defined as a narrow inclined region over moderately steep topography separating a quasi-homogeneous shelf water mass from a denser oceanic water mass.

The vernal progression destroys the simple winter frontal structure just described. Increasing solar radiation and diminishing storm intensity cause the formation of the seasonal thermocline over both the shelf and slope regions. A cold band of shelf water, generally delineated by the 10°C isotherm, occupies the mid-shelf region below

the seasonal thermocline. This band is surrounded, inshore, above, and offshore by warmer waters. Thus, a well-defined temperature front remains below the thermocline as the offshore boundary of the cold band. Increased fresh water runoff in the spring decreases the shelf water salinity to its minimum by early summer, thus enhancing the salinity front even in the near surface waters. However, the seasonal thermocline dominates the density variation of the near surface waters so that the seasonal pycnocline extends from the shelf well out into the slope waters and the sharp winter surface density front essentially disappears. A small density front is maintained at the offshore edge of the cold band below the seasonal pycnocline. The important point here is that although the front is altered, weakened, sometimes disrupted by intrusions, the formation of "bubbles", and other advective processes, a frontal zone exists throughout the year and occupies essentially the same place relative to the shelf break.

In summary, the frontal zone of the Middle Atlantic Bight has three distinguishing characteristics: 1) the front is always present; 2) the water property isopleths which delineate the front always intersect both the bottom and the surface (or the bottom of the seasonal thermocline in summer); and 3) the front is always located over the shelf break.

We want to describe in this section some of the important physical processes which occur in the winter frontal zone south of New England. Our discussion is based on hydrographic and moored current observations made in and near the frontal zone during the March 1974 experiment lasting 35 days and the 5 day long January 1975 experiment. We will look at the thermal wind relation together with observed current shears to

determine to what extent the frontal zone exhibits a geostrophic balance. Second, we investigate the variability of the front for frequencies ranging from the internal wave band to motions with periods of several days.

3.2 The Thermal Wind Relation and Geostrophic Balance in the Frontal Zone

In this subsection we attempt to discover to what extent the shelf frontal zone is in geostrophic balance. There is no a priori necessity for a geostrophic balance to exist. In fact, if the front was maintained by very vigorous mixing against an encroaching slope water mass, such a balance would be rather surprising. The permanence of the front near the shelf break suggests some topographic control perhaps through partial conservation of potential vorticity. As we shall show, the predominantly alongshore currents do seem to be in near-geostrophic balance with the density field in the frontal zone.

The largest geostrophic current shears should occur across the front, the zone of maximum horizontal density gradients. If we idealize the front as a sharp interface between two homogeneous fluids of different densities, the velocity difference across the front is given by the Margules equation,

$$\frac{dh}{dy} = \frac{f(\rho_1 u_1 - \rho_2 u_2)}{g(\rho_1 - \rho_2)} \approx \frac{f \Delta u}{g \Delta \rho / \bar{\rho}},$$

where $h(y)$ is the depth of the interface with x positive eastward along-shore, y positive northward, and fluid 2 being the lighter shelf water.

During the March 1974 experiment, a total of ten cross-front density sections were occupied (Flagg and Beardsley, 1975) giving an average offshore slope of 2×10^{-3} for the $26.5 \sigma_t$ contour¹. With an average

¹ This agrees well with the frontal slope obtained by Wright (1976), $100\text{m}/52\text{km} = 1.9 \times 10^{-3}$, from an average over many years and all seasons.

change in σ_t across the front of approximately 0.5, the computed velocity difference across the front is 10.2 cm/sec, with the shelf water flowing westward relative to the slope water.

The mean currents measured on the New England shelf during the March 1974 experiment and current observations over the continental slope and rise obtained in other experiments are shown in an isometric projection in Figure 3.2; the measured currents are also listed in Table 3.1. Also shown is the mean position of the front as given by the 26.5 σ_t surface during the March 1974 experiment. The depth is plotted using a logarithmic scale to accommodate the large depth change; this results in an apparent distortion of the frontal interface. The mean currents at the upper two current meters at mooring 3 are between 6 and 8 cm/sec westward so that a 10 cm/sec horizontal shear across the front would produce a 3 cm/sec eastward flow of slope water. This is clearly not the case. The mean currents measured on the slope are also toward the west and generally only slightly smaller. The vertical shear between instruments 31 and 35 is about 7 cm/sec; in the correct sense, however, current meter 35 is located 1.2 meters above the bottom and is thus embedded in the bottom boundary layer. In light of these mean current observations, the actuality of the large mean geostrophic shear remains in question. (It is clearly desirable to put a vertical current meter array at the 250 to 300 m isobath to simultaneously monitor currents on both sides of the front.)

We now compare essentially instantaneous observed current shears with predicted geostrophic shears computed using the thermal wind relation and concurrent hydrographic data. Three density sections were made along the moored array transect during the March 1974 experiment.

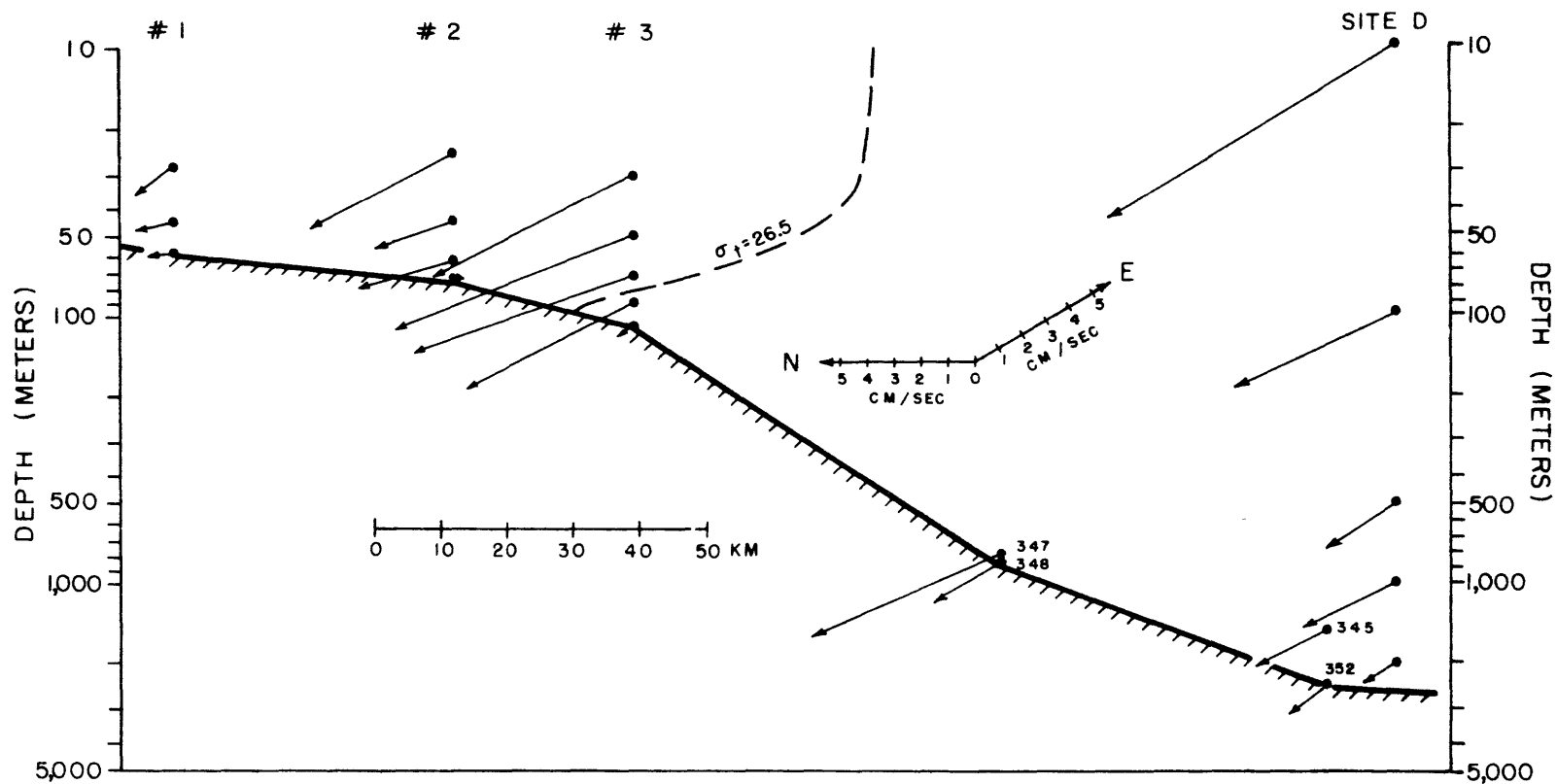


Figure 3.2 Isometric projection of mean currents across the continental shelf, slope, and rise south of New England. Moorings labeled 1, 2, and 3 are from the March 1974 experiment, 345 through 352 are from Schmitz (1974) and the Site D results are from Webster (1969). The east and north components of the currents, the mooring positions, and the instruments are tabulated in Table 3.1 The approximate position of the front during the March 1974 experiment as typified by the 26.5 sigma-t contour is also shown.

TABLE 3.1

MOORING DESIGNATION	POSITION AND DATE	$\overline{\text{EAST}}$	$\overline{\text{NORTH}}$	DEPTH	WATER DEPTH
		(cm/sec)			
Mar 1974	Feb. 28 - Mar. 4, 1974				
1	40°54.0'N 71°04.3'W	-2.1	-0.5	27	58
		-0.6	-0.9	44	
		-0.2	0.8	57	
2	40°54.0'N 70°55.6'W	-5.7	0.5	24	72
		-2.2	1.0	44	
		-2.2	1.8	62	
		-0.0	-0.5	71	
3	40°18.2'N 70°51.4'W	-7.8	0.7	30	112
		-7.2	2.9	50	
		-5.9	3.3	70	
		-6.7	0.7	90	
		-0.8	0.0	108	
Schmitz (1974)	Aug. - Dec. 1970				
345	39°23'N 70°59'W	-2.8	0.3	1508	2527
347	39°50'N 70°40'W	-6.4	1.6	776	876
348	39°50'N 70°56'W	-2.0	0.4	933	943
352	39°23'N 71°01'W	-2.4	-0.5	2394	2509
Webster (1969)	Feb. '65 - Aug. '67			Nominal Depths	
SITE D	39°20'N 70°00'W	-13.0	-0.6	10	2640
		-5.7	1.1	100	
		-3.7	-0.6	500	
		-3.5	0.3	1000	
		-1.6	-0.1	2000	

Table 3.1 Tabulation of time averaged east and north currents from moored current meter arrays on the New England continental shelf, slope, and rise. The March 1974 data are from the MIT experiment and the other sources are indicated.

During the period, the frontal zone was spread over a vertical extent of 15-60 m (see Figure 1) and a horizontal extent of 7 to 40 km. Only mooring 3 was actually located in the frontal zone. A cross front density section was also made during the January 1975 experiment. From both data sets, we can obtain a total of 25 pairs of measured and predicted shear values.

Vertical shear is predicted from the density sections using the thermal wind relation:

$$\Delta u_{\text{PRED}} = u_1 - u_2 = \frac{10f(\Delta D_a - \Delta D_b)}{\Delta L},$$

where ΔD_a and ΔD_b are the dynamic height anomalies at stations a and b between pressure levels 1 and 2, and ΔL is the horizontal distance between the two stations. Estimated measurement errors in density of $\sigma_t = \pm 0.036$ causes a relatively large uncertainty in prediction shear; for a vertical shear of 2 cm/sec in 20 m, computed with a station spacing of 15 km, the estimated error in shear is ± 0.6 cm/sec.

The observed current shears were obtained from low-pass filtered current meter data. The March 1974 data were filtered using a low pass filter with 50% amplitude attenuation at 33 hours and 10% attenuation at 44.7 hours. Essentially all diurnal and semidiurnal tidal energy and inertial energy is eliminated. The average velocity normal to the hydrographic transect was then calculated from the low-passed current data for the time between bracketing hydrographic stations. We have used one-half the range in velocity over the averaging period as an estimate of the experimental uncertainty. This error is generally comparable with the uncertainty in shear computed from the hydrographic data. The January 1975 experiment was so short that a simple 12.40

hour running average filter was used to "detide" the current series. The results still contain considerable inertial energy so that the measurement uncertainty in the vertical shears is considerably larger by a factor of 5 to 10 than in the March 1974 experiment.

The resulting pairs of predicted and measured current shears for the March 1974 and January 1975 experiments are listed in Table 3.2 and plotted in Figure 3.3. Also shown are the principal axes of the data and regression lines of Δv_{PRED} and Δv_{MEAS} computed using the more accurate March 1974 data. The data clearly indicate a one to one relationship between predicted and measured shears, although the correlation coefficient is not large. The angle of the computed principal axis is 44.7° , close enough to 45° considering the possible errors. The correlation between predicted and measured shears is better at mooring 3 which is located in the frontal zone where the horizontal density gradients are generally larger than on the shelf side of the front. This analysis suggests that the cross-shelf balance is predominantly geostrophic in the frontal zone.

TABLE 3.2

INSTRUMENTS	DEPTH RANGE (m)	DALLAS		VERRILL I		VERRILL II	
		MEASURED	PREDICTED	MEASURED	PREDICTED	MEASURED	PREDICTED
13 - 11	29.8	3.9 \pm 0.8	—	7.3 \pm 0.8	0.9 \pm 0.6	—	—
23 - 21	38.0	3.5 \pm 0.3	2.2 \pm 0.6	-1.1 \pm 0.3	-0.6 \pm 0.6	2.7 \pm 0.5	2.3 \pm 0.6
32 - 31	20.0	1.2 \pm 1.2	-0.3 \pm 0.6	3.4 \pm 0.4	-0.1 \pm 0.6	1.4 \pm 0.7	1.8 \pm 0.6
33 - 31	40.0	-0.8 \pm 1.4	-0.8 \pm 0.6	7.8 \pm 0.4	2.9 \pm 0.6	0.9 \pm 0.6	6.0 \pm 0.6
35 - 31	78.0	3.4 \pm 1.2	—	11.5 \pm 0.5	10.1 \pm 0.6	6.0 \pm 0.5	9.2 \pm 0.6
33 - 32	20.0	-2.0 \pm 1.0	-0.5 \pm 0.6	4.4 \pm 0.4	3.1 \pm 0.6	0.5 \pm 0.5	4.1 \pm 0.6
35 - 32	58.8	2.2 \pm 0.8	—	8.1 \pm 0.5	10.0 \pm 0.6	4.6 \pm 0.4	7.4 \pm 0.6
35 - 33	38.8	4.2 \pm 1.0	—	3.7 \pm 0.5	6.9 \pm 0.6	5.1 \pm 0.3	3.3 \pm 0.6
BNL		KNORR 46					
2 - 1	33	3.3 \pm 3.5	3.8 \pm 0.6				
3 - 1	66	4.6 \pm 3.8	1.5 \pm 0.6				
3 - 2	33	1.3 \pm 4.7	-2.3 \pm 0.6				

Table 3.2 A comparison of measured and geostrophically predicted shears between pairs of instruments in the vertical at each of the three moorings of the March 1974 experiment and for the January 1975 experiment.

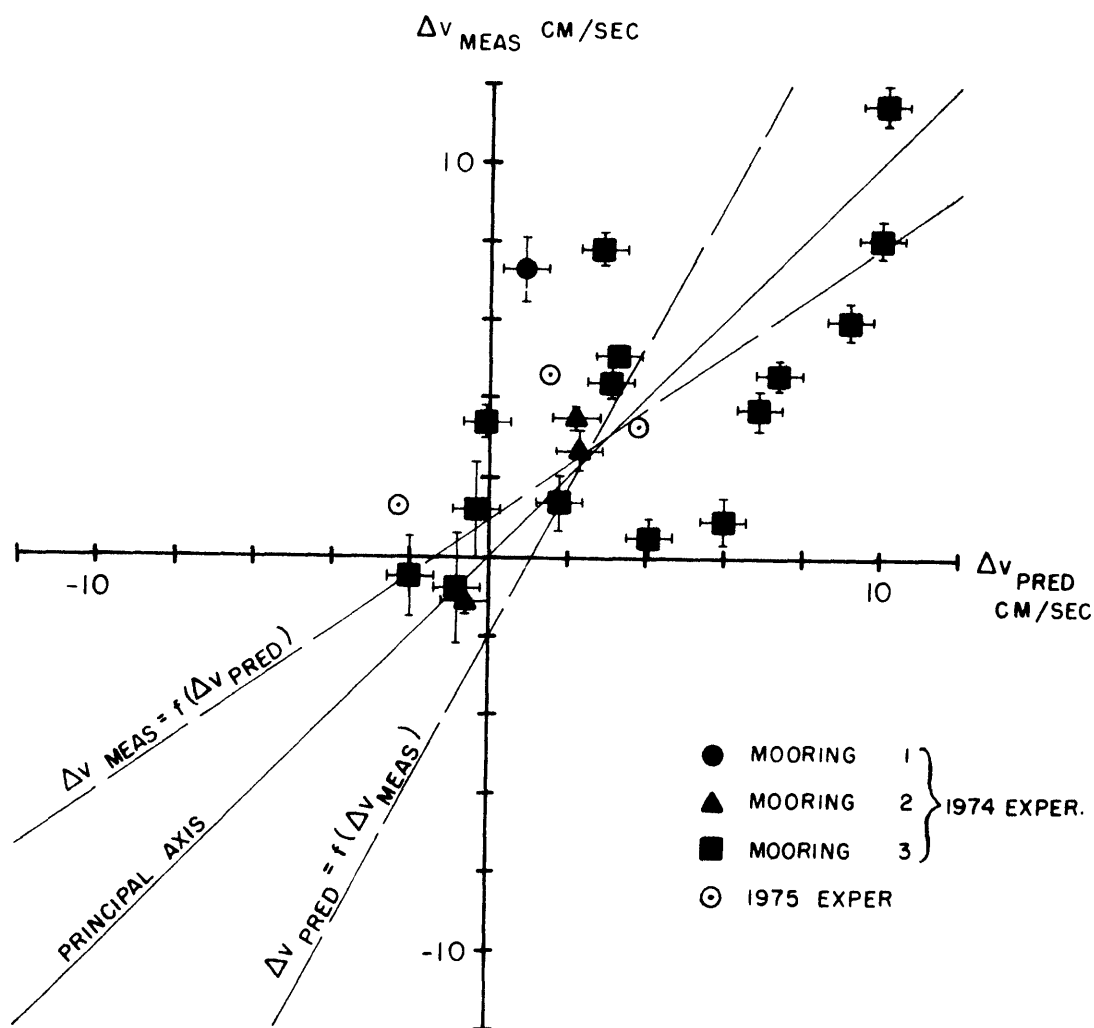


Figure 3.3 Scatter plot of the predicted vertical shear as given by the thermal wind relation versus the actual measured shear between pairs of instruments in the vertical at all three moorings of the March 1974 experiment for the cruises of the USCGC DALLAS and R/V VERRILL cruises I and II, and from the mooring and hydrographic data of the January 1975 experiment. Error bars in the predicted shears are estimated to be ± 0.6 cm/sec. Error bars for the measured shears are estimated to be equal to one-half the averaged velocity range between the pair of instruments. The regression lines and the principal axis of the data scatter are shown. The predicted and actual shears are tabulated in Table 3.2.

3.3 The Alongshore Geostrophic Transport

From the last section, we can now use the simultaneous current and hydrographic data to compute velocity and transport sections across the shelf. The velocity sections, though clearly approximate, illustrate the cross-shelf structure through the front and allow computation of the alongshelf transport of shelf water. These transports are important factors in box models of the shelf (Beardsley, Boicourt, and Hansen, 1976), for determining resident times, and to predict where cross-frontal mixing might occur along the shelf.

The velocity sections were constructed in the following manner. The low passed measured alongshelf velocities were extrapolated to 30 m at each mooring. (This depth was chosen since all moorings had a VACM located within 5 m of this depth.) The three extrapolated velocities were used to determine, by horizontal interpolation, the 30 m velocity for each pair of hydrographic stations out to the 120 m isobath. To determine the absolute alongshore velocity past the 120 m isobath, velocities at adjacent sections were equated at depths of minimum horizontal density difference. The results of this analysis for the March 1974 experiment are shown in Figures 3.4, 3.5, and 3.6 for the Dallas, Verrill I, and Verrill II cruises respectively. The underlined velocities are from the 30 m across-shelf current profile and arrows indicate where the relatively arbitrary velocity equivalences have been made.

These velocity sections illustrate several important features. A region of slow eastward velocity occurs beneath the front in all three sections. The Dallas section with better offshore coverage suggests that below the zone of eastward flow directly under the front, the deeper

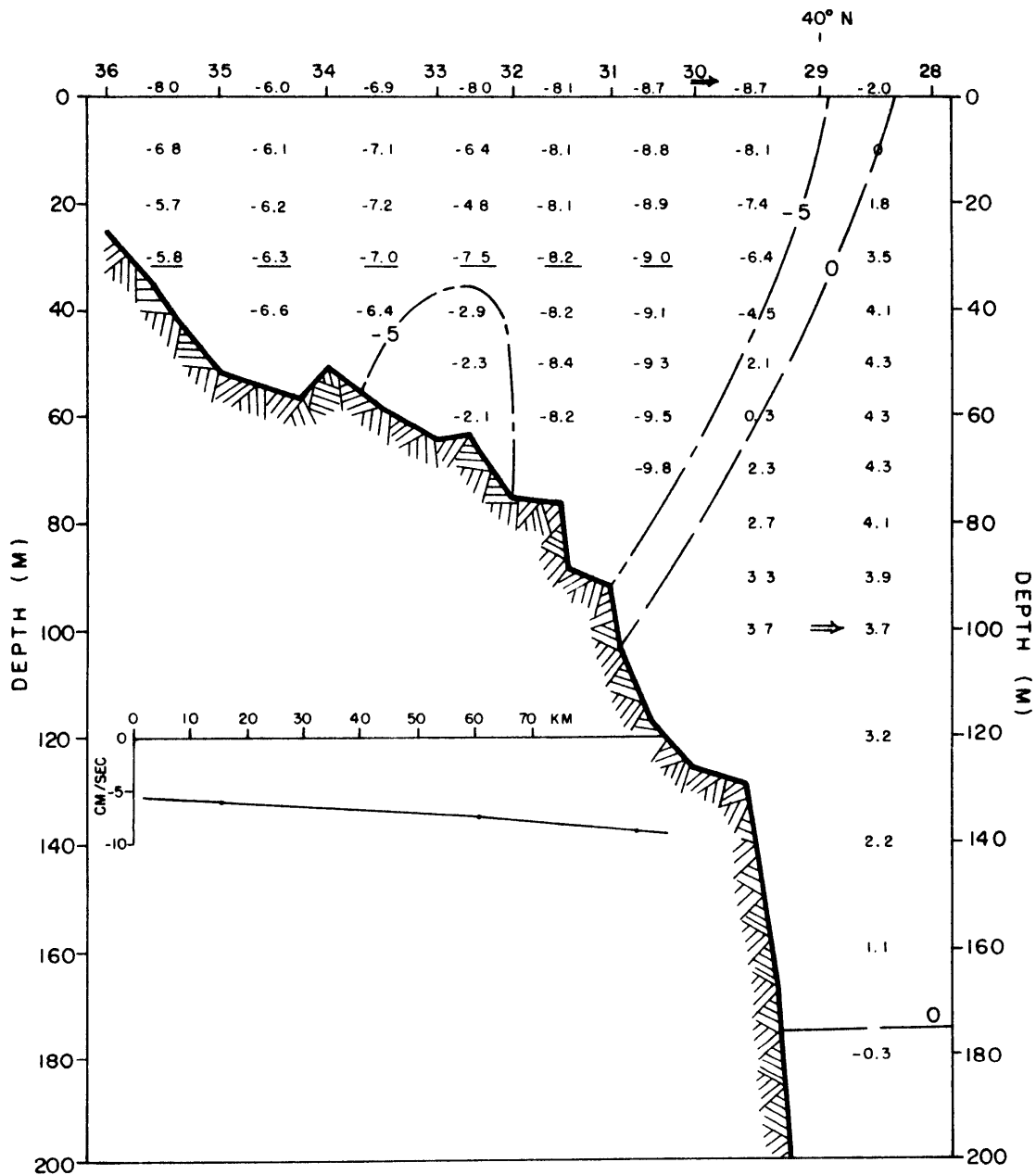


Figure 3.4 Alongshelf velocity section along the mooring array transect from the hydrographic survey of the USCGC DALLAS during the March 1974 experiment. Current velocities are given in cm/sec, positive numbers indicate current alongshore toward the east. Underlined numbers are interpolated from the cross-shelf current profile shown below obtained from the current meter moorings at nominally 30 m. Arrows indicate where somewhat arbitrary current equivalences were made based upon the density structure offshore of mooring 3.

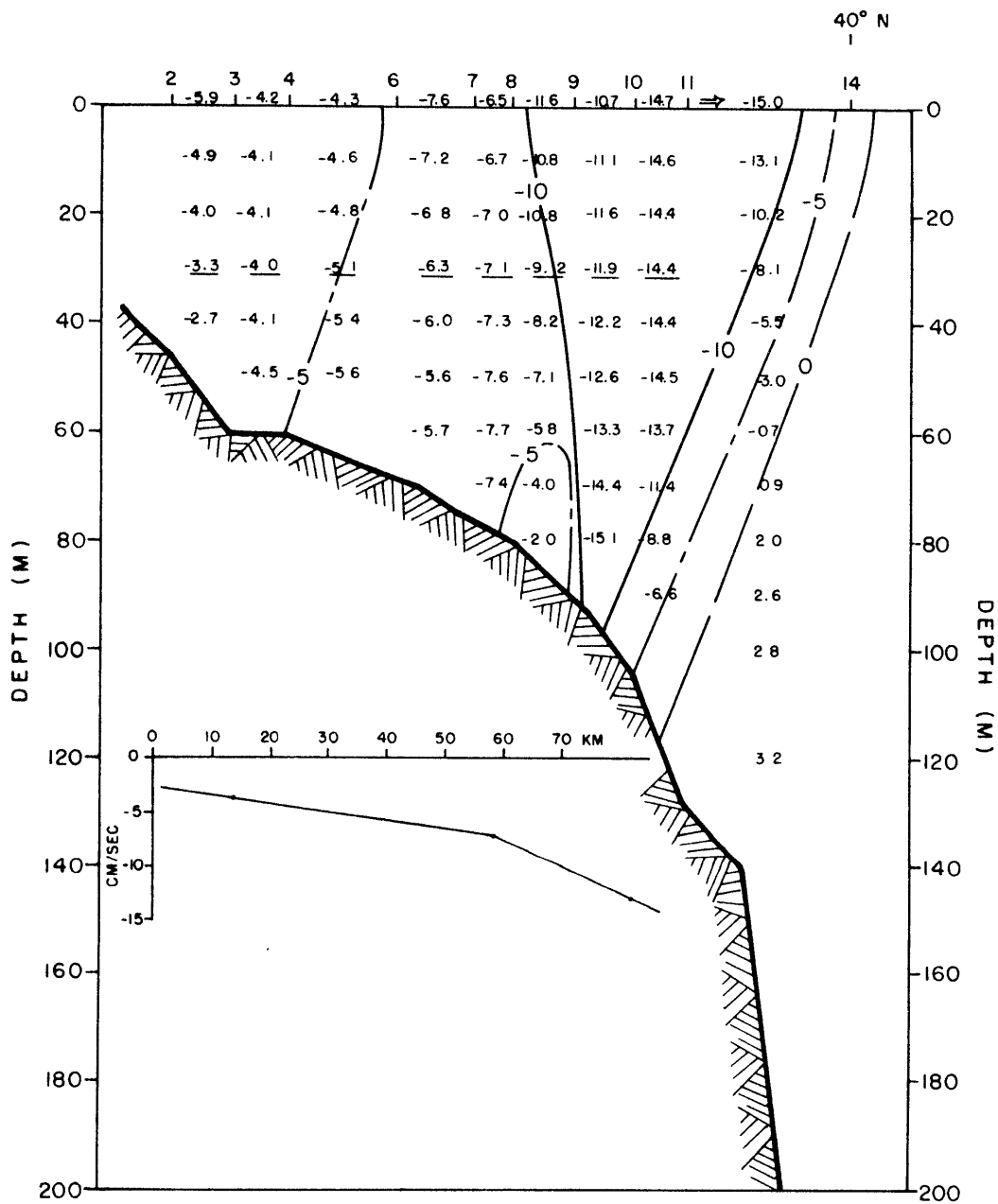


Figure 3.5 Same as Figure 3.4 but for the hydrographic survey section obtained during R/V VERRILL cruise I.

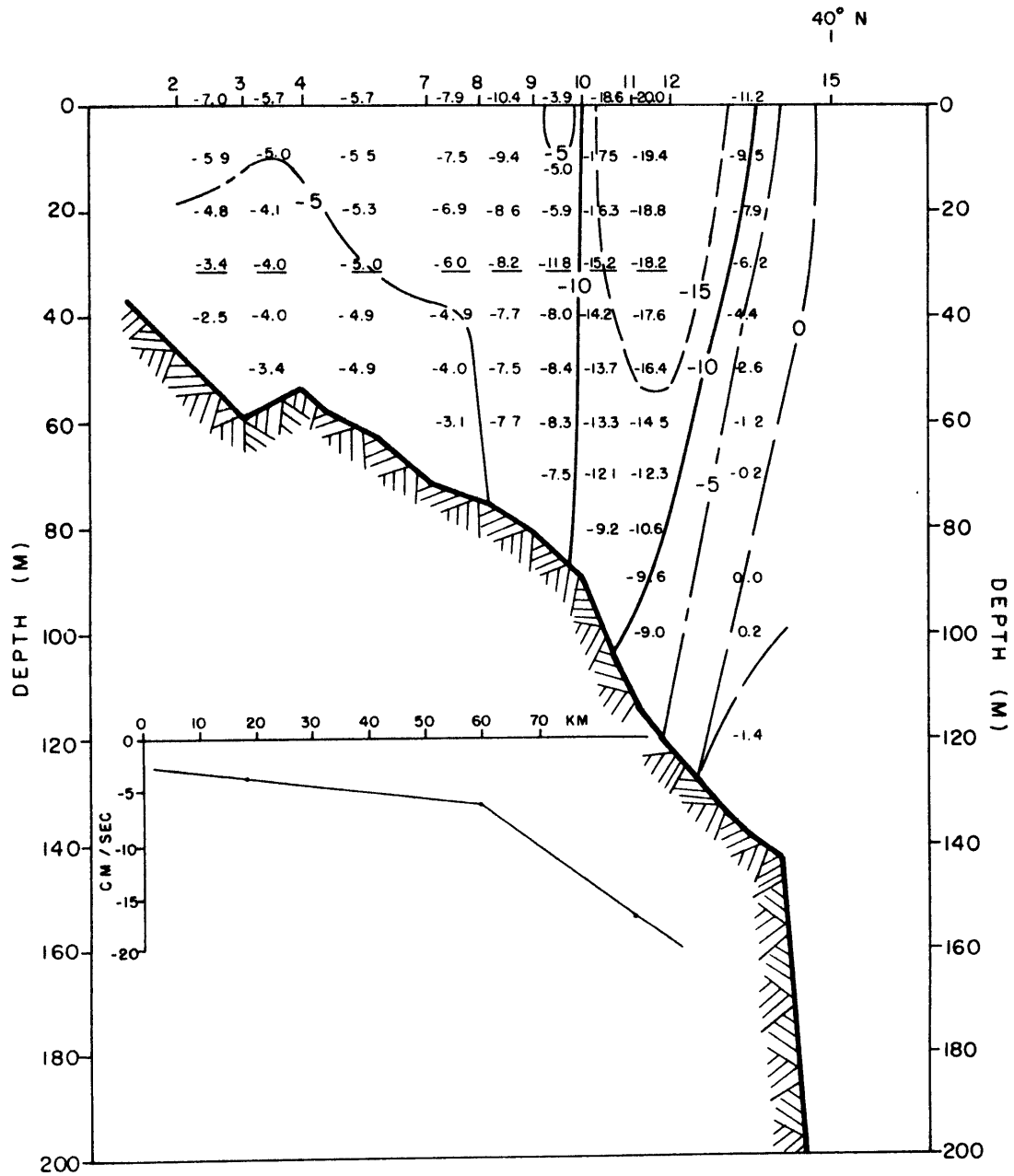


Figure 3.6 Same as Figure 3.4 but for the hydrographic survey section obtained during R/V VERRILL cruise II.

flow is westward again. Inside the frontal zone, the westward flow generally is greatest near the surface and increases offshore at all depths except near bottom at mid-shelf. This pattern agrees with the monthly mean current structure observed for this period. The maximum currents are found just inside the front, approximately near the 120 m isobath, a results correctly predicted by Iselin (1955) before the advent of modern current meters.

The following general picture emerges of the alongshelf current structure. Flow is westward at 5-6 cm/sec in 50 m, increasing offshore to a maximum of 10-20 cm/sec just inside the front. Over the mid-shelf region the velocity decreases slightly with depth by 2-4 cm/sec. Beneath the front and above 200 m, there is a wedgelike region of slow flow, possibly eastward or westward at 0-5 cm/sec; below this the flow is westward again. Outside the surface expression of the front, the velocity is westward at all depths at 5-10 cm/sec, decreasing somewhat with depth. A schematic of this description is shown in Figure 3.7. Our evidence for a velocity deficient zone under the front is sketchy at best but the scheme suggested here is also consistent with the behavior of the neutrally buoyant floats of Voorhis, Webb, and Millard (1976).

A simple integration of the velocity section has been made, and the resulting transport estimates are listed in Table 3.3. The average westward transport of shelf water between the 20 meter isobath and the front is 0.62 Sv ($1 \text{ Sv} = 10^6 \text{ m}^3/\text{sec}$). Of this total, about 0.40 Sv occurred within the 100 m isobath, and approximately 0.22 Sv occurred in the wedge shaped region between the 100 m isobath and the front. Thus, approximately one third of the total transport occurs in the frontal zone. Beardsley, Boicourt, and Hansen (1976) calculated a mean

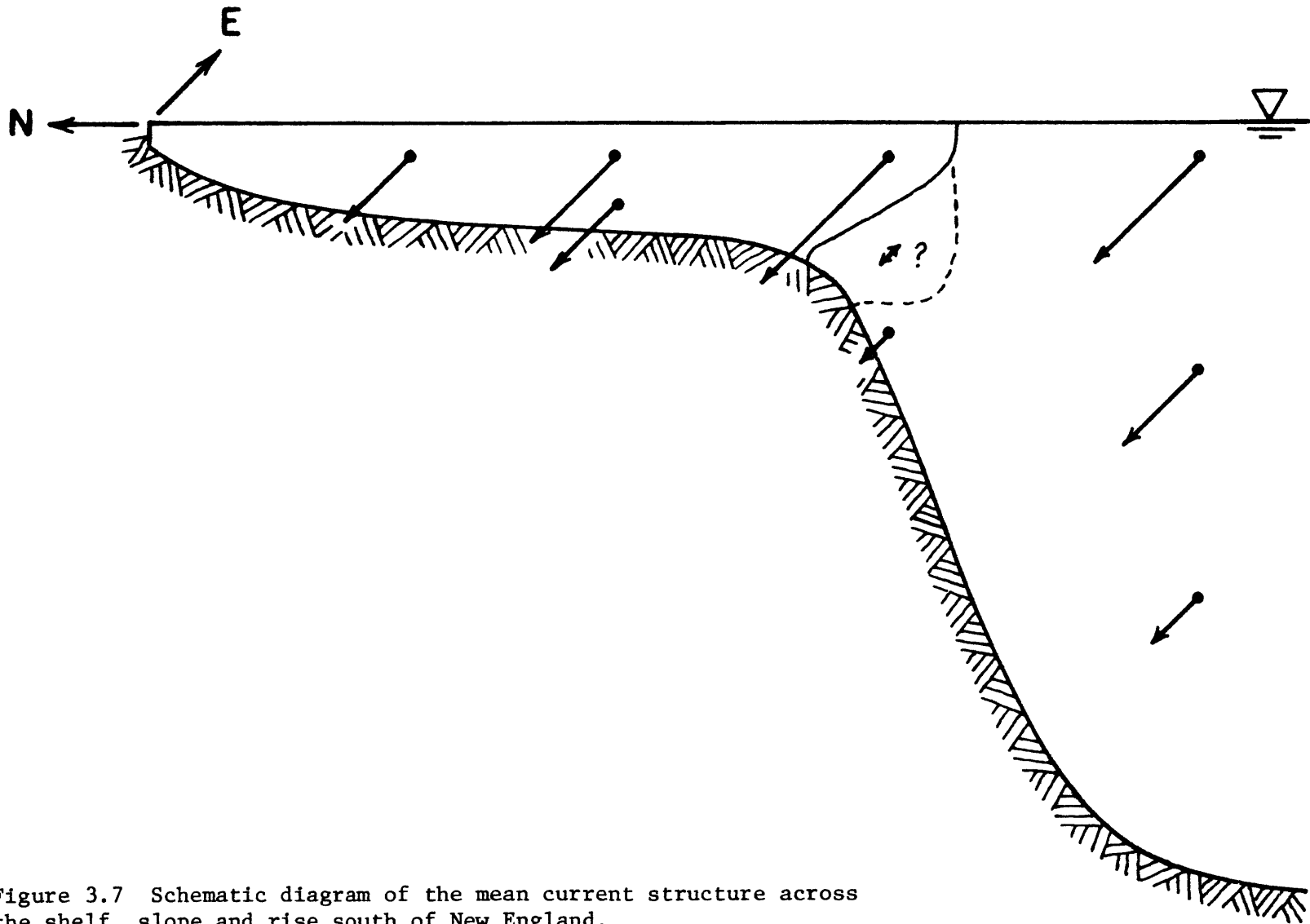


Figure 3.7 Schematic diagram of the mean current structure across the shelf, slope and rise south of New England.

TABLE 3.3

CRUISE	TOTAL (Sv)	INSIDE 100m (Sv)	OUTSIDE 100m (Sv)
DALLAS	-0.522	-0.338	-0.184
VERRILL I	-0.681	-0.437	-0.244
VERRILL II	-0.654	-0.428	-0.226
AVERAGE	-0.619	-0.401	-0.218
STD DEV	0.085	0.055	0.031

Table 3.3 Alongshore transports inside the front through the mooring array transect determined from the combined data of the moored current meter array and the first three hydrographic cruises.

alongshore transport inside the 100 m isobath for this section of the shelf using the monthly averaged current meter values from the March 1974 experiment and obtained a westward transport of approximately 0.17 Sv. An estimate of the total mean transport of shelf water inside the front is then $(0.17) \times (1.5) = 0.26$ Sv. This mean value is significantly smaller than the average value of 0.62 Sv from the three velocity sections discussed here. The discrepancy has several likely causes. Near surface velocities were probably underestimated in the "mean" calculations. The velocity section based on the combined hydrographic and current data probably overestimate near bottom currents and certainly represents only three fair weather samples of the alongshore current pattern. Thus, a reasonable estimate for the total alongshore transport is ~ 0.40 Sv.

3.4 The Variability of the Frontal Zone

The New England frontal zone exhibits significant variability on every time scale that has been examined. Repeated observations at a point would show variability ranging from the internal wave band to the seasonal cycle. In this section we examine the vertical and temporal variability of the winter frontal zone during the March 1974 and January 1975 experiments. With this data set, we can look at motions with periods ranging from several minutes to several days. The two experiments are complimentary; a sample rate of 5 or 7.5 minutes for current and temperature was used in the 35 day long 1974 experiment, while a 5 second sample rate for current was used in the 3 1/2 day January 1975 experiment. The relative position of the shelf/slope front was well documented throughout the 1975 experiment but only determined four times at intervals of about 10 days for the 1974 experiment.

3.4.1 The Internal Wave Band

In this section we examine the character and distribution of the horizontal and vertical kinetic energy in the internal wave band in and near the frontal zone. Zenk and Briscoe (1974) have examined the summertime internal wave band at the 500m isobath offshore of the front with current meters located at 60 and 85 m. They found that the temperature spectra exhibits a cutoff at N , the local Brunt-Vaisala frequency, and the kinetic energy distribution scaled in the vertical in reasonable accord with linear internal wave theory. Voorhis, Webb, and Millard (1976), using neutrally buoyant floats placed in and near the frontal zone, found a significant amount of internal wave energy which was modulated at tidal and inertial frequencies.

Only mooring 3 in the March 1974 experiment penetrated the frontal zone; instruments 31 and 32 were located above and inshore of the front, 33 and 34 were approximately in the front, and 35 was below the front. CM's 31 and 33 were VACM's, which record current and temperature every 7.5 minutes. CM 32 was an EG&G CT-3 electromagnetic current meter which uses a vane to orient the instrument into the current. Due to a possible sluggish response of the vane, we use only the spectrum results at frequencies below 0.5 cph. A similar cutoff is used on the current data from instrument 35, an EG&G model 102 current meter which burst sampled for one minute at five minute intervals. Instrument 34 had severe time base problems and cannot be used here. Instrument 36, a bottom mounted Draper Lab. pressure/temperature recorder sampled temperature every 7.5 minutes but had a 17 minute time constant making it unsuitable for frequencies greater than 1.0 cph. During the January 1975 experiment, current meter 1 (19 m) was placed above the front, 2 (52 m) was in the

front, and 3 (85 m) was below the front. These current meters were EG&G model 102's set to sample continuously every 5 seconds.

The Brunt-Vaisala frequency, N , at mooring 3 during the March 1974 experiment has been calculated from the four hydrographic cruises; the averaged N profile with error bars estimated by one standard deviation is shown in Figure 3.8. Above and below the frontal zone, N is approximately constant at about 1 cph. N is quite large within the frontal zone, with minimum buoyancy periods of order 5-10 minutes. The average maximum N found corresponds to an average minimum buoyancy period of 6.6 minutes. The increased variability of N within the frontal zone is caused by horizontal and vertical motions of the front itself. Data taken during the January 1975 experiment were not sufficient to clearly define the N profile. However, the average maximum values of N obtained from the four hydrographic stations nearest the current meter mooring was 6.25 cph, or a buoyancy period of about 9.6 minutes. Thus the maximum vertical density gradients in the front were of similar magnitude in both experiments.

Table 3.4 shows the percentage of the total variance in current spectra that occurs in the internal wave band at frequencies greater than 0.1 cph for the March 1974 data. The table indicates that energy in this band is generally insignificant compared to the total. However, the importance of the internal wave band is considerable because of the vertical and horizontal mixing associated with internal waves and because of the triggering effect that internal waves have for bottom erosion (B. Butman, personal communication). The relatively large percentage of internal wave variance at 35 is due to the low level of low frequency energy under the front rather than an increase in internal wave

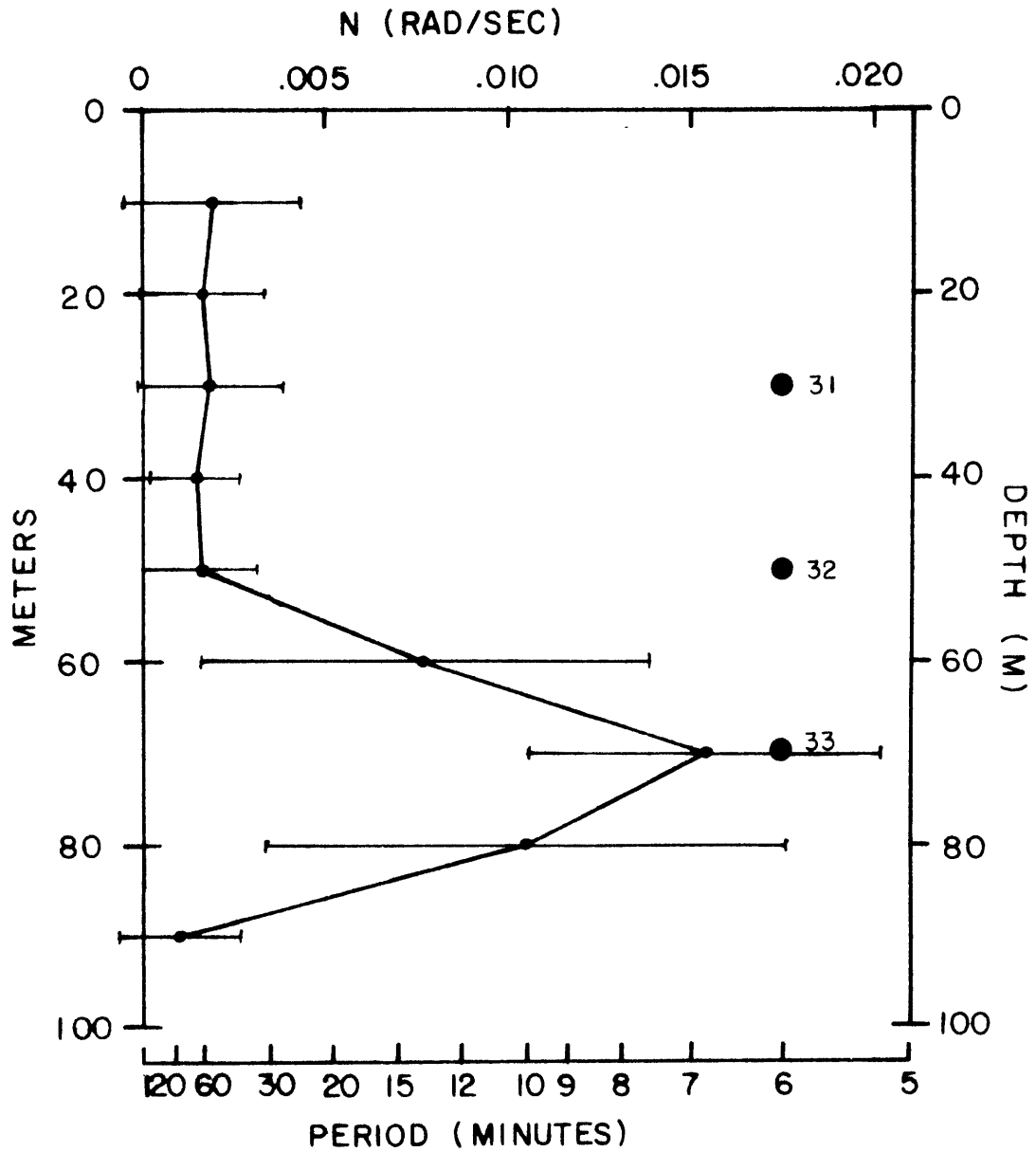


Figure 3.8 Vertical profile of the average Brunt-Vaisala frequency estimated from four hydrographic cruises during the March 1974 experiment at mooring 3. Error bars are one standard deviation of the scatter at that depth. The relative vertical positions of the instruments on mooring 3 are shown.

TABLE 3.4

INSTRUMENT	DEPTH (m)	TOTAL VARIANCE (cm ² /sec ²)	PERCENTAGE OF TOTAL VARIANCE				
			LOW FREQUENCY $f < 1/33 \text{ hr}^{-1}$	DIURNAL	INERTIAL	S-DIURNAL	INTERNAL-W $f > 1/10 \text{ hr}^{-1}$
31	30	209	31.0	12.5	28.4	22.8	5.2
32	50	150	24.7	13.2	25.9	28.3	7.8
33	70	212	24.9	31.3	15.9	20.2	7.2
34	90	688	—	—	—	—	—
35	108	45	30.8	18.8	9.4	26.3	14.7

Table 3.4 For mooring 3 of the March 1974 experiment, a tabulation of the total horizontal current variances and the percentage of the variance in each of four frequency bands: 1) Low Frequency for $f \leq 1/33 \text{ hr}^{-1}$; 2) the Diurnal tidal band; 3) the Inertial band; 4) the Semi-Diurnal tidal band; and 5) the Internal Wave band for $f \geq 1/10 \text{ hr}^{-1}$.

energy. The percentages of total variance in the internal wave band for the temperature spectra of instruments 31, 33, and 36 are 3.7, 19.4, and 4.6% respectively. The large increase in relative temperature variance for 33 together with no increase of horizontal current variance indicates the large amount of vertical motion in the internal wave band.

The frontal spectra of horizontal kinetic energy from the March 1974 and January 1975 experiments, and of temperature from the March 1974 experiment, are shown in Figures 3.9 - 3.14. In order to resolve to lower frequencies spectra were first calculated using little band averaging; 5 and 6 adjacent frequency bands for the 1974 and 1975 experiments respectively. Where it was possible to look at the high frequencies a second spectrum with a higher Nyquist frequency was calculated using more band averaging; 104 and 44 adjacent frequency bands for the '74 and '75 experiments respectively. The high frequency spectra were prewhitened and a Hanning window used.

In the frequency band 0.09 cph to 0.50 cph the shape of the horizontal kinetic energy spectra are similar at all depths for the March 1974 experiment exhibiting a spectral taper of $\sim f^{-5/2}$. For frequencies from 0.50 cph to the Nyquist frequency, which for the VACM's is 4.0 cph, the spectra flatten out somewhat, tapering as $f^{-2/3}$. The flattening of the spectra at higher frequencies does not seem to be the result of aliasing as the energy levels are too large to be aliased $f^{-5/2}$ spectra. The energy levels are all about equal for instruments 31, 32, and 35, and are slightly less than 1/2 that of 33.

Figures 3.11 and 3.12 show the energy distribution in the frontal zone for the short and stormy period of the January 1975 experiment.

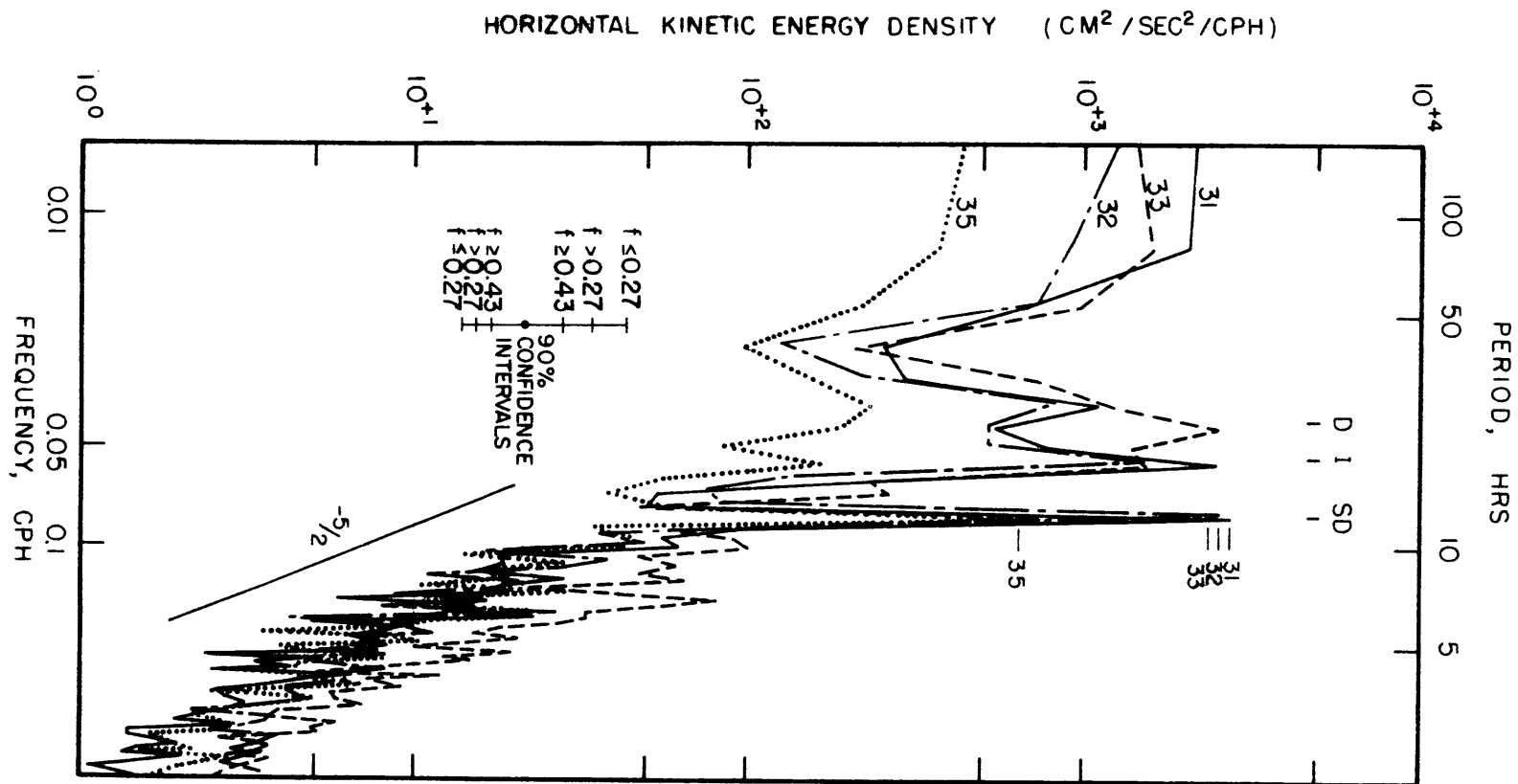


Figure 3.9 Auto spectra of the east and north current components for instruments 31, 32, 33, and 35 from the March 1974 experiment. Spectra are estimated with 400 estimates averaged over 5 adjacent frequency bands. Spectra are normalized such that a unit sine wave has energy of 1/2. The spectral taper of the internal wave band between 5 and 10 hours is close to $f^{-5/2}$.

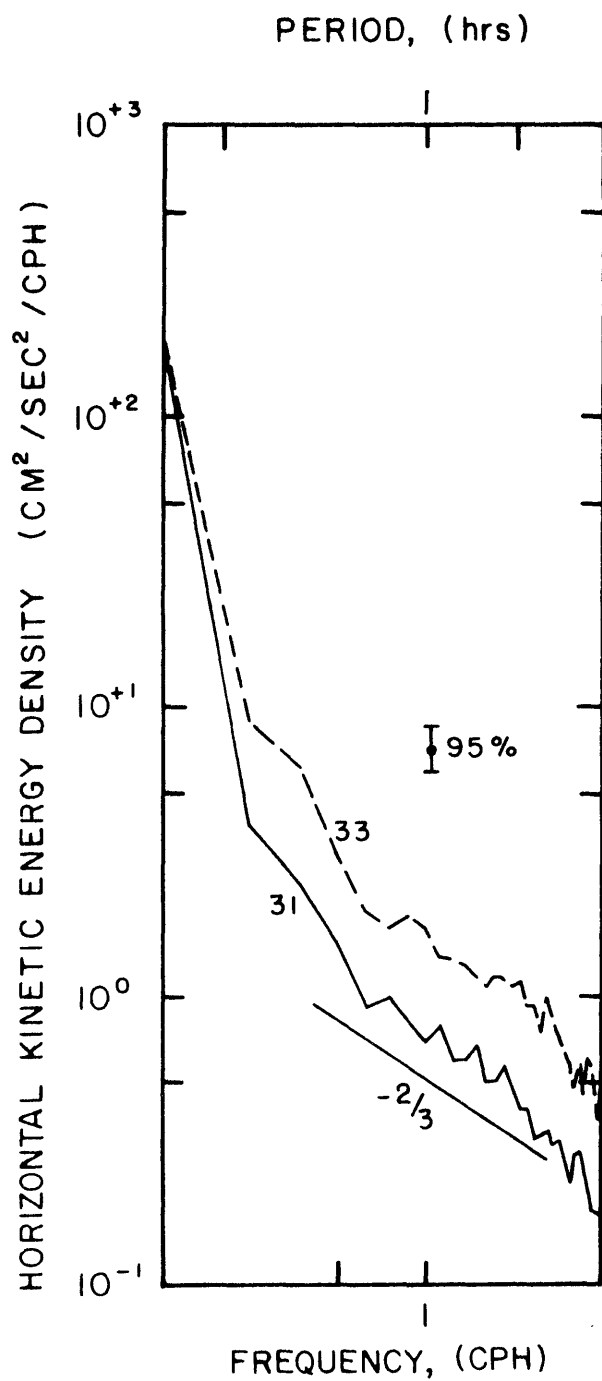


Figure 3.10 Auto spectra of the east and north current components for instruments 31 and 33 from the March 1974 experiment. Spectra are computed from 13 pieces with 256 estimates each averaged over 8 adjacent frequency bands. A spectral taper of $f^{-2/3}$ is shown.

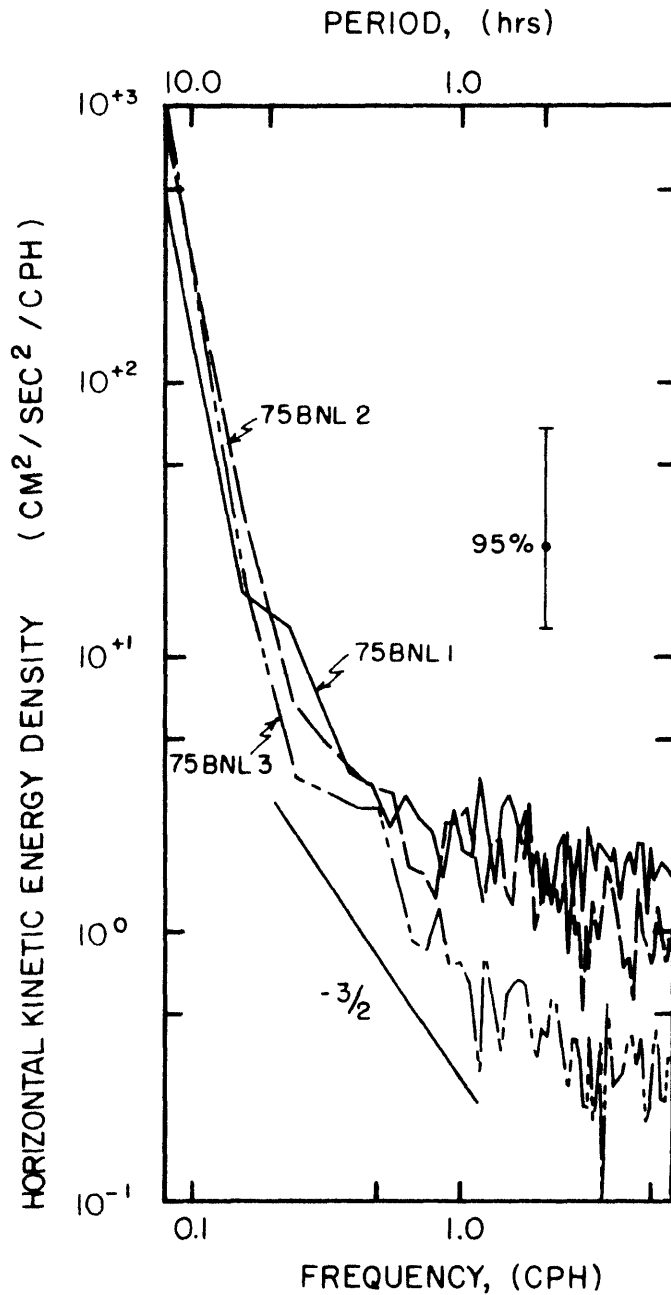


Figure 3.11 Auto spectra of east and north current components for instruments BNL 1, 2, and 3 from the January 1975 shelf edge experiment. Spectra were computed with 450 estimates averaged over 6 adjacent frequency bands. A $f^{-3/2}$ spectral taper is illustrated.

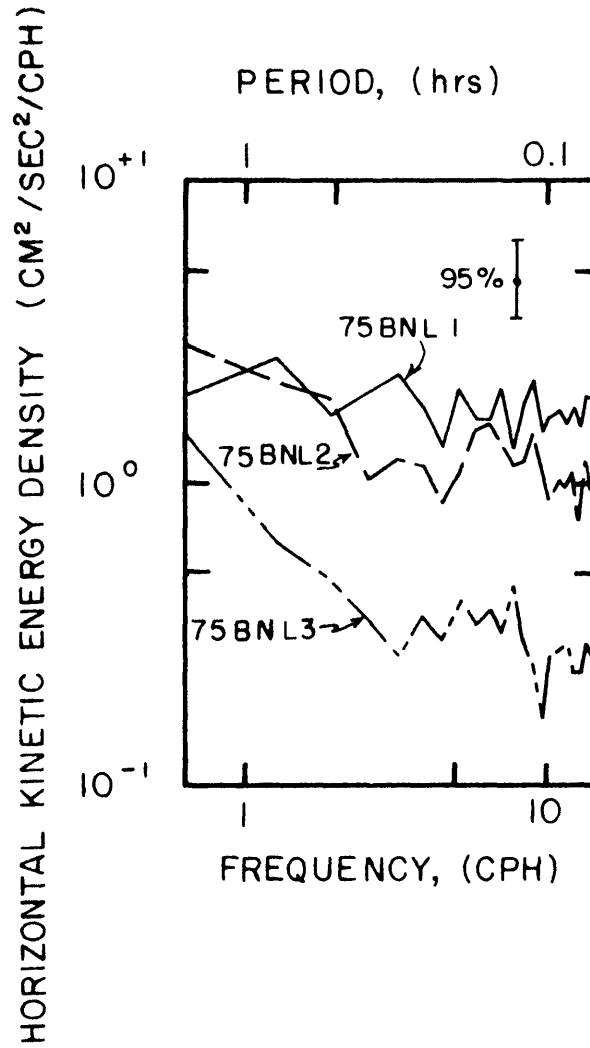


Figure 3.12 Auto spectra of east and north current components for instruments BNL 1, 2, and 3 from the January 1975 shelf edge experiment. Spectra were computed from 4 pieces with 256 estimates each, averaged over 11 adjacent frequency bands.

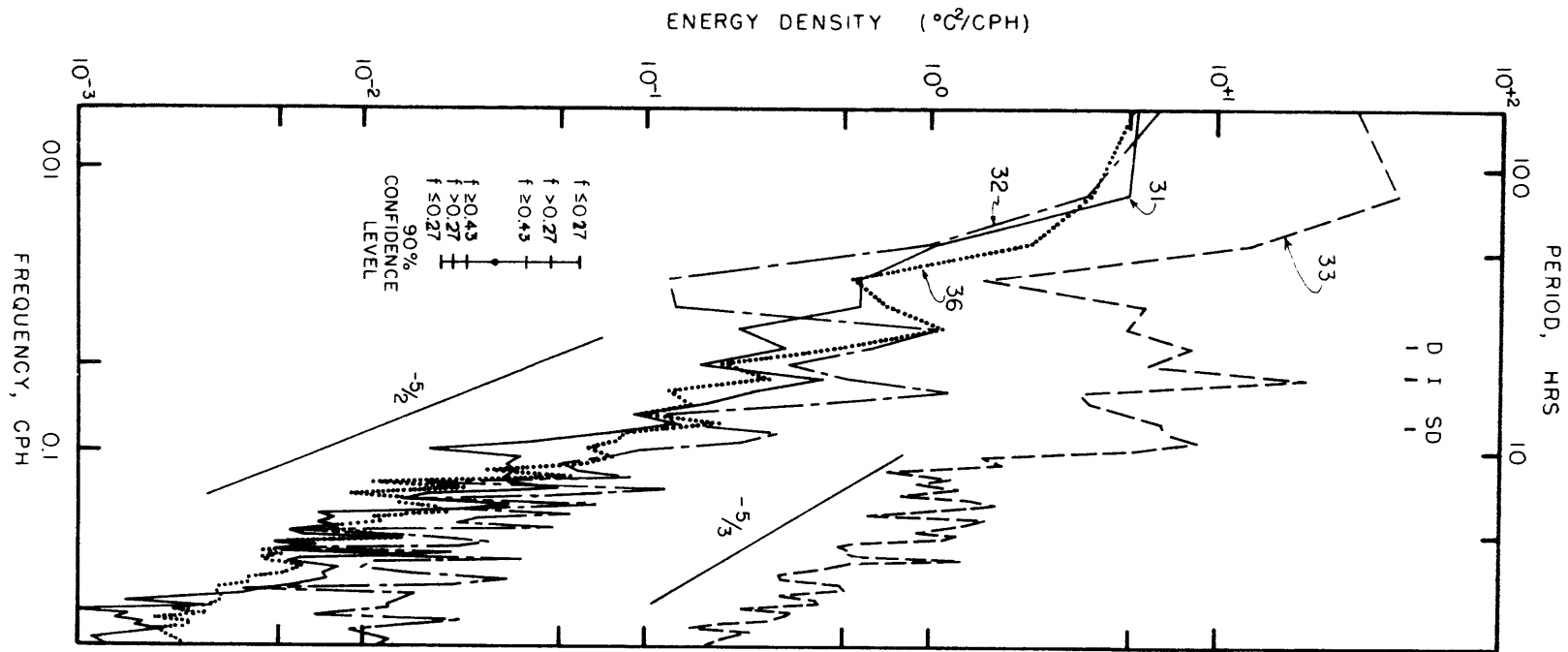


Figure 3.13 Auto spectra of temperature for instruments 31, 32, 33, and 36 from the March 1974 experiment. Spectra were computed with 400 estimates averaged over 5 adjacent frequency bands.

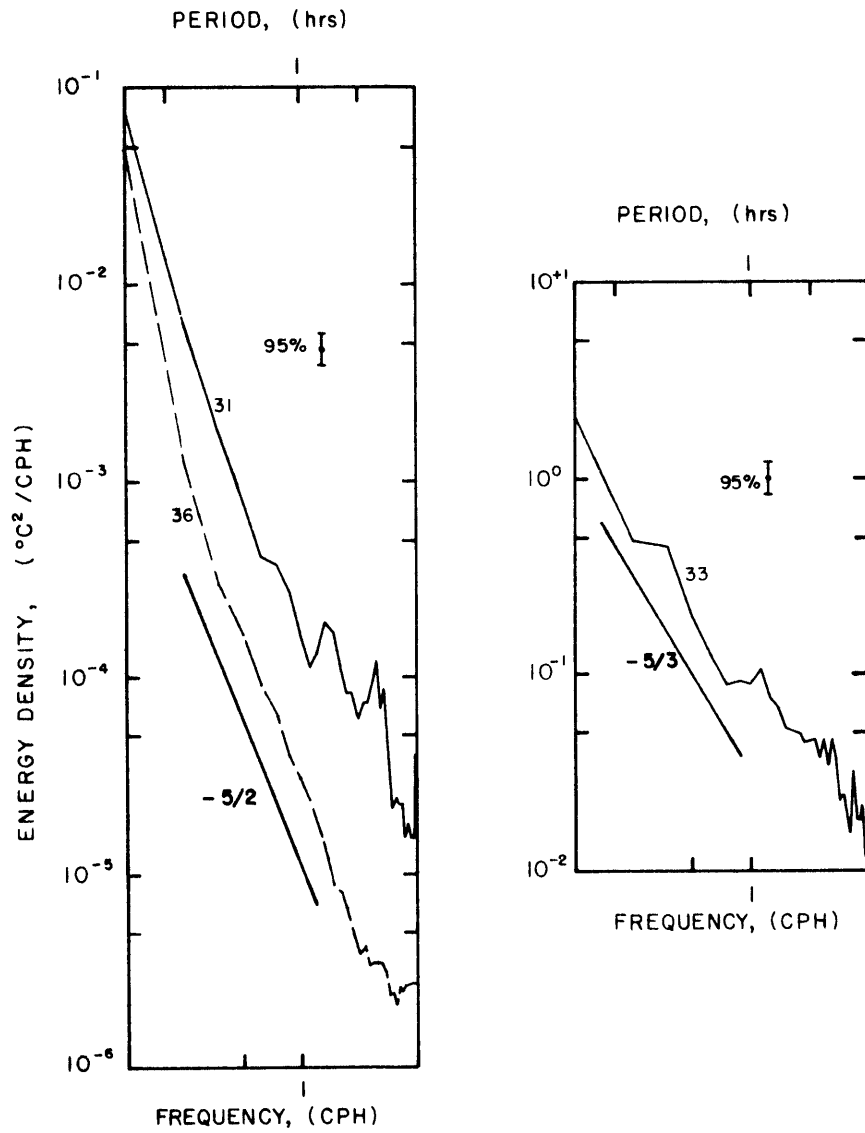


Figure 3.14 Auto spectra of temperature for instruments 31, 33, and 36 from the March 1974 experiment. Spectra were computed from 13 pieces averaged over 8 adjacent frequency bands.

Below 0.50 cph the spectra are not well resolved. Above approximately 0.50 cph, the spectra show a more pronounced flattening than the 1974 experiment with a slope between $-1/2$ and 0. Again, the energy levels are much larger than would occur by aliasing alone. In contrast to the results of the 1974 experiment, the horizontal kinetic energy density is not the largest in the intense part of the front. The greatest energy level is in the upper layer where it is about 1.5 times greater at BNL 1 as compared to BNL 2 for periods longer than 3 hours. It is probable that the surface stress is the source of high frequency energy which propagates downward. The records of current direction (see Appendix) show an increased fluctuation first at BNL 1 followed two hours later by BNL 2. The energy density below the front was considerably less than the upper two current meters with the ratio of the energy density between 52 and 85 meters being approximately 3.7. Thus, the intense front served to isolate the lower instrument from the storm induced oscillations.

The magnitude of the horizontal kinetic energy density at 19 and 52 meters from the January 1975 experiment was only slightly larger than the energy level at 70 m in the center of the front during the 1974 period. The internal wave energy below the front at 85 m in 1975 was about the same as those 1974 records which were out of the front itself. Thus, it would seem that the region of large density gradient maintains a high level of internal wave energy while above the front there are periods of high and low energy. It would also seem that the water below the front has a small, relatively constant, amount of internal wave energy.

An investigation of the linear internal wave theory (WKBJ) prediction about the behavior of the spectra indicates that the theory is probably not applicable to the frontal region. Temperature spectra which should indicate a high frequency cutoff at the local Brunt-Vaisala frequency indicate only the most tenuous sign of a cutoff and then the cutoff frequencies seem to be constant with depth (Figure 3.14). Vertical scaling of the horizontal and vertical energy spectra, again, is not particularly successful. It would seem that the intense frontal activity combined with the rather narrow and strong pycnocline invalidates the hypotheses of the linear wave theories in the frontal zone.

3.4.2 The Semi-Diurnal and Diurnal Tides

The tides are the largest single source of variance in the frontal zone as well as on the shelf (see Table 3.4). Much of the interesting tidal behavior occurs in the cross-shelf direction covered in Chapter 2. The diurnal tide shows the same baroclinic nature observed at mooring 2 with an increase in energy with depth. According to Traschen (WHOI, unpublished manuscript) the diurnal tidal ellipses have significant ellipticity and are oriented along the isobaths. In contrast to the diurnal tide, the semi-diurnal tide is nearly barotropic and essentially completely clockwise polarized. Because of the circular tidal ellipse, the barotropic amplitude distribution, and the nearness of mooring 3 to the shelf edge, simple one-dimensional continuity describes the relation between the semi-diurnal tidal currents and surface tide.

3.4.3 The Inertial Band

The inertial oscillations are greater in magnitude in the frontal zone than anywhere else on the shelf. As indicated in Table 3.4, the inertial energy is concentrated above the front, decreasing by approximately 50% in the front. In the bottom boundary layer the energy level is an order of magnitude smaller, partially due to frictional effects. Figure 2.5 shows the amplitude of the inertial oscillations as a function of time. While on the average the energy of the inertial oscillations and the tides is about equivalent in the surface layer, during an inertial burst, the inertial amplitudes are as much as 3 times the tidal amplitudes. The inertial energy level at mooring 3 in the upper layer is an order of magnitude larger than at 120 m at Site D (Webster, 1969). However, within 12 m of the surface at Site D, Pollard and Millard (1970) show inertial currents as high as 50 cm/sec as compared to a maximum observed at mooring 3 of almost 20 cm/sec. It is likely that the inertial oscillations are of about the same magnitude above the front and in the slope water. That the average inertial energy decreases with depth and is clearly associated with the wind stress is consistent with the generations of theories in Pollard (1970), Niiler (1975), and de Szoeke and Rhines (1976) even though the depth is finite.

As mentioned in Chapter 2, inertial oscillations play an important role in the behavior of the low frequency, wind driven currents. In particular, it seems that if conditions are right, the water below the surface layer will either respond predominantly as a steady current with little inertial motion or as predominantly inertial oscillations with

little mean current. Part of the cause for this behavior is suggested by the generation theories. Specifically, storms can be efficient generators of inertial waves if, 1) the stress vector is constant in direction but varies in magnitude with the inertial frequency, or if, 2) the stress vector rotates clockwise with the inertial frequency.

The January 1975 shelf edge experiment provides an ideal opportunity to study the first type of generation mechanism. The experiment lasted only 78 hours, but during the middle 48 hours of the deployment the wind stress was greater than or equal to 4 dynes/cm^2 . Figure 3.15 shows a stick plot of the wind stress and the 12.42 hour averaged currents at 19, 52, and 85 meters. The wind stress record indicates that following an initial period of calm, an eastward stress built to a maximum of almost 10 dynes/cm^2 in ~ 6 hours. This was followed by a lull and a gradual increase to another, but lower, maximum 16 to 20 hours later. After the second maximum of $\sim 7 \text{ dynes/cm}^2$, the wind slowly diminished over the next 24 hours. The wind stress had an approximate inertial period, so we should expect large inertial oscillations. The current records show that during the maximum wind stress, the current at 19 m was directed to the right of the wind, in the Ekman sense. When the wind started to die down the current started to rotate clockwise. The eastward components of the lower two records are quite coherent, but do not become coherent with the current at 19 m until after the second peak in the wind stress. To see the oscillations better, hodographs of the low passed currents are shown in Figure 3.16. With only inertial oscillations impressed upon a mean current, the hodograph would be an inertial circle displaced from the origin by the mean current plus the Ekman layer velocity. It is clear that more is actually happening than

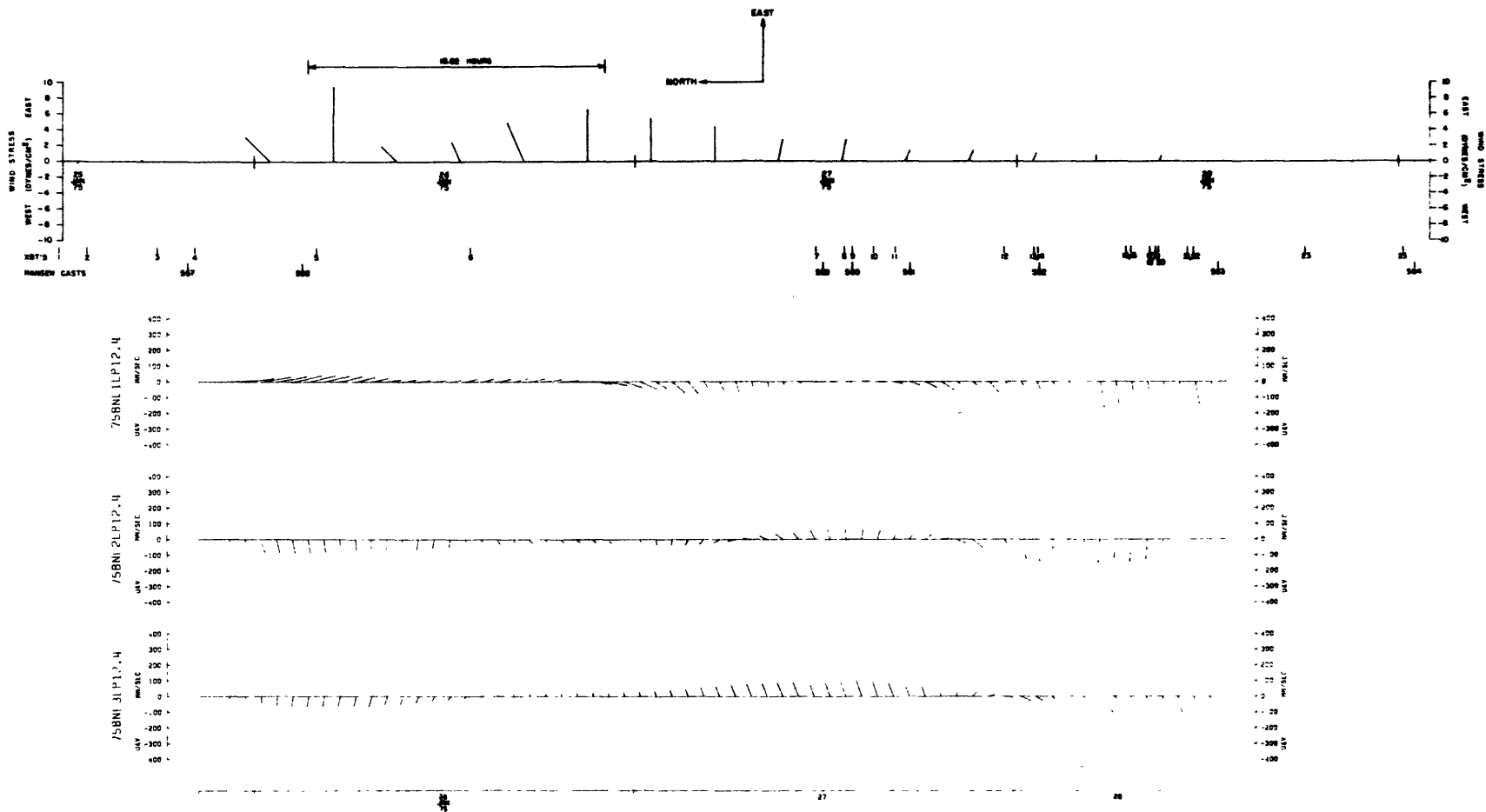


Figure 3.15 Vector plots of wind stress and 12.4 running averaged currents from the January 1975 shelf edge experiment. East is upward and north is to the left. The relative timing of the Nansen casts and XBT launches are shown below the wind stress plot.

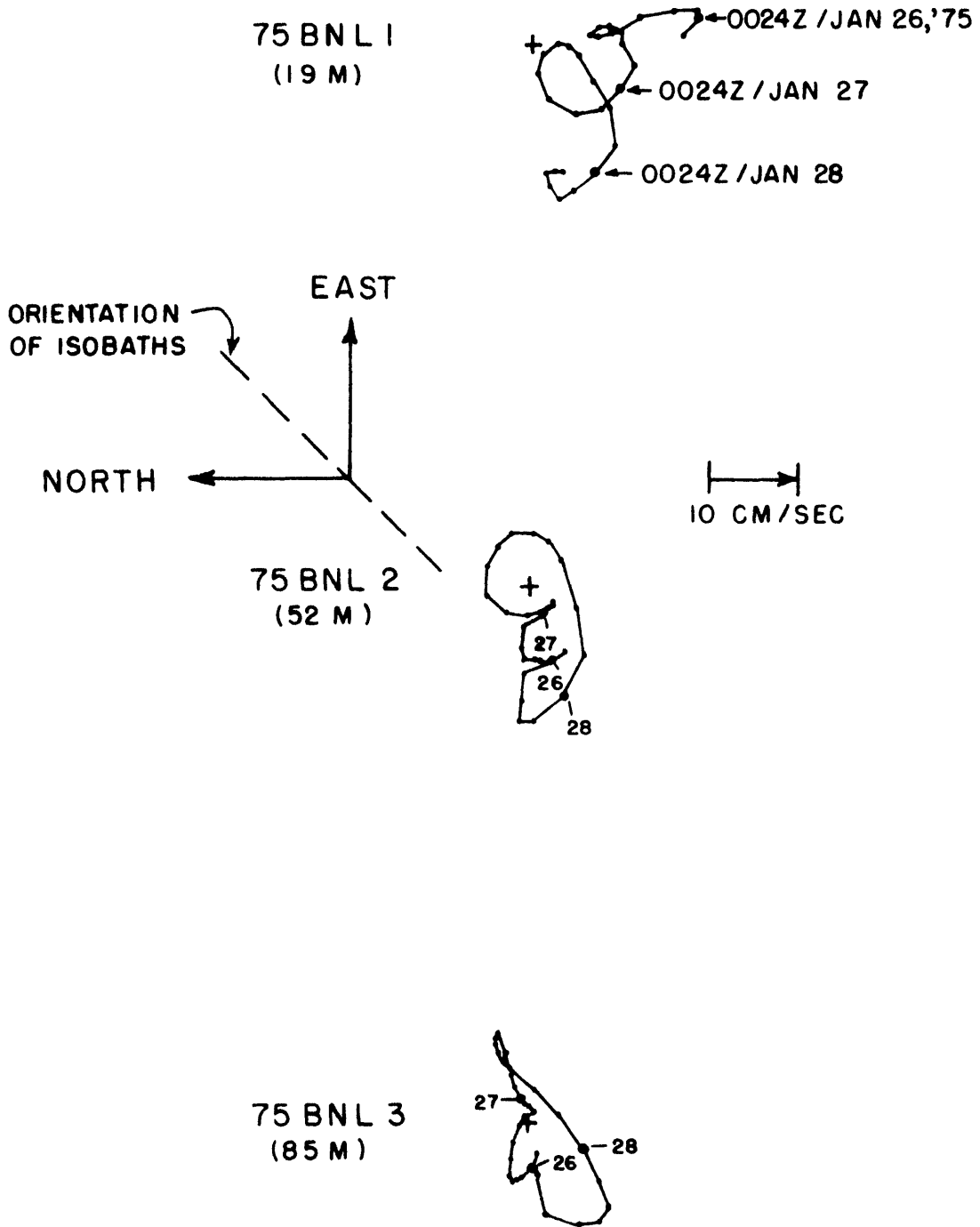


Figure 3.16 Hodograph of the running 12.4 hour averaged currents from the January 1975 shelf edge experiment.

this simple concept, but there is certainly clockwise polarized motion of near inertial period together with a mean toward the south-southwest. The currents show the clearest inertial motion at 19 m and seem to be more and more contaminated by lower frequencies with depth. At 85 m, which is ~ 25 m off the bottom, the oscillations seem to be partially constrained to follow the isobaths. The amplitude of the oscillations is on the order of 5 cm/sec, which is less than expected in light of the March 1974 experiment where amplitudes two to three times this were common. Note also that the resultant currents at the three instruments are not toward the east. It appears that inertial oscillations are important in determining the response to storms on the shelf and that this importance increases in the frontal zone.

3.4.4 Subtidal Frontal Variability

The subtidal frequencies are the most important on the shelf and slope in terms of actual displacement of water and for the on-offshore movements of the front. The March 1974 experiment lasted only a month so we are restricted to relatively short time scales. Ingham (1976a, b) has studied the seasonal variations of the front primarily by examining satellite photographs. In this subsection motions with periods ranging from little over a day to slightly longer than a week in the wintertime frontal zone are explored.

The spectra of Figure 3.9 indicate that in the frontal zone the energy density for frequencies lower than a day decreases with depth by a small amount. Instrument 35 is in the bottom boundary layer accounting for the reduction there. Clockwise and anti-clockwise spectra show that the degree of circular polarization is nowhere near as large as in the tidal and inertial currents. The flow has a clockwise polarization but the clockwise energy level is only about twice the anti-clockwise. Table 3.5 lists the variances for the east and north currents in the subtidal band. The variance of the alongshore flow is two to four times the cross-shelf variance. This is consistent with the degree of polarization. The ratio of eastward variance to northward variance increases toward the bottom indicating that some topographic control is exerted. There is a tendency for the spectra in Figure 3.9 to flatten out at the lowest frequency. This is in contrast to the results of Webster (1969) at Site D or those of Schmitz (1974) on the continental slope. There is a slight peak at three to four days.

Figure 3.17 shows the auto correlations of the low-passed east and north currents for mooring 3 of the March 1974 experiment. The eastward

TABLE 3.5

DEPTH (m)	VARIANCE IN SUBTIDAL BAND (cm^2/sec^2)			VARIANCE OF FRONT POSITION (km^2)
	TOTAL	EAST	NORTH	
0	—	—	—	68.9
20	—	—	—	49.0
30	111.3	83.5	27.8	41.0
40	—	—	—	31.8
50	71.2	49.7	21.5	13.7
60	—	—	—	11.6
70	82.2	65.4	16.8	43.6
80	—	—	—	174.2
108	20.2	16.7	3.5	—

Table 3.5 A comparison of the vertical distribution of the total, east, and north horizontal current variances with the vertical distribution of on-offshore position variance of the 26.5 sigma-t contour from the four hydrographic cruises along the mooring array cross-shelf transect from the March 1974 experiment.

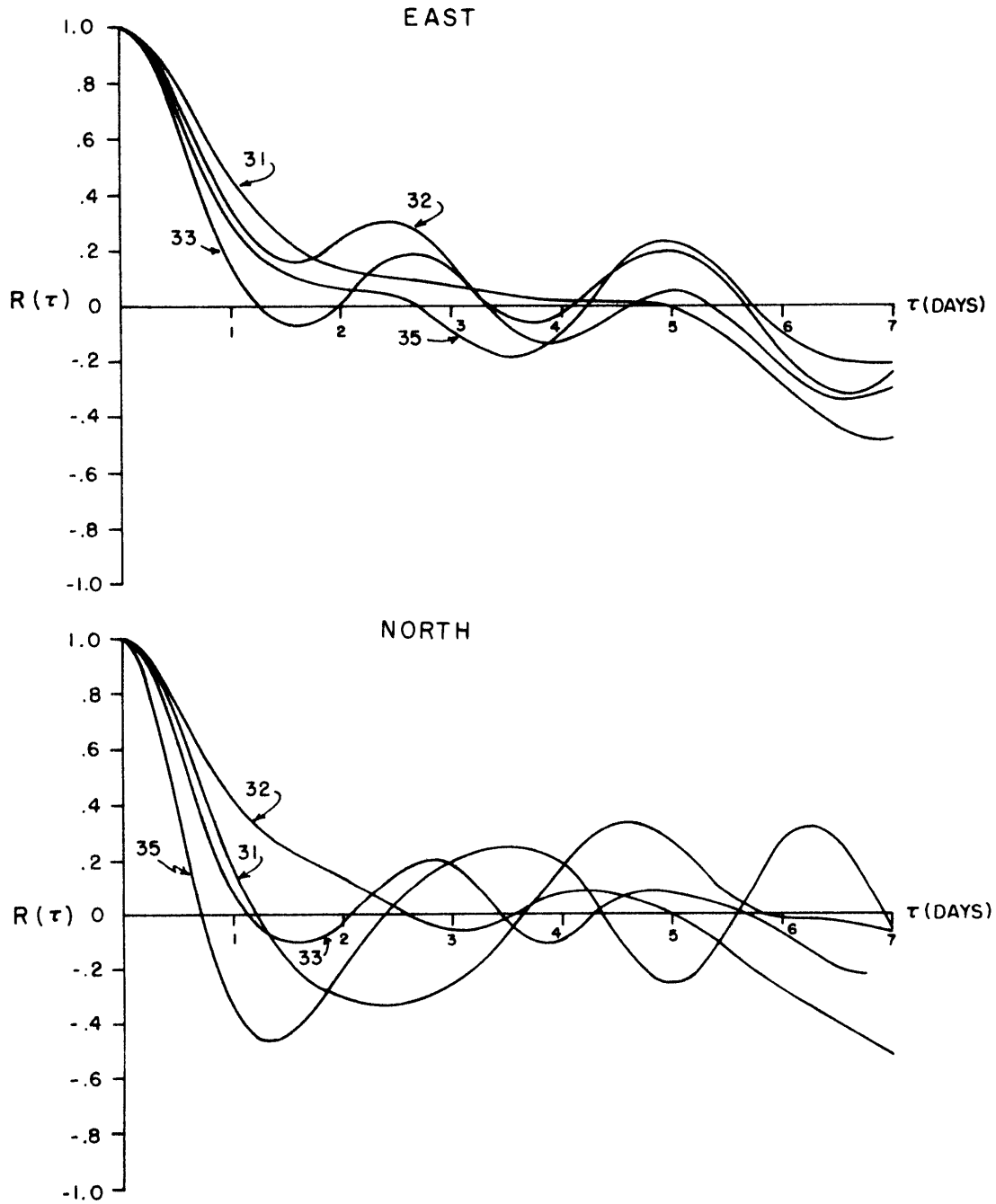


Figure 3.17 Autocorrelation plot of the low passed east and north currents from the March 1974 experiment for instruments 31, 32, 33, and 35.

correlation for 31 indicates low frequency oscillations of periods on the order of two weeks, while the records at 32 and 33 show periods of 2 to 3 days. The record just off the bottom and under the front shows alongshore oscillations of about 5 days. The vertical EOM's at mooring 3 (see Figure 2.9) show a high degree of alongshore vertical coherence but less than further on the shelf. The auto-correlations for the onshore velocities show a completely different behavior with little indication of common oscillation periods. The two upper current meters show oscillations of ~ 4.5 day period decreasing in amplitude with depth. At mid-depth, the onshore oscillations have a shorter period, ~ 2.8 days. At the bottom, there is again a strong oscillatory motion with a period of ~ 4.2 days. The onshore vertical EOM's at mooring 3 (see Figure 2.10) show a different structure as compared to moorings 1 and 2. The predominant on-offshore motion involves the upper three instruments moving in concert, but there is a significant amount of motion where 31 and 33 move opposite to each other. Thus to some extent, the waters above the front act as a continuation of the motion further on the shelf.

During the March 1974 experiment, one hydrographic survey was carried out with sufficient dispatch that we obtained a quasi-synoptic picture from Hudson Canyon to Nantucket Shoals. This has yielded what is probably a fairly accurate map of the alongshore position of the shelf/slope front. Figure 3.18 is a topographic chart of the $26.5 \sigma_t$ surface which represents the position of the middle of the front. This shows that while the front follows the shelf break in general, the front actually undulates on and offshore by a considerable amount. A wavelike feature in Figure 3.18, where the sampling seems dense enough to avoid aliasing, near $70^{\circ}30'N$, has a peak amplitude of ~ 20 km and a wavelength

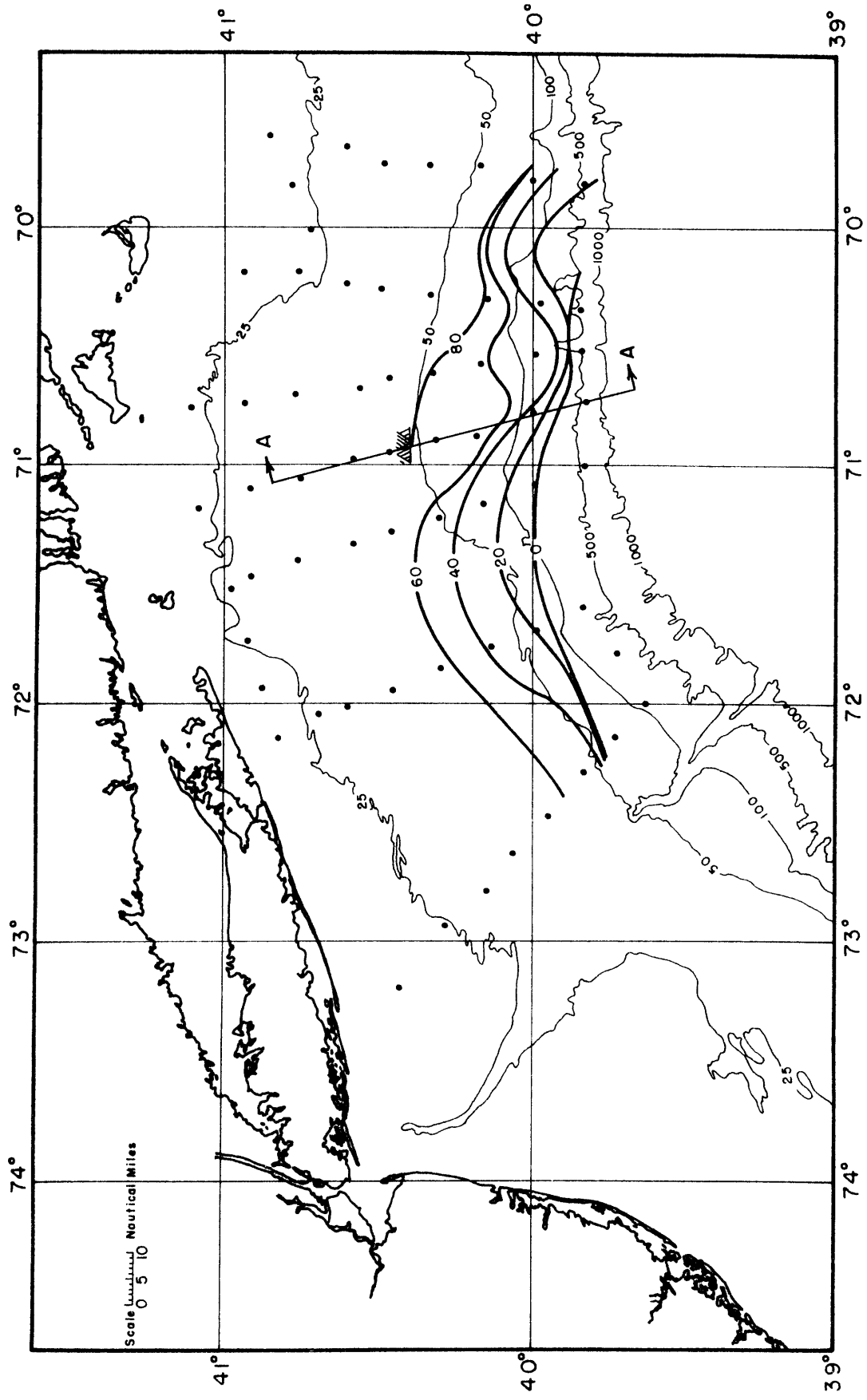


Figure 3.18 A quasi-synoptic topographic map of the 26.5 sigma-t surface taken from the cruise of the USCGC DALLAS, February 28 - March 4, 1974 at 20 meter increments from the surface. Depth contours are in fathoms. Line A-A is the cross-shelf section of Figure 3.20.

of ~ 80 km. NOAA satellite photographs indicated that there was a warm core eddy located offshore of the shelf break in the vicinity of the feature. Saunders (1973) conducted an airborne radiometry survey of an area south of Georges Bank during the last week of September 1971. Although September is not the normal time for a surface front to exist, Saunders found a strong temperature gradient occurring between Gulf of Maine and slope water. A distinctly wavelike feature was evident on the front with a wavelength of ~ 65 km, and from a succession of flights, it moved along the shelf break to the west at ~ 9 cm/sec, implying a period of 8-9 days. In particular there was no evidence for at least 100 km to the south of the presence of a Gulf Stream eddy. In 1974 we were not able to measure the propagation speed with only a single large cruise. Figure 3.19 from Ingham (1976a) shows the position of the thermal front over a 13 month period as given by satellite photographs showing large on-offshore variability. The envelope of the variation south of New England is about 250 km wide. Most of this envelope represents variations of a longer time scale than that of the single waves. Although it is hard to see, the undulations of the front at any one time are considerably smaller perhaps by a factor of ten. Thus, the front is seen to have alongshore wavelike features with wavelengths perhaps on the order of 50 to 100 km, peak to peak amplitudes of 20 to 40 km, and which from Saunders' single example, seem to propagate to the west with speeds of 5-10 cm/sec.

Although the March 1974 experiment had only one synoptic cruise, we did occupy the same cross-shelf section along the line marked A-A in Figure 3.18 four times at 8 to 10 day intervals. The position of the $26.5 \sigma_t$ contour for each cruise is shown in Figure 3.20 together with the

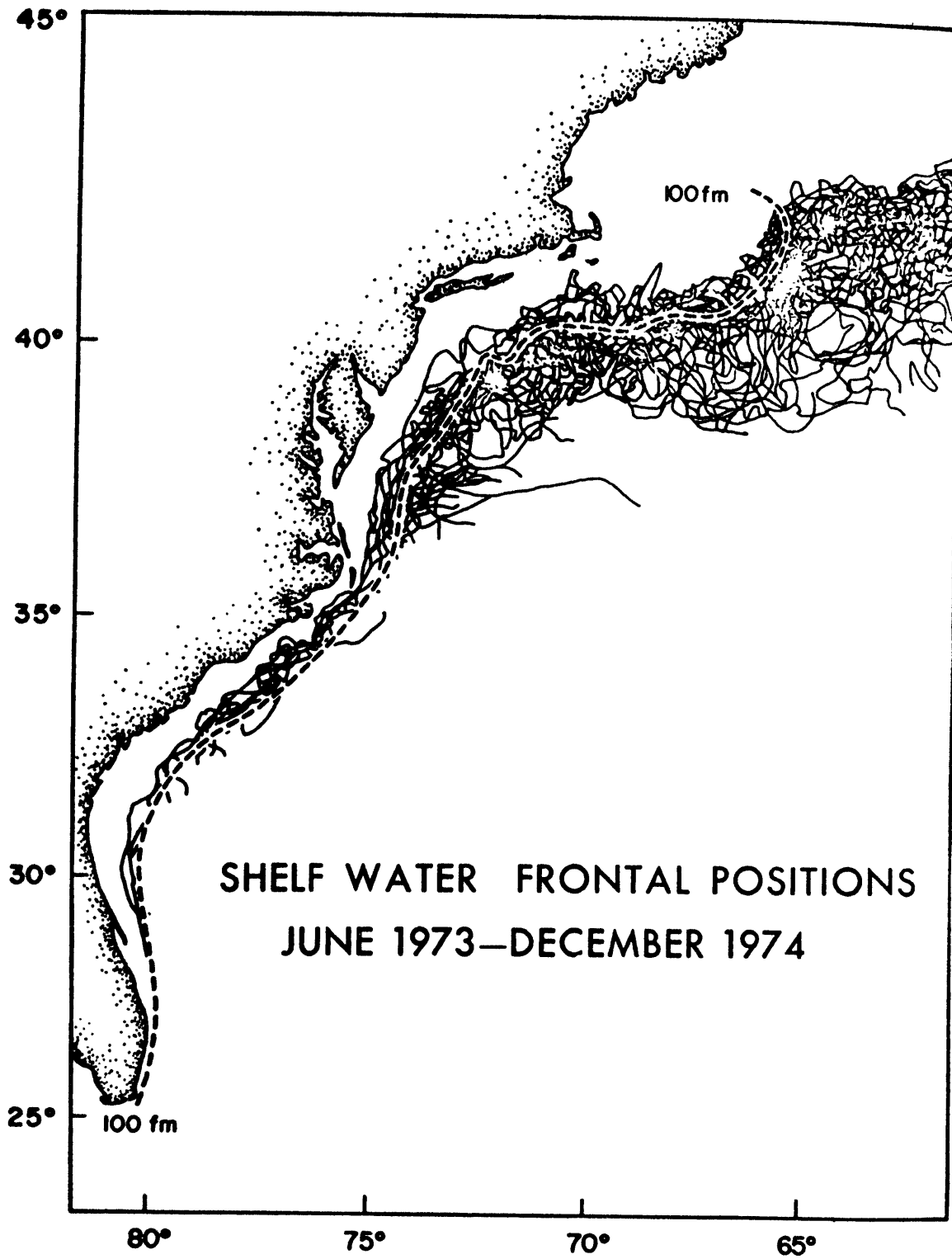


Figure 3.19 Composite plot of the positions of the shelf/slope front as observed by satellite from June 1973 to December 1974. Heavy dashed line indicates the position of the shelf break. (Taken from Ingham, 1976.)

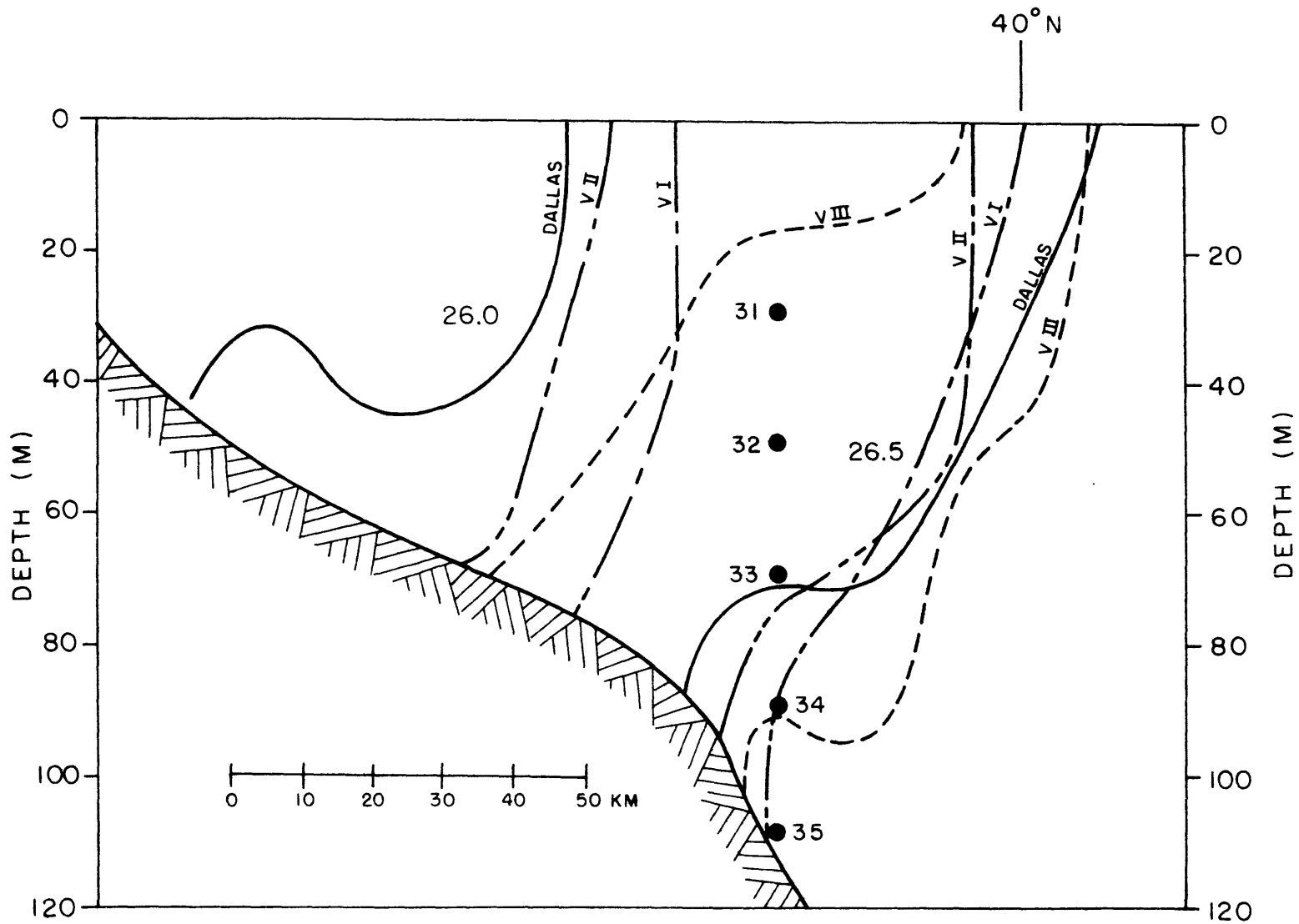


Figure 3.20 Cross-shelf profiles of the 26.0 and 26.5 sigma-t contours for each of the four cruises of the March 1974 experiment. The relative positions of the instruments on mooring 3 are illustrated.

26.0 σ_t contour which was well onto the shelf. One of the first things which is apparent is that there is a minimum in on-offshore oscillations at a depth of 50-60 m. The variation of the 26.0 σ_t contour, in relatively unstratified water, in contrast, is much larger. The mean slope of the front changes by as much as 50% which in turn implies a 50% variation in the geostrophic shear.

Table 3.5 shows the vertical dependence of the frontal position variance over the four cruises as well as the variance of the low passed currents. The table shows a variation of about ± 8 km near the surface, a minimum of ± 3.5 km at mid-depth, increasing to ± 13 km at 80 m. There is also a minimum of low-passed current variance at mid-depths which is primarily related to the alongshore component. There is one tantalizing, but perhaps questionable, piece of information about the vertical distribution of horizontal energy. Instrument 34 at 90 m had severe time base problems, but it should be possible to use the total variance since the device was recording during the whole period. The total variance at 34 was $687 \text{ cm}^2/\text{sec}^2$, or three times the level at any other depth. That large difference makes one skeptical, but it is interesting to note that it occurs at a depth corresponding to the maximum frontal position variance. The result is that the vertical distribution of frontal movement seems to be associated with a similar distribution of horizontal along-shore currents.

The only concrete evidence we have of the type of low frequency motion of the front is the oscillations forced by the wind stress discussed in Chapter 2. The important features of this motion are: 1) the forcing mechanism is the wind stress forcing an Ekman flow near surface and return flow along the bottom; 2) the front oscillated approximately

about its mean position at mid-depth; and 3) the observed period of oscillation was 3 1/2 to 4 days. The movement of the front about its mid-depth position is consistent with the vertical distributions of frontal position and horizontal current variances. It is quite probable that this behavior is symmetric with respect to the alongshore wind. There is no direct information about the alongshore behavior of the front for these oscillations. However, the length scale of the forcing storm was over 1000 km suggesting that the front moved in phase over a large portion of the coastline. In this respect, and in terms of the oscillation periods, there seems to be a clear difference between this type of motion and the alongshore undulations of Figure 3.18.

3.5 Discussion

We are at only the beginning stages of understanding the kinematics and dynamics of frontal motions especially the low frequency, short along-shore wavelength motions. At present, there seem to be three types of forcing that could be important in frontal motions. The first is advection by wind stress. We have shown one effect above but it is possible that mesoscale wind forcing could force the shorter wavelength oscillations as well. Thus, a short wavelength impulse could distort the front which then oscillates with a low frequency.

A second mechanism is the flow induced by warm core eddies thrown off by the Gulf Stream. These eddies tend to have diameters on the order of 100 km and to move along the shelf edge toward the west at a speed which varies from ~ 7 cm/sec south of Georges Bank to 3 cm/sec off the New Jersey coast (C. Parker, personal communication). These numbers are of the same order as the alongshore undulations of the front. Satellite photographs, Saunders (1973), and Morgan and Bishop (1975) have all shown the relatively large effect an eddy can have on the shelf. However, there seems to be relatively few eddies per year, something on the order of 10, to account for the seemingly more ubiquitous features in the front.

The third candidate is that frontal distortions could also be associated with low frequency energy propagating up the slope from the deep ocean. Schmitz (1974) found an energy peak for periods of ~ 10 days over the continental slope at depths of ~ 1000 m. This is close to the period of the oscillations estimated for the alongshore undulations. Niiler and Kroll (1975) suggest that barotropic energy of this time

scale could penetrate up the slope to the continental shelf. The along-shore undulations could then be passive advective effects of the shoreward propagating waves.

A last possible mechanism for explaining the frontal waves is baroclinic or barotropic instabilities caused by the 5-10 cm/sec geostrophic shear across the front. An analysis of the stability of the front is carried out in Chapter 4 with the rather discouraging result that it does not seem likely, if the model assumptions are correct, that instabilities are an active possibility. The front is indeed unstable, but the growth rates are much too slow.

To progress further in our understanding of the frontal dynamics we will need longer data series with measurements taken along the shelf break, and on the continental slope as well as on the shelf itself. There is a need for current measurements below the front to verify the existence of the velocity deficit region and to see whether the high variability measured just under the front is real.

4. Analysis of the Dynamic Stability of the Frontal Zone

4.1 Introduction

One frontal phenomenon not explained in the last chapter was the on-off shore undulation of the front as depicted by the $26.5 \sigma_t$ surface in Figure 3.18. We have shown that a large geostrophic shear is probable across the front; the presence of the available potential energy represented by this shear suggests that the frontal zone might be baroclinically unstable to small perturbations in the frontal structure. This possibility motivates the analysis presented here.

The following factors seem to be of central importance to a dynamical model of the shelf/slope front: 1) the density change across the front occurs in a fairly narrow region both vertically and horizontally; 2) the front intersects both the top and the bottom; and 3) the front straddles a region of large increase in bottom depth. Frontal stability theory has progressed to an advanced position in meteorology so that we can borrow from existing theories. A theory which includes the first two characteristics of the frontal zone above is that presented by Orlanski (1968). Orlanski examines the stability of an interface separating fluids of different density in an infinite slab confined between two rigid parallel horizontal surfaces. We propose to perform the same analysis but include the third characteristic above, a sloping topography under the front.

The theory is a perturbation expansion of the primitive Boussinesq, hydrostatic, and constant f -plane equations for small disturbances on a Margules front. Using this general formulation, we look at two special cases: 1) where the front is vertical and 2) the limit

as the Rossby number goes to zero with a steep bottom slope. For the general case it is convenient to take advantage of the small Rossby number applicable to the frontal zone south of New England. We can then use the semi-geostrophic expansion for small Ro outlined by Duffy (1976) and include the appropriate bottom topography.

The analysis shows that there are unstable waves for the parameter range pertaining to the shelf/slope front. Moreover, the predicted phase speeds and frequencies are in qualitative agreement with the observed behavior of the front. However, the growth rates associated with these unstable waves yield e-folding times so long, relative to other forcing present, as to effectively eliminate baroclinic instability as a viable explanation for the observed phenomena. The analysis does suggest that the front should occur near the shelf break where the increased bottom slope tends to stabilize the front. The same front located over the rather flat middle shelf region would be quite baroclinically unstable.

4.2 Model Development

The model development follows that of Orlandi (1968). We consider the stability of the classic Margules-type front separating two immiscible, incompressible, homogeneous, Boussinesq fluids. The region is bounded by a rigid horizontal lid and below by a two-dimensional bottom of arbitrary shape. The geometry and coordinate system are illustrated in Figure 4.1. The interface height is given by $z^* = h_I^*(x^*, y^*, t^*)$ and the interface intersects the top at $y^* = L$ and the bottom at $y^* = 0$. The Coriolis parameter, f , is constant, the motion hydrostatic, and the horizontal velocities in each layer are independent of the vertical coordinate. Let \hat{k} be the vertical unit vector, ∇^* the horizontal gradient operator and $\underline{u}_j^* = (u_j^*, v_j^*)$ the horizontal velocity vector for $j = 1$ (lower layer) and $j = 2$ (upper layer). In Region II ($0 \leq y^* \leq L$) the dynamical equations are

$$\left[\frac{\partial}{\partial t^*} + \underline{u}_j^* \cdot \nabla^* + f \hat{k} \times \right] \underline{u}_j^* = -\frac{1}{\rho} \nabla^* p_j^* \quad j=1,2, \quad 4.1$$

and

$$p_1^* = p_2^* + (\rho_1 - \rho_2) g h_I^* + \rho_2 g H, \quad 4.2$$

where p_1^* and p_2^* are the pressures at $z^* = 0$ and $z^* = H$ respectively.

The continuity equations for the two layers can be expressed as:

$$\left[(H - h_I^*) u_2^* \right]_{x^*} + \left[(H - h_I^*) v_2^* \right]_{y^*} + (H - h_I^*)_{t^*} = 0, \quad 4.3$$

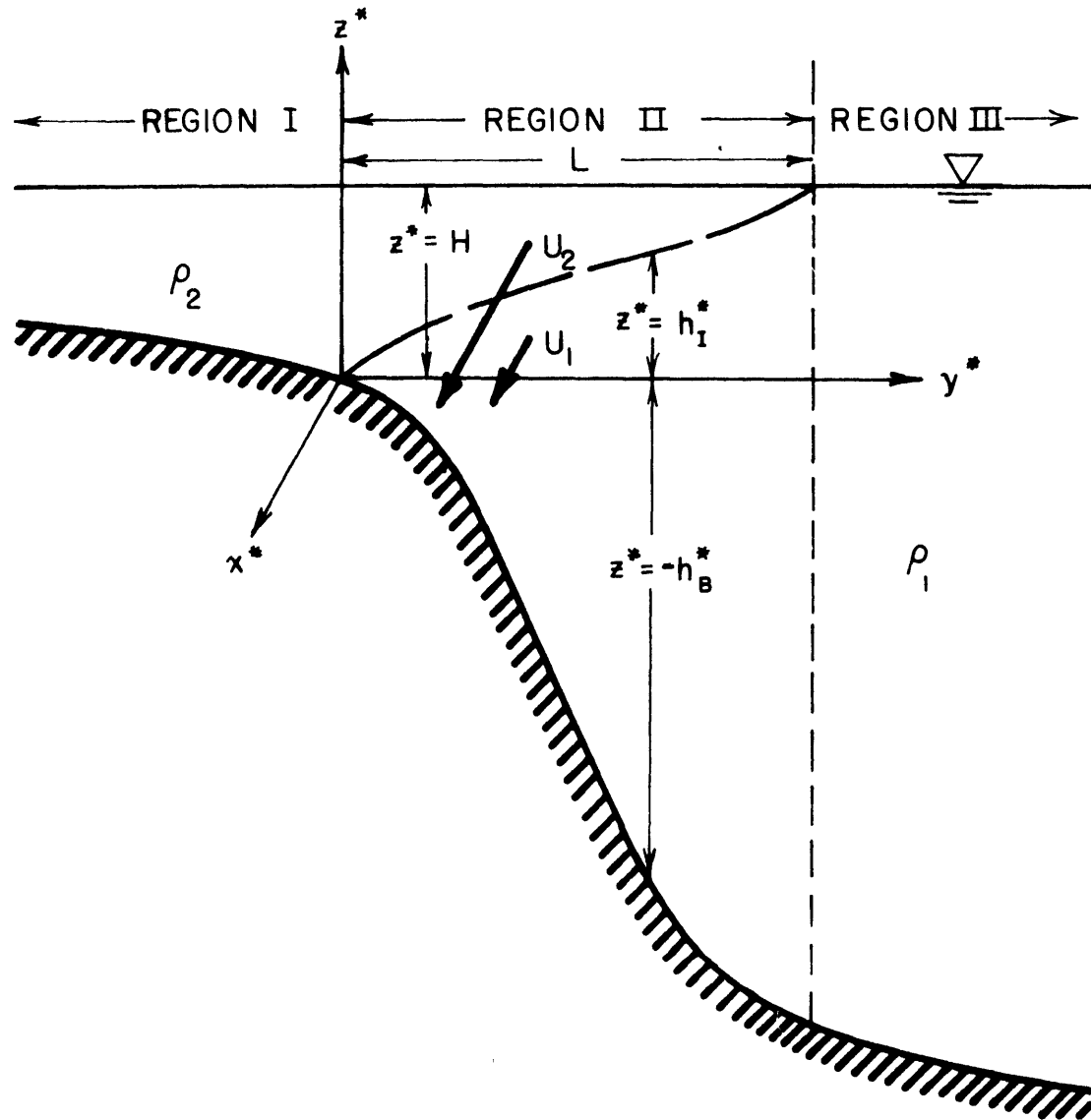


Figure 4.1 Geometry and coordinate system for the shelf/slope frontal model.

and

$$\left[(h_B^* + h_I^*) u_1^* \right]_{x^*} + \left[(h_B^* + h_I^*) v_1^* \right]_{y^*} + (h_B^* + h_I^*)_{t^*} = 0. \quad 4.4$$

The basic state is a Margules front with steady uniform along isobath flow in each layer, U_j , directed in the positive x^* direction. Equations 4.1 and 4.2 then result in a relation between the vertical shear in Region II and the slope of the interface:

$$\frac{dh_I}{dy} = \frac{f(\rho_2 U_2 - \rho_1 U_1)}{(\rho_1 - \rho_2)g} \equiv \frac{f(U_2 - U_1)}{g'} \quad 4.5$$

$$\text{where } g' = \frac{(\rho_1 - \rho_2)}{\bar{\rho}} g.$$

We non-dimensionalize the governing equations by defining

$$x = kx^*, \quad y = y^*/L, \quad z = z^*/H, \quad t = k\bar{U}t^*,$$

$$\frac{u_j}{\bar{U}} = \frac{u_j^*}{\bar{U}}, \quad w_j = \frac{w_j^*}{kH\bar{U}}, \quad \rho_1 = \frac{k}{\bar{\rho}f\bar{U}} \rho_1^*,$$

$$\rho_2 = \frac{k}{\bar{\rho}f\bar{U}} (\rho_2^* + \bar{\rho}gH), \quad h_I = h_I^*/H, \quad h_B = h_B^*/H,$$

where k will be an along-shore wavenumber and $\bar{U} \equiv 1/2(U_2 - U_1)$. This scaling results in Rossby and Richardson numbers which are defined respectively as

$$Ro = \frac{k\bar{U}}{f}, \quad Ri = \frac{gH}{(U_2 - U_1)^2} \cdot \frac{(\rho_1 - \rho_2)}{\bar{\rho}} = \frac{fL}{2\bar{U}}.$$

The scaled governing equations in Region II now become

$$R_0 \left[\frac{\partial}{\partial t} + \underline{u}_j \cdot \nabla + \hat{k} \times \right] \underline{u}_j = -\nabla p_j, \quad j = 1, 2, \quad 4.6$$

$$p_1 - p_2 = 4 R_i R_0 h_I, \quad 4.7$$

$$\left[(1 - h_I) u_2 \right]_x + \frac{1}{2 R_i R_0} \left[(1 - h_I) v_2 \right]_y - h_{I_t} = 0, \quad 4.8$$

and

$$\left[(h_B + h_I) u_1 \right]_x + \frac{1}{2 R_i R_0} \left[(h_B + h_I) v_1 \right]_y + h_{I_t} = 0, \quad 4.9$$

where the horizontal gradient operator is defined as

$$\nabla \equiv \hat{i} \left(\frac{\partial}{\partial x} \right) + \hat{j} \left(\frac{1}{2 R_i R_0} \frac{\partial}{\partial y} \right).$$

We now perturb the basic flow with a small motion of amplitude ε and use the perturbation amplitude as an expansion parameter allowing us to linearize the governing equations about the basic state. Thus we define

$$\begin{aligned} u_j &= \frac{U_j}{U} + \varepsilon u_j, & v_j &= \varepsilon v_j, \\ p_j &= \bar{p}_j + \varepsilon p_j, & \text{and } h_I &= \bar{h}_I + \varepsilon h. \end{aligned} \quad 4.10$$

The zeroth order problem is simply the basic state while the first order

equations are

$$R_0 \left[\frac{\partial}{\partial t} + \frac{u_j}{\bar{u}} \frac{\partial}{\partial x} + \hat{k} \times \right] u_j = -\nabla p_j, \quad 4.11$$

$$p_1 - p_2 = 4 R_i R_0 h, \quad 4.12$$

$$(1 - \bar{h}_I) \left(u_{2x} + \frac{1}{2 R_i R_0} v_{2y} \right) - \frac{v_2 \bar{h}_{Iy}}{2 R_i R_0} - \frac{u_2}{\bar{u}} h_x - h_t = 0, \quad 4.13$$

and

$$(h_B + \bar{h}_I) \left(u_{1x} + \frac{1}{2 R_i R_0} v_{1y} \right) + \frac{v_1 (h_B + \bar{h}_I)_y}{2 R_i R_0} + \frac{u_1}{\bar{u}} h_x + h_t = 0 \quad 4.14$$

The solution is assumed to be wavelike in x^* and t^* with an along-shore wavenumber k and a frequency σ so that u_j, v_j, p_j and $h \propto e^{i\psi}$ where $\psi = kx^* + \sigma t^* = x + \left(\frac{\sigma}{k\bar{u}}\right)t$. We will be looking for those solutions for which σ is complex and the perturbation is growing. Substitution of this form into 4.11-4.14 yields an equation for the perturbation pressures in each layer

$$p_{1yy} + \frac{(h_B + \bar{h}_I)_y}{(h_B + \bar{h}_I)} p_{1y} - \left\{ 4 R_i^2 R_0^2 + \frac{2 R_i (h_B + \bar{h}_I)_y}{(\tau-1) (h_B + \bar{h}_I)} \right\} p_1 \quad 4.15$$

$$= \frac{R_i (1 - R_0^2 (\tau-1)^2)}{(h_B + \bar{h}_I)} (p_1 - p_2),$$

$$\begin{aligned}
p_{2yy} + \frac{(1-\bar{h}_I)_y}{(1-\bar{h}_I)} p_{2y} - \left\{ 4R_i^2 R_o^2 + \frac{2R_i}{(\tau+1)} \frac{(1-\bar{h}_I)_y}{(1-\bar{h}_I)} \right\} p_2 \\
= - \frac{R_i (1 - R_o^2 (\tau+1)^2)}{(1-\bar{h}_I)} (p_1 - p_2), \quad 4.16
\end{aligned}$$

where τ is the ratio of the phase velocity plus the mean velocity to one-half the vertical shear, i.e.,

$$\tau \equiv \left(\frac{\sigma}{k} + \frac{1}{2}(u_1 + u_2) \right) / \frac{1}{2}(u_2 - u_1).$$

For Regions I and III where there is no interface, the equations for the perturbation pressures are simply

$$p_{1yy} + \frac{h_{By}}{h_B} p_{1y} - \left\{ 4R_i^2 R_o^2 + \frac{2R_i}{(\tau-1)} \frac{h_{By}}{h_B} \right\} p_1 = 0 \quad 4.17$$

$$p_{2yy} + \frac{h_{By}}{h_B} p_{2y} - \left\{ 4R_i^2 R_o^2 + \frac{2R_i}{(\tau+1)} \frac{h_{By}}{h_B} \right\} p_2 = 0.$$

The boundary conditions on the solutions are

$$\begin{aligned}
p_j &\rightarrow 0 \text{ as } x \rightarrow \pm \infty, \\
p_j &\text{ continuous at } y = 0, 1, \\
p_j &\text{ be regular at } y = 0, 1.
\end{aligned} \quad 4.18$$

The regularity condition is necessitated by the requirement that p_j and its derivatives be finite in the apex regions where the interface intersects the top and bottom and where equations 4.15 and 4.16 are singular. This can be translated into quantitative boundary conditions

on p_j by insisting that the vertical velocity at the interface match the required vertical velocity where the interface contacts the top or bottom. This yields the boundary condition that

$$p_{1y} - \frac{2R_i}{(\tau-1)} p_1 = \frac{R_i(1-R_o^2(\tau-1)^2)}{(h_o + \bar{h}_I)_y} (p_1 - p_2) \text{ at } y=0, \quad 4.19$$

$$p_{2y} - \frac{2R_i}{(\tau+1)} p_2 = -\frac{R_i(1-R_o^2(\tau+1)^2)}{(1 - \bar{h}_I)_y} (p_1 - p_2) \text{ at } y=1.$$

We let the depths in Region I and III be constant, for analytical simplicity and because it is not expected that the details of the bottom topography in these regions have much effect on the stability of the interface. This results in a continental slope region confined to be only under the front and a relatively shallow ocean depth. Figure 4.2 illustrates the cross-shelf bottom topography south of New England with the idealized model topography superposed. Equation 4.17 then becomes simply

$$p_{jyy} - 4R_i^2 R_o^2 p_j = 0$$

so that $p_j \propto e^{\pm 2R_i R_o y}$. The boundary conditions at infinity then give

$$p_1 \propto e^{-2R_i R_o (y-1)}, \quad y \geq 1, \quad 4.20$$

$$p_2 \propto e^{2R_i R_o y}, \quad y \leq 0.$$

From this result and the condition that the solutions be continuous at $y = 0, 1$, we get the remaining necessary boundary conditions that

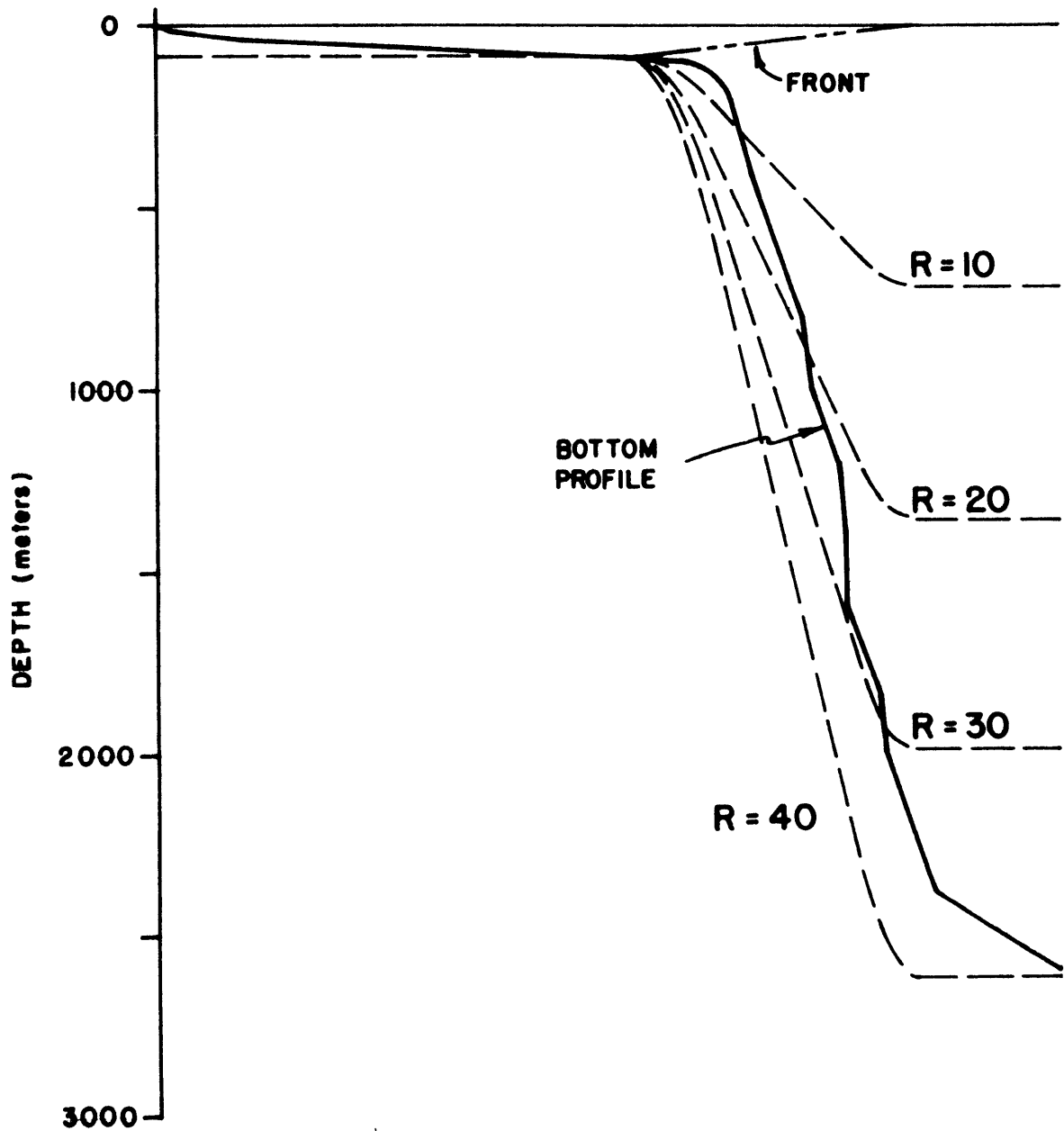


Figure 4.2 Topography of the shelf, slope, and rise along a cross-shelf transect south of New England with the idealized model topography for values of R of 10, 20, 30, and 40 superposed.

$$\frac{dP_2}{d\gamma} = 2 Ri Ro P_2 \quad \text{at } \gamma = 0,$$

4.21

$$\frac{dP_1}{d\gamma} = -2 Ri Ro P_1 \quad \text{at } \gamma = 1.$$

Equations 4.15 and 4.16 together with the boundary conditions 4.19 and 4.21 form an eigenvalue problem for τ . Note that the eigenvalue is non-linear in the interior and boundary equations so that the problem cannot be cast in a simple canonical form.

From the hydrographic data of the 1974 MIT Shelf Dynamics Experiment (Flagg and Beardsley, 1975) and the historical data given by Bigelow (1933), Bigelow and Sears (1935), Cresswell (1967), and Wright (1976), we can construct a fairly complete picture of the alongshelf as well as the cross-shelf structure of the wintertime frontal zone south of New England. This data base indicates that the center of the front is generally marked by the 10°C isotherm, the 34.5 ‰ isohaline, and the 26.5 isopycnal. Using this as a basis, we estimate the values or ranges of the different scaling parameters to be

$$L \cong 25-60 \text{ km},$$

$$H \cong 85 \text{ m},$$

$$U_2 - U_1 \cong 5-10 \text{ cm/sec},$$

$$\lambda \cong 25-100 \text{ km},$$

$$f = .9375 \times 10^{-4} \text{ sec}^{-1}.$$

From these we estimate that the Richardson and Rossby numbers vary between $23 \leq Ri \leq 113$ and $0.02 \leq Ro \leq 0.13$.

The other important parameter to be considered characterizes the slope of the bottom. If we let s be the maximum slope of the bottom, then we can define a bottom slope parameter as

$$R \equiv sL/H.$$

The maximum slope of the continental slope region south of New England ranges from 0.03 to 0.05 so that the parameter, R , has a range

$$10 \leq R \leq 50.$$

Solution of the theoretical problem yields eigenvalues, τ , which will have non-zero imaginary parts, τ_i , for unstable modes. These eigenvalues determine the important characteristics of the modes, i.e., their growth rates, phase speeds, and periods. Figures 4.3, 4.4, and 4.5 illustrate how the growth rate, phase speed, and periods vary respectively with alongshore wavelength and cross-frontal shear.

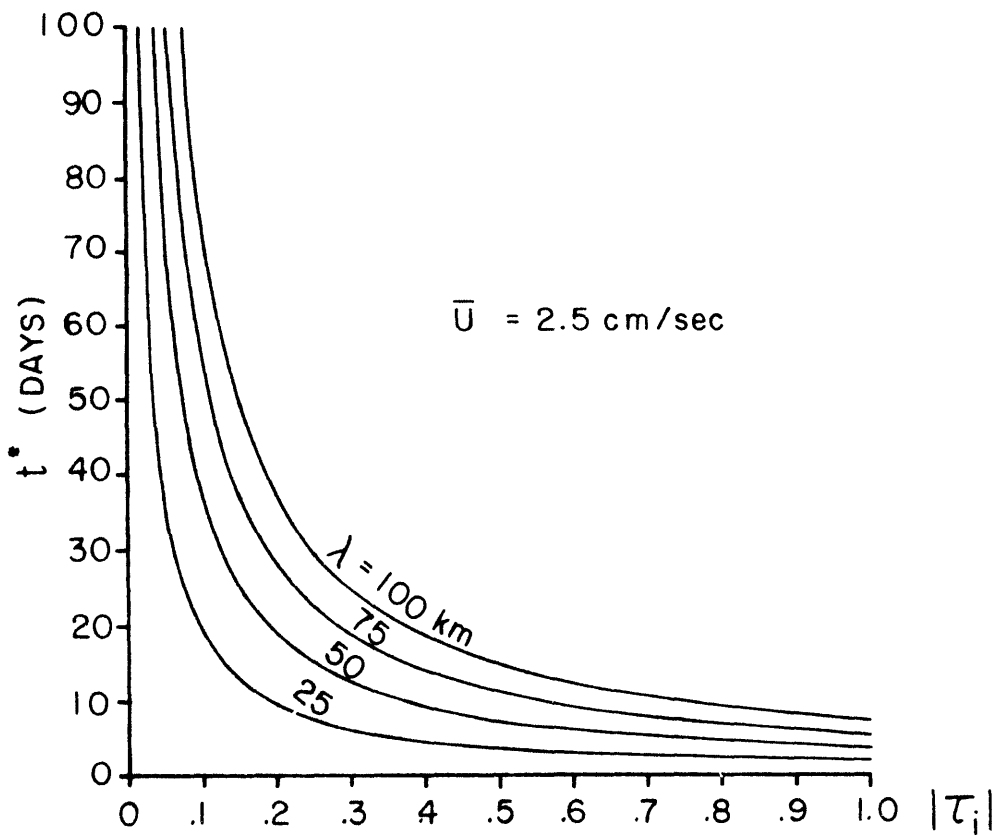
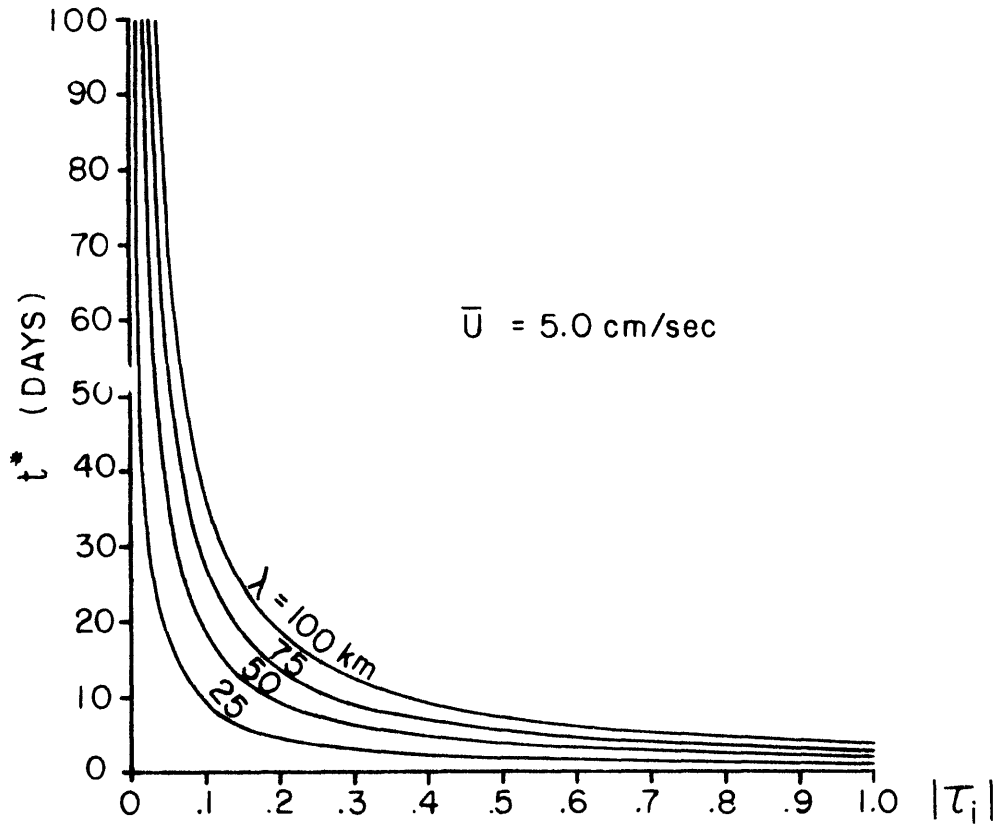


Figure 4.3 The dependence of the e-folding time, t^* , upon the imaginary part of the eigenvalue, $|\tau_i|$, the alongshore wavelength, λ , and the vertical shear.

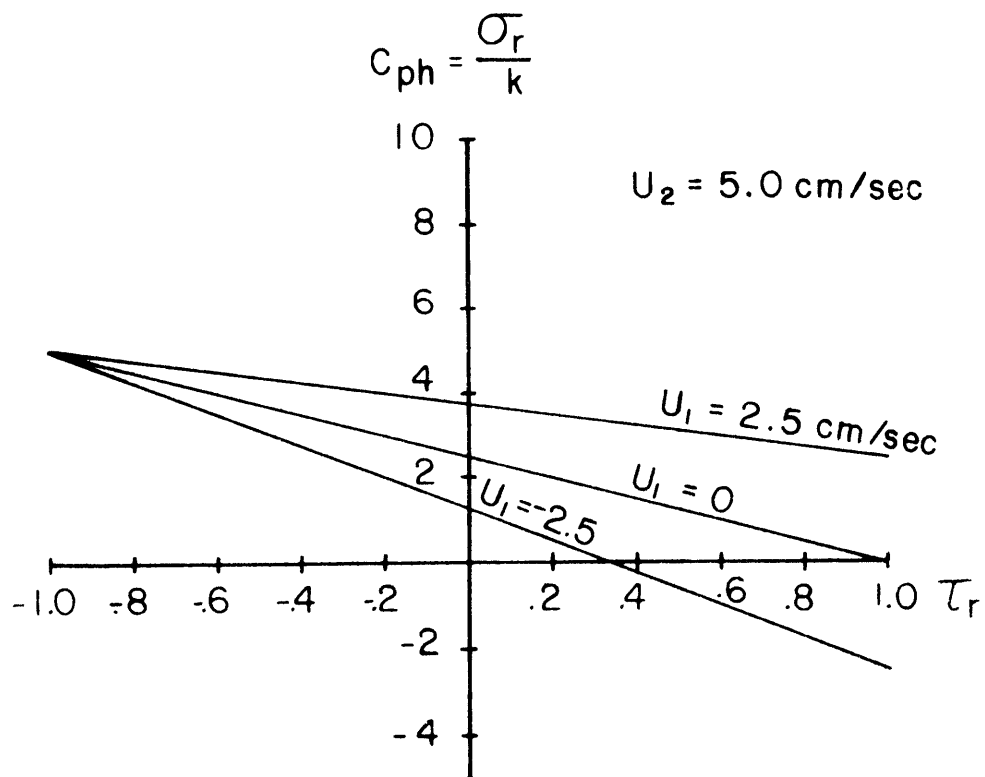
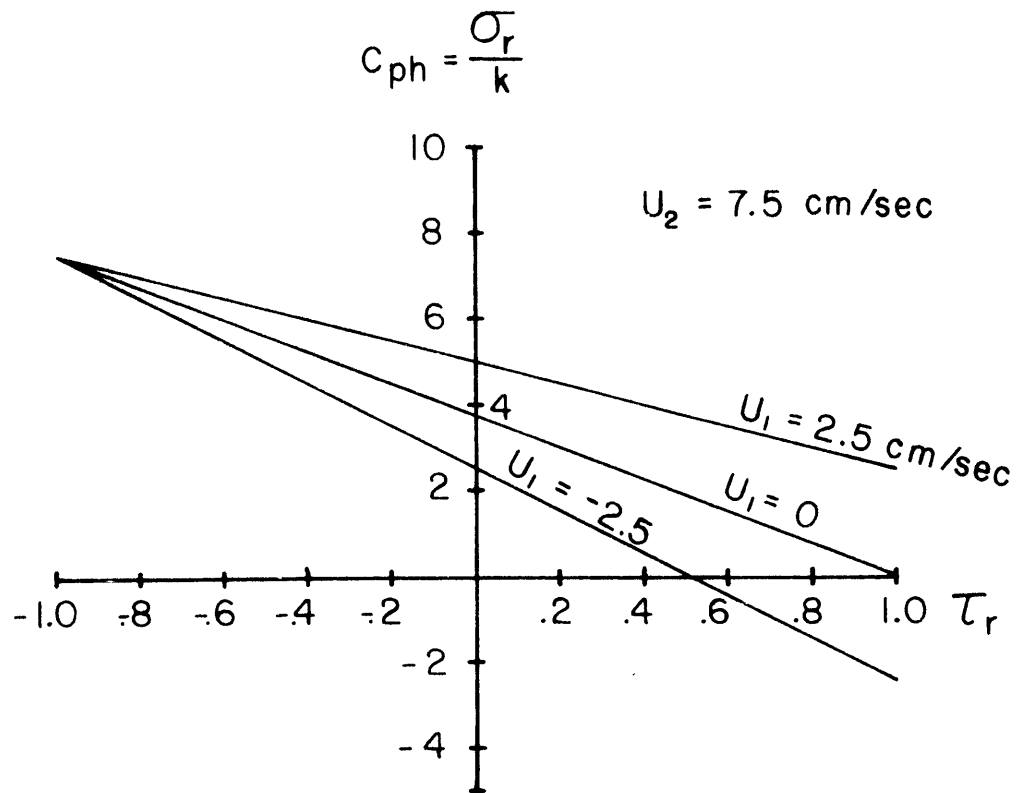


Figure 4.4 The dependence of the alongshore phase speed upon the real part of the eigenvalue and the vertical shear.

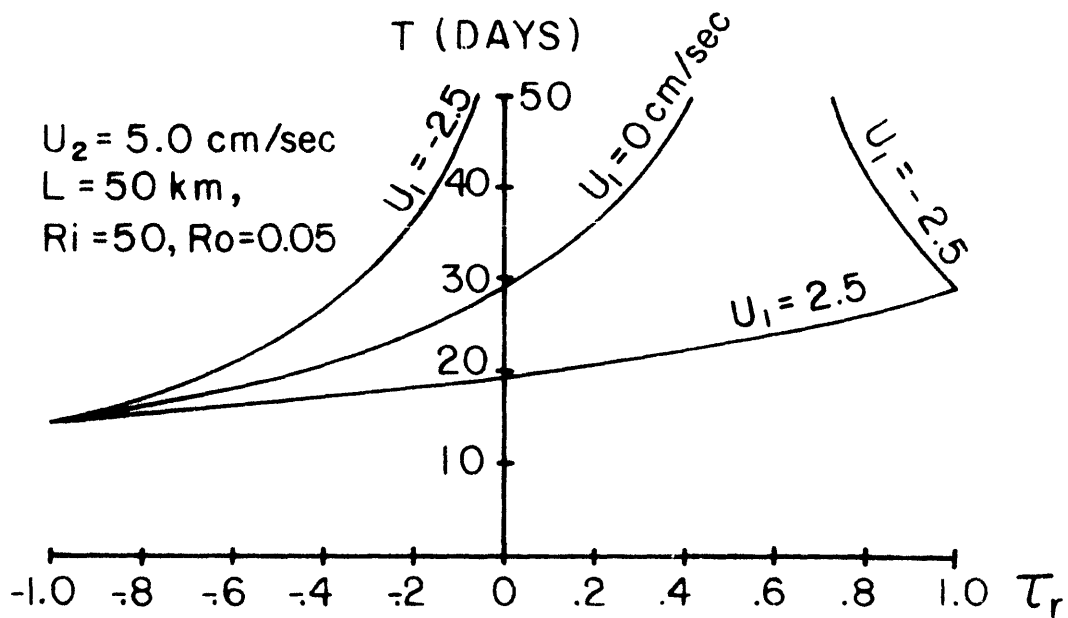
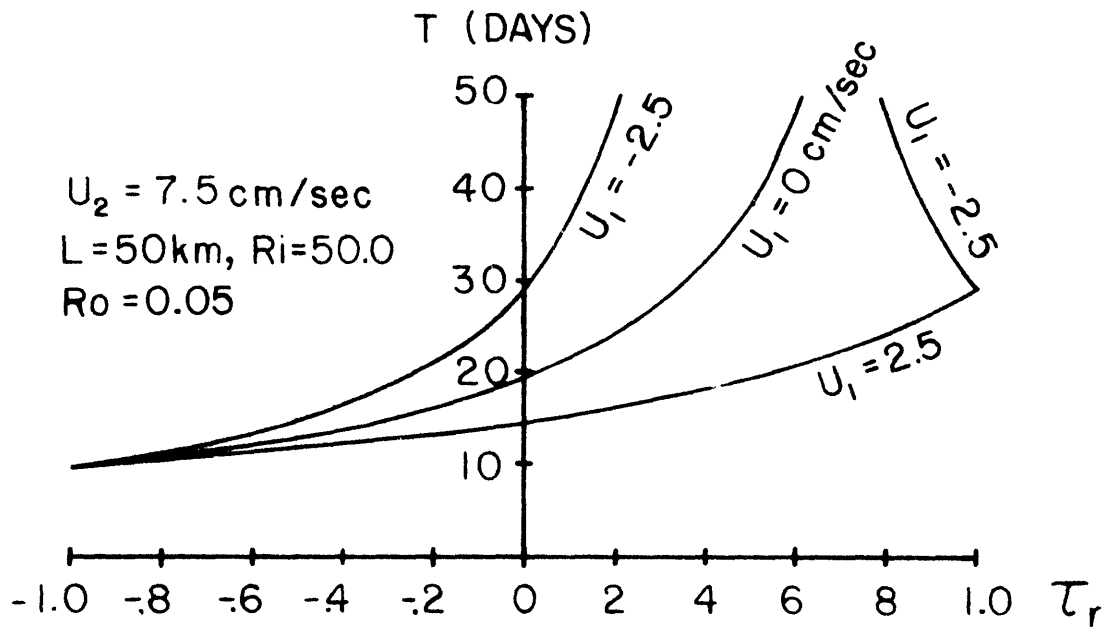


Figure 4.5 The dependence of the wave period upon the real part of the eigenvalue and the vertical shear for a frontal zone width of 50 km with $Ro = 0.05$, and $Ri = 50.0$.

4.3 Special Cases

4.3.1 Shear Waves

Before discussing the general results, let us consider the special case where the fluid interface is vertical, i.e., $\rho_1 = \rho_2$, and any instabilities present are due to the horizontal shear, the Rayleigh instability limit. This is similar to the situation that exists over the main part of the shelf during the winter months when the isopycnals are nearly vertical to within a few meters of the bottom. We proceed similar to Orlanski (1968).

For this case, the interface becomes vertical ($L \rightarrow 0$) and the density difference ($\Delta\rho$) and Region II disappear. Using the dimensional forms of the variables but dropping the (*) notation, we now have a horizontal displacement of the interface given by

$$\Delta(x, t) = \text{Re } D e^{i\psi}, \quad 4.22$$

where D is a constant. In Regions I and III, the governing equations are the dimensional form of equation 4.17, i.e.,

$$\begin{aligned} p_{jyy} + \frac{h_{By}}{h_B} p_{jy} - \left\{ k^2 + \frac{fk}{(\sigma + kU_j)} \frac{h_{By}}{h_B} \right\} p_j \\ = 0 \quad ; \quad j = 1, 2. \end{aligned} \quad 4.23$$

We take the bottom to be exponential, $h_B = h_0 e^{sy}$, so that the coefficients in equation 4.23 become constant, i.e.,

$$p_{jyy} + s p_{jy} - \left\{ k^2 + \frac{fks}{(\sigma + kU_j)} \right\} p_j = 0; \quad j = 1, 2. \quad 4.24$$

The solutions to 4.24 are of the form $p_j \propto e^{\pm l_j y}$ where the l_j 's are positive quantities given by

$$l_j = \frac{-s + \sqrt{s^2 + 4k^2 + 4fks/(\sigma + kU_j)}}{2} \quad 4.25$$

The boundary conditions at $y = \pm \infty$ imply that

$$\begin{aligned} p_1 &= A e^{-l_1 y}, \quad y \geq 0, \\ p_2 &= B e^{-l_2 y}, \quad y \leq 0, \end{aligned} \quad 4.26$$

where A and B are constants. The dynamic boundary condition at the interface (continuity of normal pressure) requires

$$(p_1 - p_2)_{y=0} = A - B = -f\rho(U_2 - U_1)D, \quad 4.27$$

while the kinematic boundary condition is

$$\begin{aligned} i(\sigma + kU_1)D &= v_1(0), \\ i(\sigma + kU_2)D &= v_2(0). \end{aligned} \quad 4.28$$

The velocities v_1 and v_2 are obtained from equation 4.1 by eliminating u_j and substituting the forms for p_j from 4.26 to get

$$\begin{aligned} v_1(0) &= \frac{i[fk + (\sigma + kU_1)l_1]A}{\rho[f^2 - (\sigma + kU_1)^2]}, \\ v_2(0) &= \frac{i[fk - (\sigma + kU_2)l_2]B}{\rho[f^2 - (\sigma + kU_2)^2]}. \end{aligned} \quad 4.29$$

Equations 4.28 and 4.29 together with equation 4.27 form a homogeneous

set of three equations for the amplitudes A, B, and D.

For a non-trivial solution to exist, the determinant must vanish, thus yielding the dispersion relationship. It is convenient to define variables ξ_1 and ξ_2 which approach unity as the bottom slope, characterized by $r \equiv s/k$, goes to zero:

$$\xi_1 = -\frac{r}{2} + \sqrt{1 + r^2/4 + r/R_0(\tau-1)},$$

$$\xi_2 = -\frac{r}{2} + \sqrt{1 + r^2/4 + r/R_0(\tau+1)}.$$

The determinant can then be written in the form

$$\begin{aligned} \delta \equiv & R_0^2(\xi_1 + \xi_2) \tau^4 + 2 R_0^2(\xi_1 - \xi_2) \tau^3 \\ & - (\xi_1 + \xi_2 + 2 R_0 \xi_1 \xi_2 - 6 R_0) \tau^2 \\ & + 2(\xi_1 - \xi_2)(1 - R_0^2) \tau - (\xi_1 + \xi_2)(1 + R_0^2) + 2 R_0 \xi_1 \xi_2 + 2 R_0 = 0. \end{aligned} \quad 4.30$$

In the limit of zero bottom slope, ξ_1 and $\xi_2 \rightarrow 1$ and 4.30 remains a quartic equation for τ with roots

$$\tau = \pm(1 - 1/R_0), \text{ and } \tau = \pm i.$$

The first set of roots are stable inertial waves while the growing root of the second set represents a Rayleigh instability for shearing flow in a homogeneous fluid.

For $r \neq 0$, equation 4.30 is no longer quartic since τ is contained in the ξ_i 's and would be formidable to solve analytically. However, it is straight forward to obtain the roots numerically. As one might expect, for small r ($\leq .05$) there are 4 roots; however, very quickly as

r increases the stable inertial roots disappear leaving only the growing and damped waves which remain as a complex conjugate pair.

The dependence of τ on the slope parameter and the Rossby number is shown in Figure 4.6, where only the growing root is included. The magnitude of the growth parameter, τ_i , decreases quickly from 1 at $r = 0$ to about 1/2 as r increases, dropping faster although not as far as R_0 is decreased. As r increases past $r = 1$, the magnitude of τ_i decreases much more gradually with the rate of decrease being less for smaller R_0 . The non-dimensionalized phase speed, τ_r , becomes negative for non-zero r . The magnitude has a relative peak for $r < 0.2$, then a relative minimum followed by a gradual increase with increasing r . τ_r is larger for larger Rossby numbers. Thus the presence of a bottom slope acts as a stabilizing factor while increasing the rotation rate or the wavelength, i.e., decreasing R_0 , is destabilizing.

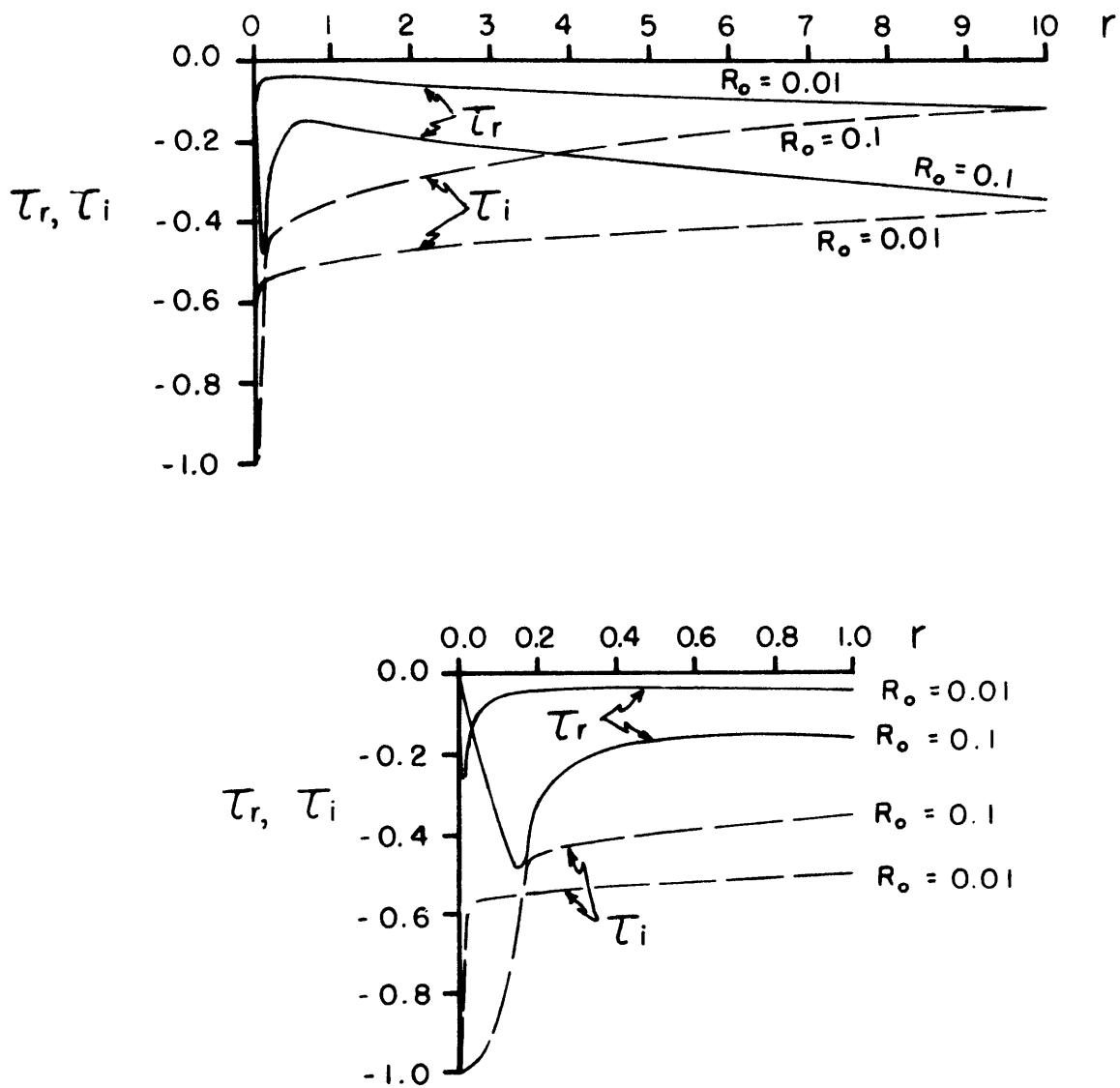


Figure 4.6 Dependence of the real and imaginary part of the eigenvalue and the vertical shear for a frontal width of 50 km and for $R_o = 0.05$, $R_i = 50.0$.

4.3.2 Large Slope and Small Rossby Number

We consider next the special case for very large slope and very small Rossby number by formally setting the non-dimensionalized bottom slope in Region II to be equal to the reciprocal of the Rossby number, i.e., $s = 1/R_0$ where $h_B = sy$. The interface depth is given by $\bar{h}_I = y$, so that equations 4.15 and 4.16 become

$$\begin{aligned} (R_0+1)y p_{1yy} + (R_0+1)p_{1y} - \left\{ 4R^2R_0^2(R_0+1)y + \frac{2R_i}{(\tau-1)}(R_0+1) \right\} p_1 \\ = R_i (1 - R_0^2(\tau-1)^2) (p_1 - p_2), \end{aligned} \quad 4.31$$

$$\begin{aligned} (1-y) p_{2yy} - p_{2y} - \left\{ 4R_i^2R_0^2(1-y) - \frac{2R_i}{(\tau+1)} \right\} p_2 \\ = -R_i (1 - R_0^2(\tau+1)^2) (p_1 - p_2). \end{aligned} \quad 4.32$$

A perturbation expansion for p_j in powers of R_0 yield for the zeroth order problem

$$y p_{1yy}^{(0)} + p_{1y}^{(0)} - \frac{2R_i}{(\tau-1)} p_1^{(0)} = 0, \quad 4.33$$

$$(1-y) p_{2yy}^{(0)} - p_{2y}^{(0)} + \frac{2R_i}{(\tau+1)} p_2^{(0)} = -R_i (p_1^{(0)} - p_2^{(0)}). \quad 4.34$$

This particular expansion decouples the dynamics of the upper layer from that of the lower layer although the lower layer acts as the forcing term

for the upper layer through the right-hand side of 4.34. The boundary conditions at $y = 0, 1$ simplify to

$$p_{1y}^{(0)} - \frac{2R_i}{(\tau-1)} p_1^{(0)} = 0, \quad p_{2y}^{(0)} = 0, \quad \text{at } y = 0, \quad 4.35$$

$$p_{1y}^{(0)} = 0, \quad p_{2y}^{(0)} + \frac{2R_i}{(\tau+1)} p_2^{(0)} = -R_i (p_1^{(0)} - p_2^{(0)}), \quad \text{at } y = 1.$$

Thus, $p_1^{(0)}$ is independent of $p_2^{(0)}$ even in the boundary conditions so that $p_1^{(0)}$ and a dispersion relationship may be found separate of $p_2^{(0)}$. The solutions to 4.33 are Bessel functions of the form (Hildebrand, 1962)

$$p_1^{(0)} = Z_0 \left(2\sqrt{\frac{2R_i}{1-\tau}} y^{1/2} \right).$$

If the quantity $\left(\sqrt{\frac{2R_i}{1-\tau}} \right)$ is real, then $Z_0 = c_1 J_0 + c_2 Y_0$ where J_0 and Y_0 are Bessel functions of the first and second kind; if

$\left(\sqrt{\frac{2R_i}{1-\tau}} \right)$ is complex, then $Z_0 = \gamma_1 I_0 + \gamma_2 K_0$ where I_0 and K_0 are modified Bessel functions of the first and second kind. τ would be complex for unstable waves; however, the boundary conditions on $p_1^{(0)}$ cannot be met by the modified Bessel functions. Since $Y_0(0)$ and $Y_1(0)$ are both infinite, $c_2 = 0$. The boundary condition at $y = 1$ then yields the dispersion relation that

$$J_1 \left(2\sqrt{\frac{2R_i}{1-\tau}} \right) = 0.$$

There is an infinity of zeros for $J_1(\lambda) = 0$; the first few roots are shown in Table 4.1 together with the values for τ for several Richardson numbers (Abramowitz and Stegun, 1964).

Orlanski (1968) showed that as $R_0 \rightarrow 0$ for the flat bottom case, unstable waves exist for $Ri \geq 2.0$ and that they have the character of

TABLE 4.1

n	$2\sqrt{\frac{2 Ri}{1-\tau}}$	τ		
		Ri = 1	Ri = 10	Ri = 100
0	0	$-\infty$	$-\infty$	$-\infty$
1	3.83171	0.4551	-4.4488	-53.4885
2	7.01559	0.8375	-0.6254	-15.2540
3	10.17347	0.9227	0.2270	-6.7295
4	13.32369	0.9549	0.5493	-3.5065
5	16.47063	0.9705	0.7051	-1.9490

Table 4.1 The eigenvalues, τ , of the large slope, small Rossby number special case given by the zeroes of the Bessel function of the first kind $J_1\left(2\sqrt{\frac{2 Ri}{1-\tau}}\right)$ for three values of the Richardson number: Ri = 1, 10, and 100.

Eady's quasi-geostrophic baroclinic instabilities receiving energy from the mean potential energy field. The present case shows that the instabilities of the Eady type are completely stabilized for sufficiently large bottom slopes and for small Rossby numbers.

4.4 The General Case

4.4.1 Flat Topography

Orlanski (1968) explored the general problem as given in equations 4.15, 4.16, 4.19, and 4.21 for a flat bottom in the parameter range: $0 \leq Ri \leq 5$, $0 \leq R_o \leq 3$. Unstable waves existed over the whole parameter range with the magnitude of the imaginary part of the eigenvalue, $|\tau_i|$, generally decreasing from 1 at $Ri = 0$ or $R_o = 0$ as Ri and/or R_o were increased. His instability diagram indicates the existence of several wave modes with the number and type of modes occurring dependent upon the values of Ri and R_o . Multimodes were shown to exist for $R_o \lesssim 1$ and $Ri \gtrsim 2$ with a new mode for small R_o appearing as Ri became successively larger than $n(n + 1)$, where $n = 1, 2, 3, \dots$. In general, each mode is characterized by the degree to which it obtains energy from three different sources. The first of these energy sources is the available potential energy of the mean flow from the sloping interface; modes deriving their growth predominantly from this source are termed baroclinically unstable. The other two instability mechanisms derive energy from the mean motion either through a Rayleigh-type instability due to the horizontal shear and/or through a Kelvin-Helmholtz-type instability due to the vertical shear interacting with gravity. Modes obtaining energy mainly from the mean kinetic energy in this manner are termed barotropic instabilities. However, only in the limiting cases are the instabilities of purely one type; energy is generally obtained from two or more sources, although often one source predominates.

4.4.2 Semi-Geostrophic Approximation

The solution of the general problem is difficult because the governing equations 4.15 and 4.16 and the boundary conditions 4.19 and 4.21 are non-linear in the eigenvalue, τ , although linear in the p_j 's. Orlanski (1968) resorted to a numerical shooting technique. With an initial guess made for the eigenvalue and the pressures at $y = 0$, the pressures were integrated across Region II and a comparison made with the desired boundary conditions at $y = 1$. If necessary, corrections were made and the process repeated. This iterative technique was suitable for the parameter regime covered by Orlanski but is not particularly adaptable to the parameter regime of the New England continental shelf. As Orlanski showed, the number of modes present increases as the Richardson number is increased. We shall see, in addition, that the presence of bottom topography also increases the number of modes. The iterative method applied to this multimode problem is very sensitive to the initial guess. The method will frequently fasten onto a stable model or one that has already been obtained. For this reason, it is difficult to be sure that all the models have been found for a given set of parameters.

This difficulty can be avoided by noting that we are interested in geophysical flows characterized by very small Rossby numbers. Thus we can make the "semi-geostrophic" approximation, valid for small Ro , which has been successfully tested by Duffy (1976), to describe the instability processes for frontal waves over flat topography. This approximation neglects the substantial derivative of the ageostrophic part of the horizontal velocity. Therefore, the scaled horizontal

momentum equations (the counterpart to equations 4.6) reduce to

$$R_0 \left\{ \frac{\partial}{\partial t} + u_j \cdot \nabla \right\} p_{jx} + \frac{1}{2R_i R_0} p_{jy} + u_j = 0,$$

$$-\frac{R_0}{2R_i R_0} \left\{ \frac{\partial}{\partial t} + u_j \cdot \nabla \right\} p_{jy} + p_{jx} - v_j = 0.$$

Equations 4.7, 4.8, and 4.9 remain the same. The small amplitude perturbation expansion can be used as before to derive the following governing equations for the perturbation pressures in Region II:

$$p_{1yy} + \frac{(h_B + \bar{h}_I)_y}{(h_B + \bar{h}_I)} p_{1y} - \left\{ 4R_i^2 R_0^2 + \frac{2R_i}{(\tau-1)} \frac{(h_B + \bar{h}_I)_y}{(h_B + \bar{h}_I)} \right\} p_1 = \frac{R_i (p_1 - p_2)}{(h_B + \bar{h}_I)}$$

4.36

$$p_{2yy} + \frac{(1 - \bar{h}_I)_y}{(1 - \bar{h}_I)} p_{2y} - \left\{ 4R_i^2 R_0^2 + \frac{2R_i}{(\tau+1)} \frac{(1 - \bar{h}_I)_y}{(1 - \bar{h}_I)} \right\} p_2 = -\frac{R_i (p_1 - p_2)}{(1 - \bar{h}_I)}$$

The boundary conditions at $y = 0, 1$ simply reduce to

$$\left. \begin{aligned} p_{1y} - \frac{2R_i}{(\tau-1)} p_1 &= \frac{R_i (p_1 - p_2)}{(h_B + \bar{h}_I)_y} \\ p_{2y} &= 2R_i R_0 p_2 \end{aligned} \right\} \text{at } y=0, \quad 4.37$$

$$\left. \begin{aligned} p_{1y} &= -2R_i R_0 p_1 \\ p_{2y} - \frac{2R_i}{(\tau+1)} p_2 &= -\frac{R_i (p_1 - p_2)}{(1 - \bar{h}_I)_y} \end{aligned} \right\} \text{at } y=1.$$

Note that the right hand side of the interior equations and the boundary conditions are everywhere independent of τ , in contrast to the nonlinear dependence exhibited in the original set (4.15, 4.16, and 4.19). With

some slight manipulations, this set can be cast into the canonical form of a standard eigenvalue problem and solved numerically. As a result, all of the eigenvalues for a given set of R_i , R_o , and R can be determined at once. Numerical values of the imaginary parts of the eigenvalues obtained by this method are somewhat less, by 2% to 7%, than values obtained by Orlanski's shooting technique applied to the complete equations.

Duffy (1976) used this formulation for the flat bottom case over the parameter range: $0 \leq R_o \leq 1$, $0 \leq R_i \leq 25$, and $R = 0$ to determine how faithfully the approximation duplicated Orlanski's results using the complete primitive equations for the frontal instability analysis. As expected, the accuracy obtained is dependent upon the Rossby number. Quite good agreement was found for $R_o \leq 0.2$, taking into account that the semi-geostrophic approximation filters out some of the high frequency oscillations. The essential character of the instabilities in terms of the mode shapes and energy transfers is retained.

The numerical solution method makes use of subroutines provided in the IMSL Scientific Subroutine Package (1975) for finding eigenvalues and eigenvectors of general matrices. Region II between $y = 0$ and $y = 1$ was divided into 40 equally spaced intervals and a simple central difference scheme used to model equations 4.36. Although it is possible to use any bottom contour in Region II, we have used a family of depth profiles composed of a linear portion between two parabolic regions. The ratio of the slope of the linear region to the slope of the basic state's interface is given by the parameter R . The two parabolic regions provide a smooth matching of the central linear slope and the flat topographies of Region I and III with the intent that short wavelength

oscillations in y are not introduced artificially by nonuniformities in the bottom profile. The parabolic portions occupy $0 \leq y \leq 0.3$ and $0.8 \leq y \leq 1$ (see Figure 4.2).

We have not exhaustively explored the whole parameter regime of the continental frontal zone but rather have concentrated upon determining the behavior of the eigenvalues for representative values of the Rossby and Richardson numbers as the slope parameter is increased. Thus we have concentrated on solutions for $Ro = 0.05$, $Ri = 5, 25, 50$ with the slope parameter $0 \leq R \leq 10$. Figure 4.7 illustrates the three-dimensional parameter space with the bold lines and dots showing those cross-sections and additional points in the space that have been examined. Most of the interesting behavior of τ_i occurs for the range of bottom slope $0 \leq R \leq 10$. We have also calculated values of τ at some of the extremes of the parameter space to verify that the general conclusions still hold.

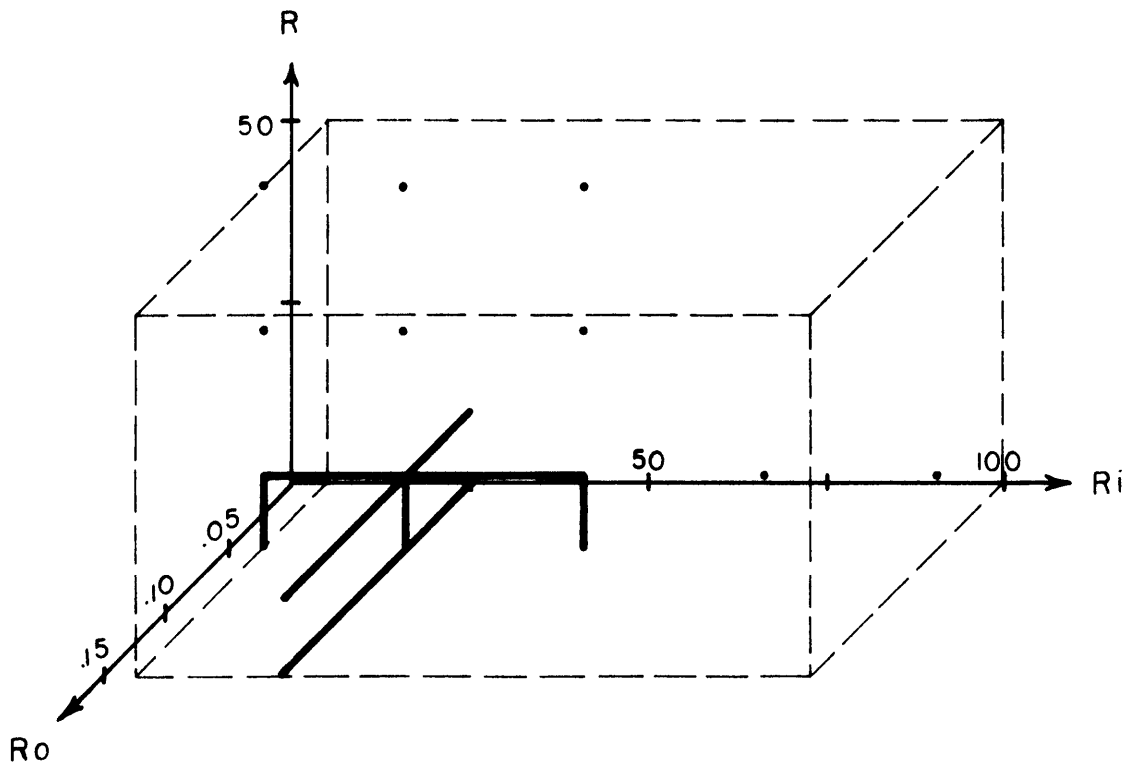


Figure 4.7 Diagram of the three-dimensional parameter space for the general stability problem pertinent to the New England shelf/slope front. The bold lines and dots indicate those cross-sections and additional points for which solutions have been computed.

4.4.3 Slope Topography

Figures 4.8, 4.9, and 4.10 illustrate the behavior of the imaginary parts of the eigenvalues with increasing bottom slope with $Ro = 0.05$ for values of Ri equal to 5.0, 25.0, and 50.0 respectively. The dominant feature of the behavior is that the magnitude of the growth rate parameter, $|\tau_i|$, decreases as the bottom slope is increased. Starting at $R = 0.0$, an envelope of the maximum values of $|\tau_i|$ decreases from 0.4 - 0.7 approximately exponentially so that at $R = 10$ the maximum values for $|\tau_i|$ are all less than 0.1. The major portion of the decrease in $|\tau_i|$ occurs for $R < 1.0$.

Inside the envelope several modes exist. At $R = 0.0$, unstable modes occur in pairs having paired negative complex conjugate eigenvalues. That is, the paired modes have phase speeds equal and opposite relative to the mean of U_1 and U_2 and equal growth rates. For those cases where there are an odd number of modes present at $R = 0.0$, the odd mode eigenvalue has zero real part corresponding to a phase velocity equal to the mean of U_1 and U_2 . As the bottom slope is increased from 0.0, the values for $|\tau_i|$ decrease, the paired modes split apart, and a non-zero negative value for τ_r appears for the odd mode. In general, those modes with positive values for τ_r are unstable over a larger range of bottom slopes. Thus waves that have a phase velocity either smaller than the mean of U_1 and U_2 , or in the opposite direction (eastward) are somewhat less affected by an increase in the bottom slope. A striking feature is the cusped nature of the instability curves. The cusps are associated with an abrupt increase in the cross-shelf wavenumber as the parameter regime passes some critical point. The appearance of a cusp is also accompanied by a sharp increase in the phase speed. The figures

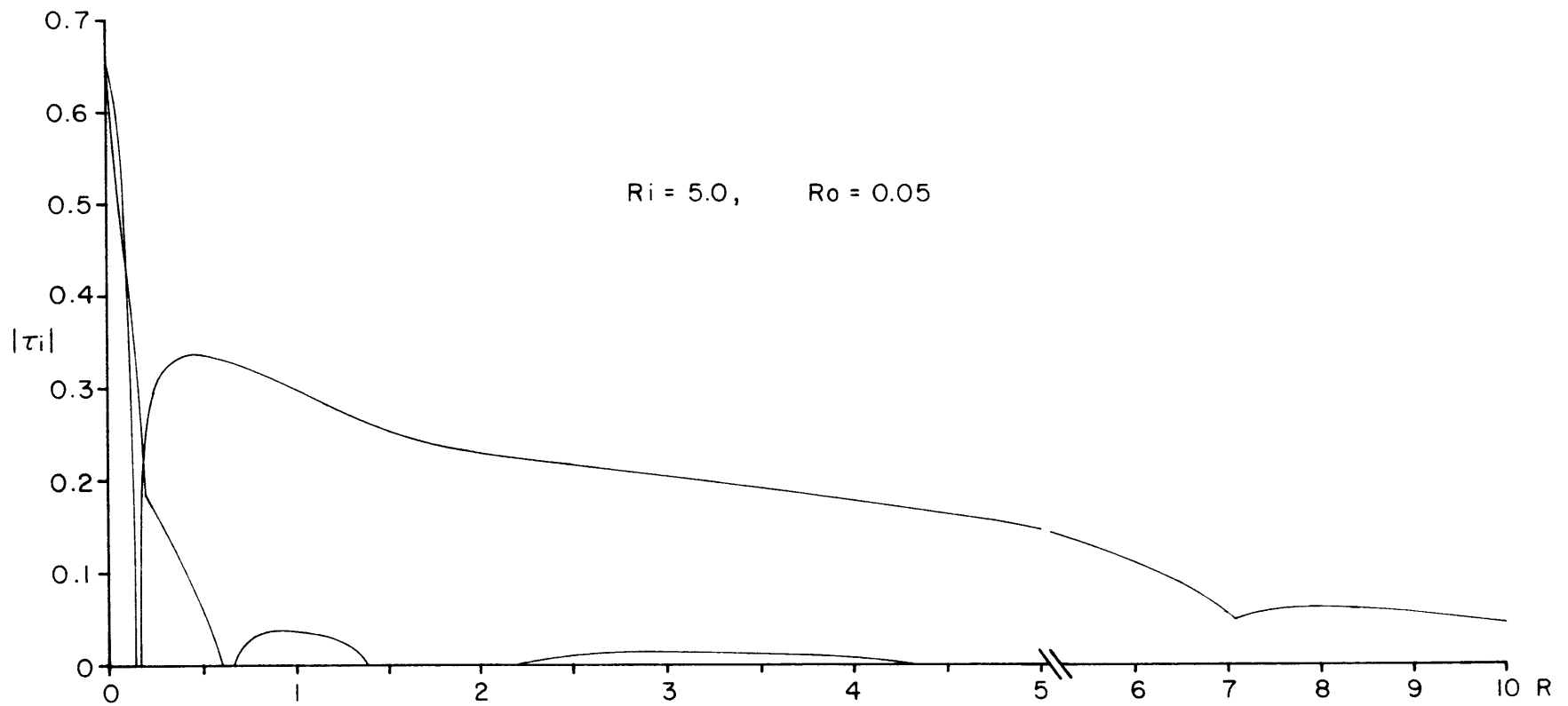


Figure 4.8 Dependence of the magnitude of the imaginary part of the eigenvalue, $|\tau_i|$, upon the bottom slope parameter, R , for $Ri = 5.0$ and $Ro = 0.05$.

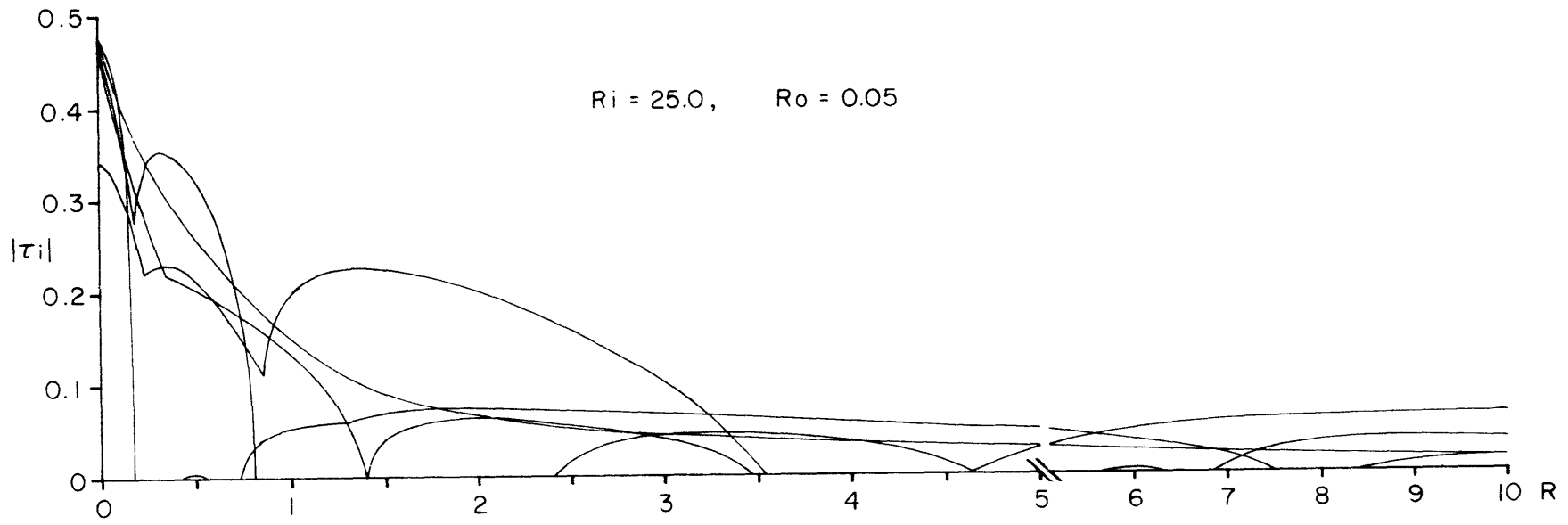


Figure 4.9 Dependence of the magnitude of the imaginary part of the eigenvalue, $|\tau_i|$, upon the bottom slope parameter, R , for $R_i = 25.0$, and $R_o = 0.05$.

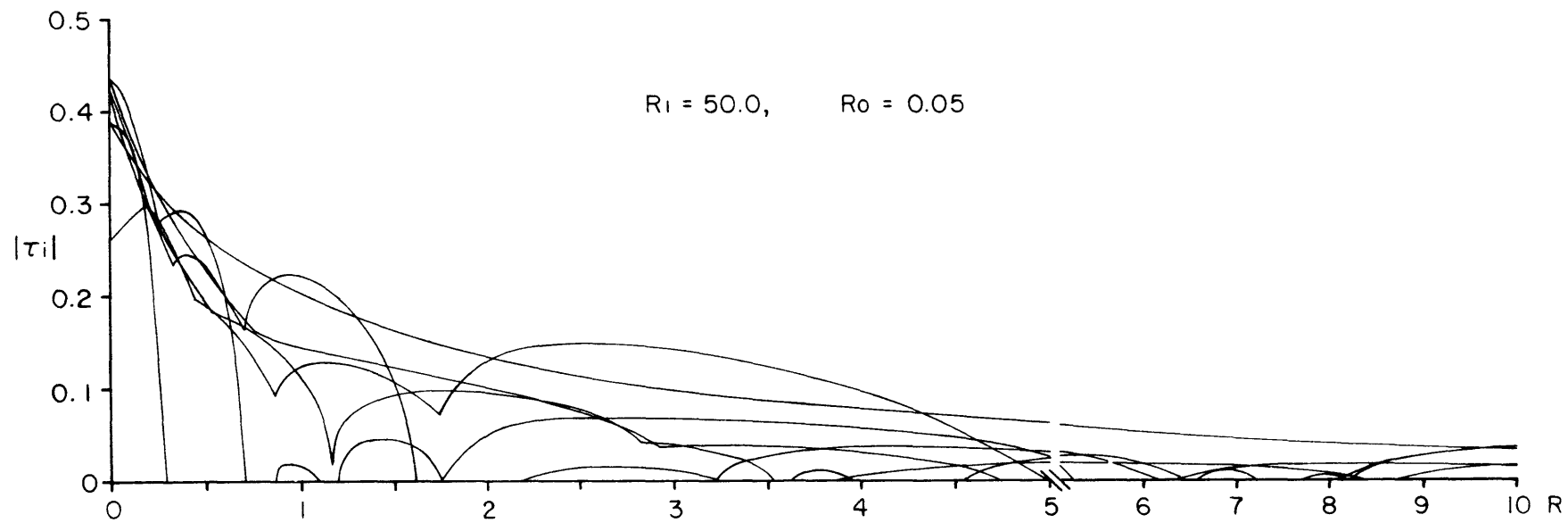


Figure 4.10 Dependence of the magnitude of the imaginary part of the eigenvalue, $|\tau_i|$, upon the bottom slope parameter, R , for $R_i = 50.0$, and $R_o = 0.05$.

show that increasing the bottom slope destabilizes some modes that were stable over flat topography.

Figure 4.11 indicates a general trend of decreasing $|\tau_i|$ with increasing Ri , but because of the cusped nature of the stability curves, the decrease is anything but monotonic. There are some ranges of Ri which are two to three times more unstable than their adjacent ranges. For fixed Ro , Ri is proportional to kL ; therefore, for a given width of the frontal zone, particular bands of wavenumbers will be especially unstable. Figure 4.12 shows the behavior as a function of Ro at $Ri = 25.0$ for two values of the bottom slope parameter: $R = 0.0$ and 10.0 . Both plots indicate a general decrease in maximum $|\tau_i|$ with increasing Ro . The effect of the bottom slope on the stability curves is evident in this figure with the curves for $R = 10.0$ being much more complicated than for $R = 0.0$. At $R = 10.0$ only one unstable wave remains which was also unstable at $R = 0.0$, the one marked (2). Note that this wave becomes less stable for increasing Ro .

We have calculated eigenvalues for some of the extreme points of the parameter space. The maximum values of the imaginary parts for each point are indicated in Table 4.2. It is interesting to note that while increasing the bottom slope stabilizes the flow, for a given value of R , increasing Ri will ultimately destabilize the flow. However, none of the values for $|\tau_i|$ are very large.

A perturbation energy analysis shows that in the flat bottom limit, all of the unstable modes are predominantly baroclinic; that is, most of the perturbation energy is obtained from the mean potential energy feeding the eddy kinetic energy through the eddy potential energy. In this case there is a net increase in the mean kinetic energy as the

TABLE 4.2

Ri	R = 10	R = 25	R = 50
5	0.046	0.001	STABLE
25	0.063	0.001	STABLE
50	0.038	0.028	0.010
75	0.044		
100	0.049		

Table 4.2 Magnitudes of the imaginary part of the eigenvalue, $|\tau_i|$, in the general case for a few extreme points in the parameter range pertaining to the New England continental shelf.

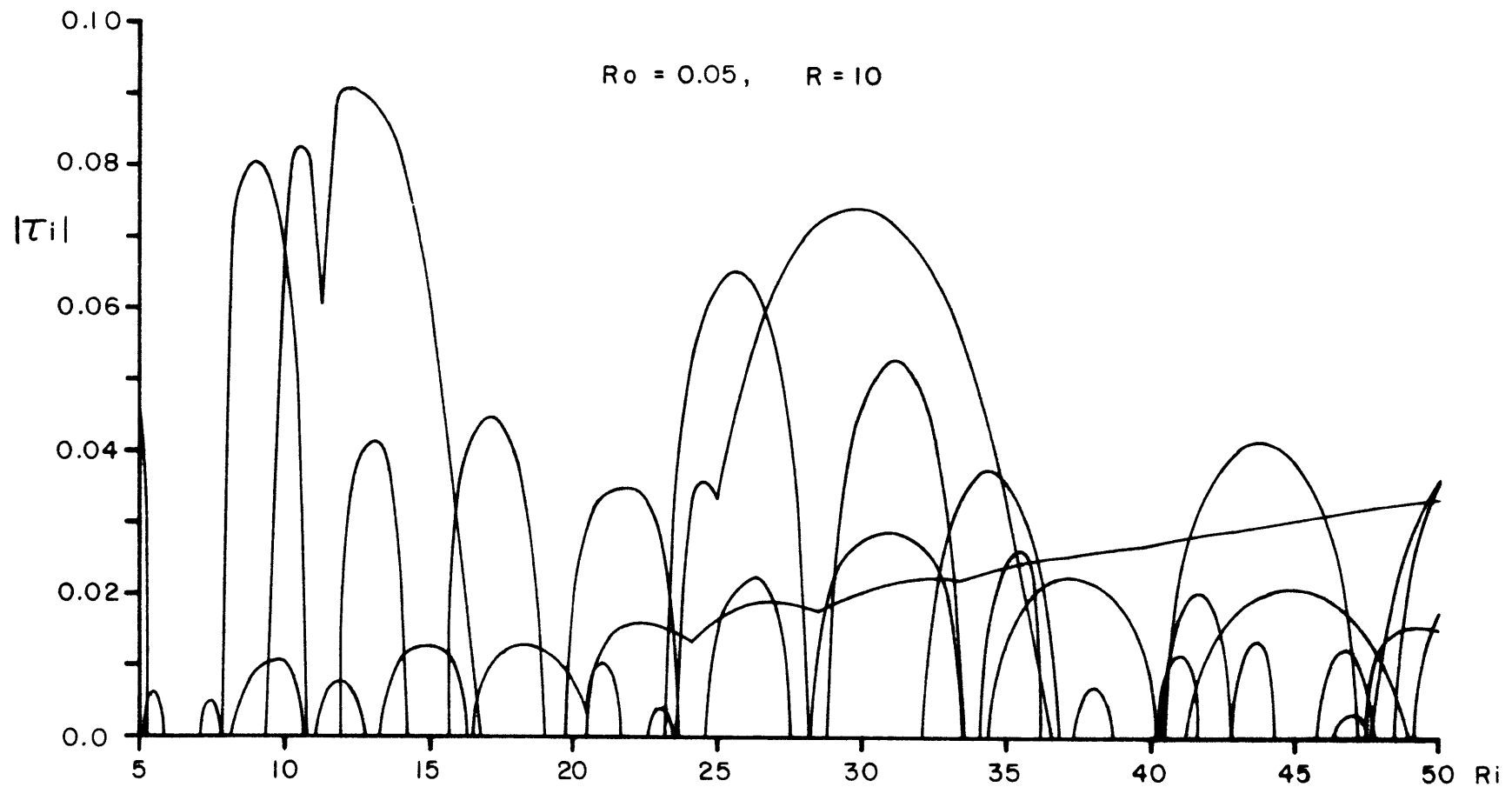


Figure 4.11 Dependence of the magnitude of the imaginary part of the eigenvalue, $|\tau_i|$, upon the Richardson number, Ri , for $R = 10.0$ and $Ro = 0.05$.

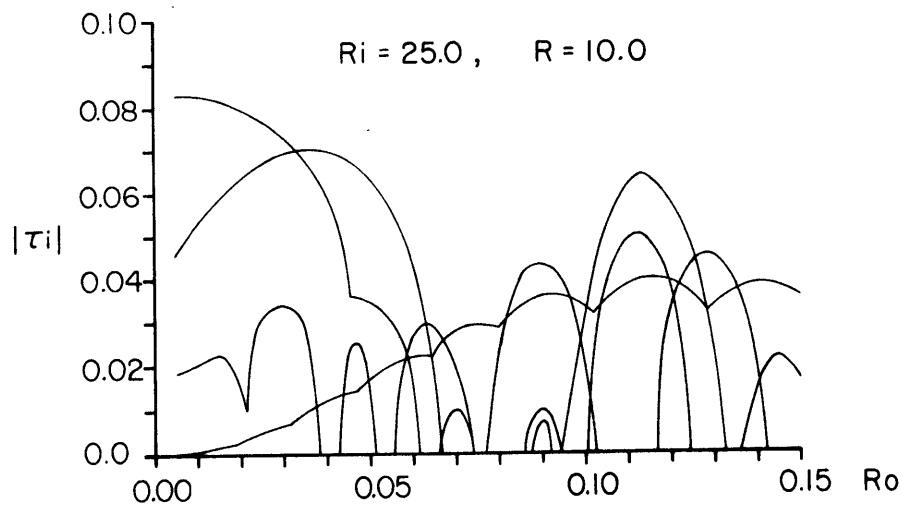
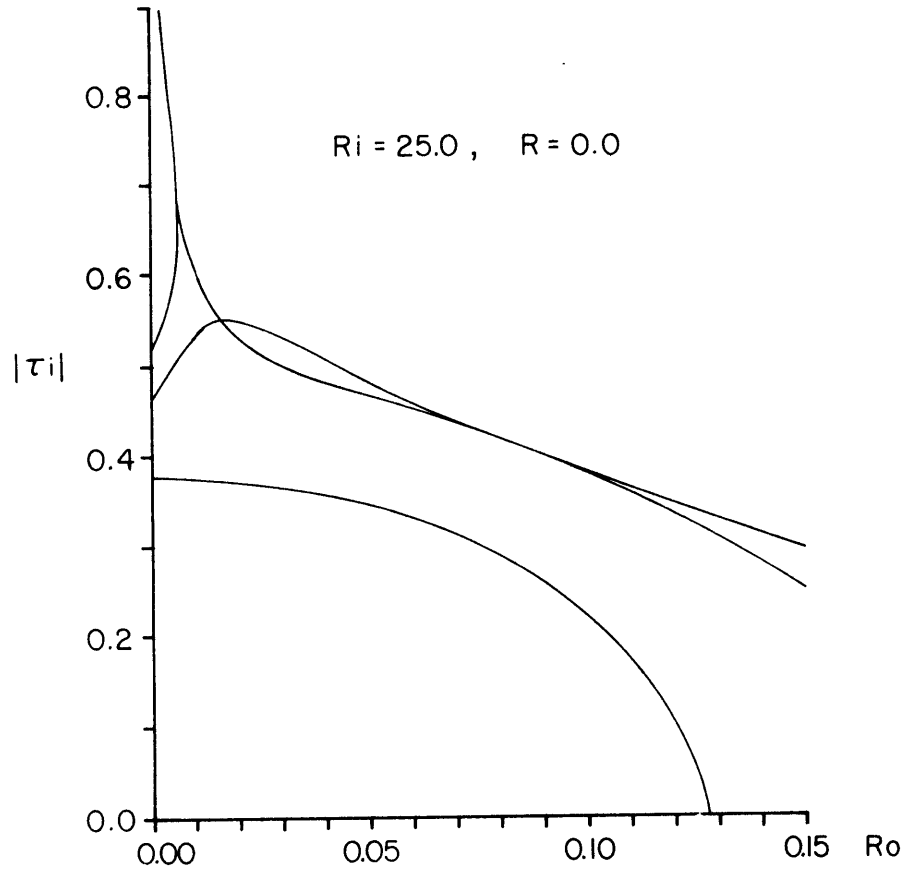


Figure 4.12 Dependence of the magnitude of the imaginary part of the eigenvalue, $|\tau_i|$, upon the Rossby number, Ro , for $Ri = 25.0$, and $R = 0.0$ and 10.0 .

eddy kinetic energy yields up energy to the mean. As the bottom slope is increased, some of the modes remain predominantly baroclinic, others become nearly purely barotropic, and some are mixed. Barotropic means that the mean kinetic energy is the energy source with energy extracted by a combination of Kelvin-Helmholtz instability and Rayleigh shearing instability. The Rayleigh source term is generally larger. Some of the predominantly barotropic instabilities feed energy to the mean potential energy.

4.6 Discussion

In this chapter we have investigated the stability of the classic Margules front as it might apply to the steep topography of the shelf water/slope water frontal zone in the Mid-Atlantic Bight. For two special cases, the first for a vertical interface and the second in the limit of steep slope and small Ro , use is made of a perturbed primitive equation model similar to Orlandi (1968). The special cases indicate that increasing the bottom slope indefinitely will eventually completely stabilize the flow, while for realistic slopes decreasing Ro has a destabilizing effect. For the general case, it is convenient to use the semi-geostrophic approximation to recast the problem into a canonical eigenvalue form. It becomes evident that decreasing Ro generally destabilizes the front (although the dependence is not large) and increasing Ri also had a destabilizing effect. Because of the cusped structure of the stability curves, the maximum growth rates may vary considerably between neighboring ranges.

By using the length and time scales that pertain to the frontal zone south of New England, we obtain the growth rates, phase velocities, and periods for the unstable modes that might be expected (see Figures 4.3 to 4.5). For $R = 10$ and $Ri = 50$, the e-folding time for the most unstable wave will be a minimum of 20 to 30 days. Phase velocities for this parameter range vary from 2 cm/sec to the east to 6 cm/sec to the west along the front with periods in excess of 10 days. It would appear that the range of phase velocities and periods are consistent with the observed alongshelf behavior. As a particular example for the New England shelf break let $R = 10$, $Ro = 0.05$, and $Ri = 50.0$ yielding for the most unstable mode an eigenvalue $\tau = (-0.74 - 0.04i)$. Further if

we assume a rather large value for the vertical shear of 10 cm/sec and an alongshore wavelength of 75 km, we obtain a phase speed of 6.2 cm/sec to the west and period of 11.5 days. This solution is indeed like that observed by Saunders (1968) south of Georges Bank. The next most unstable solution for this parameter range has a speed of 1.8 cm/sec to the west and a period of 49 days. It is likely that the faster wave would stand out in short term observations. On the other hand, the e-folding times for these two waves are 75 and 85 days, so 200 days or more are required for these waves to grow to discernable size. As this is an optimum example it is inconceivable that a front progressing through a regular annual cycle and subjected to many strong forcing phenomena with much shorter time scales would exhibit instabilities of this type.

Thus it seems that the alongshore undulations are not obvious manifestations of baroclinic instabilities and some other, probably more involved processes, are responsible. For instance, it is possible, since stable or slowly growing waves can exist along the shelf break, that mesoscale wind forcing could excite oscillations which then persist and propagate along the break. We have not as yet carried out the analysis of the type of forcing and the dynamics necessary for this to occur. One area on which some light has been shed is the question as to why the front always seems to straddle the steepest topography of the shelf/slope junction. If it is assumed that a front of the type observed existed over flat topography, the growth rates for the unstable modes would be, at a minimum, 20 times faster than those for $R = 10.0$. This brings the e-folding time down to as little as 1.5 days. It is likely that the front would be destructively unstable under these conditions. Thus the front would tend to migrate from the shelf offshore until an

equilibrium was established between the instabilities and frictional dissipation.

5. Summary and Conclusions

This section summarizes the features of the shelf and frontal circulation south of New England that we have observed and some of their dynamical consequences and outlines some areas requiring additional observational effort.

The mean currents during the March 1974 experiment all had a westward alongshore component, increasing in magnitude progressing offshore to a maximum at the nearshore edge of the shelf/slope front, and decreasing in magnitude with depth. There was a significant amount of mid-depth onshore flow such that the mean current vector rotated clockwise with depth. Mean currents within 1 m of the bottom were onshore on the inner half of the shelf, offshore on the outer half, and near zero under the front. There were strong indications that the predicted vertical geostrophic shear across the shelf/slope front actually existed although perhaps not as large as the simple Margules equation suggested. Evidence indicated that under the front there was a region of velocity deficit down to ~ 200 m and that below this region the flow was again alongshore toward the west. The total alongshore transport of shelf water was on the order of 0.4 Sv with approximately one-third of this occurring in the wedge of shelf water offshore of the 100 m isobath. The alongshore transport may vary by 50% primarily due to the influence of the wind events.

The steady state, frictional shelf model proposed by Csanady (1976) seemed to capture the essential features of the mean current structure on the broad New England shelf. That the salt balance is maintained by the mean circulation as well as the first order flow episodes does not seem to be dynamically critical for application of the model to winter

conditions. This is consistent with Stommel and Leetmaa's (1972) model that the shelf was in a wind driven as compared to a density driven regime. Features of the model that are supported by our observations are: 1) the intensification offshore of the alongshore current; 2) the increase in the magnitude of the cross-shelf sea level gradient offshore; and 3) the existence of a line of bottom flow divergence.

The measurements of the mean currents from the March 1974 experiment were the first from a moored array in the New England shelf area. As such it is not surprising that a number of issues remain unresolved. It required 25 to 30 days to obtain an approximately stable estimate of the mean with statistical errors of 0.5 to 3 cm/sec. These statistical errors are of the same order as the means themselves. In addition, the winter of 1974 as a whole was a particularly mild one. Thus, in order to form an adequate picture of the "climatological" mean winter current structure, observations over several winter seasons will be required. Since there is such a drastic change in the hydrography of the shelf during the spring and summer from the relatively simple winter regime, what does this do to the mean currents? Essentially nothing is known of the current structure during the summer. Does the region of low velocity under the winter front also become much reduced as the density contrast across the front decreases? Does the presence of the strong seasonal thermocline completely invalidate the frictional shelf model? Is the cold band eroded from the top and edges, or as anticipated, does it flow slowly alongshore to the west without being significantly replenished from the east around Nantucket Shoals? Is the dynamic effect of the freshwater runoff more important during the summer with the decrease in magnitude of the mean and rms wind stress?

The low frequency currents for periods longer than 33 hours contain only about 30% of the total horizontal kinetic energy on the shelf, however, they contain about 70% of the displacement variance. Thus, the low frequency motions are the dominant cause for movement of water on the shelf. The empirical orthogonal modal analysis was used to define the vertical and horizontal structure of the low frequency motions. This indicates that for alongshore motions the whole shelf together with the water above the shelf/slope front moves predominantly as a unit. The onshore current component, in contrast, is characterized by opposing flows at surface and bottom very much as one would expect of an upwelling region. The waters above the shelf/slope front move on and offshore in concert with the upper waters of the shelf. That the wind stress is the primary source of momentum for the low frequency currents is quite evident from the visual correlation between the current and wind stress records, the similarity of their spectra, and from the significant coherence levels. There is a high degree of correlation between the subsurface pressures and the currents, primarily because of the interaction between the wind stress, SSP gradients, and the currents. However, the possibility exists that the SSP gradients may be partially forced by some oceanic interaction, in turn forcing the shelf currents.

There is a considerable amount of evidence that the low frequency currents behave in a manner consistent with frictional coastal boundary layer dynamics. However, attempts made to define the nature of the low frequency behavior with more precision generally do not meet with much success. Part of the reason for this is that at times the wind stress seems to preferentially force inertial oscillations rather than a mean current while at others a mean current is forced with little

inertial motion. The cause for this is not fully understood but at least part of the answer seems to be related to the amount of clockwise energy in the wind at the inertial frequency. Another reason that the current does not always behave as one would expect relative to the wind stress is that the shelf currents also contain a significant amount of inertio-gravitational wave motion. Beardsley et al. (1977) and Munk, Snodgrass, and Carrier (1956) have demonstrated the presence of edge waves of approximately 6 hour periods, initiated by wind events, in the pressure records of the Mid-Atlantic Bight. In this thesis we have demonstrated the existence of oscillations on the shelf/slope front about its mid-depth position with periods of 3 1/2 to 4 days. The shelf currents were also shown to oscillate in accord with this motion. Niiler and Kroll (1976) have indicated that the propagation of low frequency energy up the continental slope and onto the shelf is quite possible. All these effects would serve to degrade the simple relation between wind and current expected from frictional boundary layer dynamics. It is clear that a complete shelf model will have to take into account at least some of these added complications. The most difficult, but perhaps the most important, will be the inclusion of the actual shelf/slope boundary condition. It seems that at the moment this is the greatest barrier to a thorough understanding of the shelf response.

That the shelf/slope front is central to understanding the shelf/ocean boundary condition is obvious. In this thesis we have examined current meter and hydrographic observations of the frontal zone to obtain a better understanding of its kinematics and the possible relationships between the front and the shelf. The shelf/slope front of the Mid-Atlantic Bight has three distinguishing characteristics: 1) the front is

always present in one form or another; 2) the water property isopleths delineating the front always intersect both the bottom and the surface (or the bottom of the seasonal thermocline in summer); and 3) the front is always located over the shelf break.

The frontal zone is quite active in the internal wave band with what appears to be a nearly constant and large amount of energy in the front itself, a variable amount above the front, perhaps stimulated by wind events, and a relatively small but constant amount below the front. The presence of the sharp density gradient and the proximity of the surface and bottom seem to invalidate the assumptions of linear internal wave theory in the frontal zone. The semi-diurnal and diurnal tides account for the largest percentage of horizontal current variance in the front. The semi-diurnal tide appears to be barotropic and one-dimensional continuity predicts the horizontal currents reasonably well in the frontal zone. The diurnal tide increases toward the bottom, is less clockwise polarized than the semi-diurnal, and has tidal ellipses aligned with the isobaths. Inertial energy is important on the shelf and relatively more so in the frontal zone where it has about the same average value as the semi-diurnal tide above the front. Below the front the inertial energy is relatively smaller. We have discussed the importance of inertial oscillations in determining the character of the current response to wind stress. This implies an as yet undefined interaction between inertial motion and movement of the front.

We have demonstrated two types of low frequency motion of the front. From hydrographic sections, and from airborne and satellite borne radiometry measurements, the surface expression of the front is known to exhibit on and offshore undulations from some mean position more or less

along the shelf break fundamentally different from the entrainment of shelf water by eddies. These undulations appear to have amplitudes of 20 to 40 km and alongshore wavelengths from 50 to 150 km. The only measurement that we have so far indicates a westward migration along the shelf break at 5 to 10 cm/sec., hence we deduce periods of oscillation of 7 to 10 days. However we know little or nothing about the cross-shelf behavior of these motions. The second type of frontal motion observed was that forced by a sudden onset of a large wind event causing an oscillation of the front about its mid-depth position. It would seem that this motion was a free oscillation, however, there exists the possibility that subsequent wind stress oscillations were the cause for the repeated frontal movements. The period of these oscillations was 3 1/2 to 4 days. Thus, this later type of motion may be different than the above alongshore undulations because of the mismatch in observed periods. We can do little more than speculate about the relationship because there is no information on the alongshore behavior of these shorter period motions.

To proceed further, progress is required in two complimentary directions. To fill the gaps in our knowledge of the kinematics of the front, we need an observational program which includes at least three current meter moorings spaced along the shelf break at 20 to 40 km spacings and three cross frontal moorings spaced about 15 km apart centered near the 150 m isobath. This program should concentrate on the winter front as it is conceptually the simplest to interpret. The goals of such an experiment would be among others to: 1) confirm present concepts on the vertical and horizontal shears across the front; 2) monitor movements of the front to obtain as nearly as possible a three-dimensional description of the low frequency frontal movement; 3) increase our understanding of

the role of inertial oscillations in the frontal zone; and 4) obtain more precise data on the structure of the internal wave field. In conjunction with the observational effort progress is needed in forming conceptual theories which might explain the front's presence and perhaps as a separate issue, the length and time scales of motion that we should expect. Apparently a simple diffusive model with the appropriate boundary conditions can explain the mean distribution of temperature in the winter (M. Bowman, personal communication). If this is so, a mechanism is needed to cause frontogenesis or a tightening of the isotherms along the shelf break. Perhaps meteorological theories can be extended to this application. If we assume that a front is present, how does it respond to various types of forcing such as wind stress and low frequency energy propagation from the deep ocean? Even with the rather limited data and information presently available it may not be too early for theoretical progress to be made on these issues.

REFERENCES

- Abramowitz, M. and I. Stegun (1964) Handbook of Mathematical Functions. U.S. Department of Commerce, Applied Mathematics Series - 55.
- Barvenik, F. (1975) Brookhaven National Laboratory Coastal Shelf Productivity Program. Data Report on KNORR Cruise 46.
- Beardsley, R.C. and B. Butman (1974) Circulation on the New England continental shelf: response to strong winter storms. Geophys. Res. Lett., 1, 4, 181-184.
- Beardsley, R.C. and C.N. Flagg (1975) The water structure, mean currents, and shelf-water/slope-water front of the New England continental shelf. Seventh Liege Colloquium on Ocean Hydrodynamics, 10, 209-226.
- Beardsley, R.C., W.C. Boicourt, and D. Hansen (1976) Physical oceanography of the Middle Atlantic Bight. Limnol. Oceanog., Special Symposium, 2, 20-34.
- Beardsley, R.C., H. Mofjeld, M. Wimbush, C. Flagg, J. Vermersch (1977) Ocean tides and weather induced bottom pressure fluctuations in the Middle Atlantic Bight. Submitted to J. Geophys. Res.
- Bigelow, H.B. (1933) Studies of the waters on the continental shelf, Cape Cod to Chesapeake Bay I, the cycle of temperature. Massachusetts Institute of Technology and Woods Hole Oceanographic Institution Papers in Phys. Oceanog. and Meteor., 2, 4.
- Bigelow, H.B. and M. Sears (1933) Studies of the waters on the continental shelf, Cape Cod to Chesapeake Bay II, Salinity. Massachusetts Institute of Technology and Woods Hole Oceanographic Institution Papers in Phys. Oceanog. and Meteor., 4, 1.
- Boicourt, W.C. (1973) The circulation of water on the continental shelf from Chesapeake Bay to Cape Hatteras. Doctoral Dissertation, John Hopkins University.
- Boicourt, W.C. and P.W. Hacker (1975) Circulation on the Atlantic continental shelf of the United States, Cape May to Cape Hatteras. Seventh Liege Colloquium on Ocean Hydrodynamics, 10, 187-200.
- Bumpus, D.F. (1973) A description of the circulation on the continental shelf of the east coast of the United States. Prog. in Oceanog., 6, 111-158.
- Butman, B. (1975) On the dynamics of shallow water currents in Massachusetts Bay and on the New England continental shelf. Doctoral Dissertation, Massachusetts Institute of Technology, and Woods Hole Oceanographic Institution.

- Cresswell, G.M. (1958) The quasi-synoptic monthly hydrography of the transition region between coastal and slope water, to the south of Cape Code, Massachusetts. Unpublished Manuscript, Woods Hole Oceanographic Institution Reference No. 67-35.
- Csanady, G. (1976) Mean circulation in shallow seas. J. Geophys. Res., 81, 30, 5389-5399.
- De Szoeke, R. and P. Rhines (1976) Asymptotic regimes in mixed-layer deepening. J. Mar. Res., 34, 1, 111-116.
- Duffy, D. (1976) The application of the semi-geostrophic equations to the frontal instability problem. Submitted to the J. Atmos. Sci.
- EG&G, Environmental Consultants (1975) Summary of Oceanographic Observations in New Jersey Coastal Waters near 39°28'N Latitude and 74°15'W Longitude during the Period May 1973 through April 1974. A Report to Public Service Electric and Gas Company, Newark, N.J.
- EG&G, Environmental Consultants (1976) Summary of Oceanographic Observations in New Jersey Coastal Waters near 39°28'N Latitude and 74°15'W Longitude during the period May 1974 through May 1975. A Report to Public Service Electric and Gas Company, Newark, N.J.
- Emery, K.O. and E. Uchupi (1972) Western North Atlantic Ocean: topography, rock structure, water life, and sedimentation. Amer. Assoc. of Petr. Geol., Memoir 17.
- Flagg, C.N. and R.C. Beardsley (1974) The 1974 Massachusetts Institute of Technology New England Shelf Dynamics Experiment, Data Report, Part I: Hydrography. Department of Meteorology, Massachusetts Institute of Technology, Report 75-1.
- Flagg, C.N., J.A. Vermersch, and R.C. Beardsley (1974) The 1974 Massachusetts Institute of Technology New England Shelf Dynamics Experiment, Data Report, Part II: The Moored Array. Department of Meteorology, Massachusetts Institute of Technology, Report 76-1.
- Hildebrand, F.B. (1962) Advanced Calculus for Applications. Prentiss-Hall Book Company, New Jersey.
- Ingham, M.C. (1976) Variations in the Shelf Water front off the Atlantic Coast between Cape Hatteras and Georges Bank. U.S. Dept. of Commerce, MARMAP Contribution No. 140.
- International Mathematical and Statistical Libraries, Inc. IMSL Library 1, Edition 5, 1975.
- Iselin, C.O. (1939) Some physical factors which may influence the productivity of New England's coastal waters. J. Mar. Res., 2, 1, 74-84.

- Iselin, C.O. (1955) Coastal currents and the fisheries. Deep Sea Res. Supplement to Vol. 3, 474-478.
- Kundu, P. (1975) A note on the Ekman veering observed on the Oregon continental shelf. Submitted to J. Phys. Oceanog.
- Kundu, P. and J. Allen (1975) Some three-dimensional characteristics of low frequency current fluctuations near the Oregon coast. Submitted to J. Phys. Oceanog.
- Kundu, P., J. Allen, and R. Smith (1975) Modal decomposition of the velocity field near the Oregon coast. J. Phys. Oceanog., 5, 4, 683-704.
- Millard, R.C. Wind measurements from Buoys: a sampling scheme. J. Geophys. Res., 76, 24, 5819-5828.
- Morgan, C.W. and J.M. Bishop (1975) Eddy inducted water exchange along the continental slope. Preprint.
- Munk, W., F. Snodgrass, and G. Carrier (1956) Edge waves on the continental shelf. Science, 123, 3817, 127-132.
- Niiler, P. (1975) Deepening of the wind-mixed layer. J. Mar. Res., 33, 3, 405-422.
- Niiler, P. and J. Kroll (1975) Propagation of topographic Rossby Waves onto a continental shelf. Preprint.
- Orlansky, I. (1968) The instability of frontal waves. J. Atmos. Sci., 25, 178-200.
- Petrie, B. (1975) M2 surface and internal tides on the Scotian shelf and slope. J. Mar. Res., 33, 3, 303-323.
- Pollard, R.T. (1970) On the generation by winds of inertial waves in the ocean. Deep Sea Res., 17, 795-812.
- Pollard, R.T. and R.C. Millard (1970) Comparison between observed and simulated wind-generated inertial oscillations. Deep Sea Res., 17, 813-821.
- Saunders, P. (1971) Anticyclonic eddies formed from shoreward meanders of the Gulf Stream. Deep Sea Res., 18, 1207-1219.
- Saunders, P. (1973) Tracing surface flow with surface isotherms. The skin temperature of the Ocean. A review. Fifth Liege Colloquium on Ocean Hydrography, 6, 93-108.
- Saunders, P. (1976) Wind stress on the ocean over the eastern continental shelf of North America. Unpublished Manuscript.

- Schmitz, W.J. (1974) Observations of low-frequency current fluctuations on the continental slope and rise near Site D. J. Mar. Res., 32, 2, 233-251.
- Scott, J. and G. Csanady (1976) The COBOLT experiment: first current meter observations. J. Geophys. Res., 81, 30.
- Stommel, H. (1966) The Gulf Stream. University of California Press.
- Stommel, H. and A. Leetmaa (1972) Circulation on the continental shelf. Proc. Nat. Acad. Sci., 69, 11, 3380-3384.
- Traschen, J. (1976) Tides of New England continental shelf. Unpublished Manuscript. Woods Hole Oceanographic Institution.
- Voorhis, A., D. Webb, and R. Millard (1976) Current Structure and Mixing in the Shelf/Slope Front South of New England. Woods Hole Oceanographic Institution Contribution No. 3718.
- Webster, F. (1968) Observations of inertial-period motions in the deep sea. Rev. of Geophysics, 6, 4, 473-490.
- Webster, F. (1969) Vertical profiles of horizontal ocean currents. Deep Sea Res., 16, 85-98.
- Wright, W.R. (1976) The limits of shelf water south of Cape Cod. J. Mar. Res., 34, 1, 1-14.
- Zenk, W. and M. Briscoe (1974) The Cape Cod Experiment on Near Surface Internal Waves. Woods Hole Oceanographic Institution Report, 74-87.

Appendix

This appendix acts as a short data report for the results of current and recorded temperature measurements of the January 1975 shelf edge experiment sponsored by the Brookhaven National Laboratory Coastal Shelf Productivity Program carried out during R/V KNORR Cruise 46. The cruise was designed to look at shelf edge exchange and coastal boundary region processes and the interaction of the physical and biological aspects. The cruise lasted from 24 to 30 January 1975 in the shelf and shelf break region along a transect from 40°48' N, 72°31' W to 39°38' N, 71°55' W.

The site of the mooring was in the center of the frontal zone at 39°49.0' N, 72°00.3' W on the 112 m isobath (see Figure 1.4). The isobaths in this area are oriented northeast-southwest. Three EG&G 102 film type Richardson current meters were positioned above, in, and below the front at depths of 19, 52, and 85 meters. Four temperature sensors borrowed from WHOI (courtesy of P. Saunders) were also hung on the mooring, three just below each current meter, and the fourth 10 m above the bottom (see Figure 1.5). The temperature sensors were an extremely primitive design using Rustrac recorders and Bourdon tube sensors and had a time constant of on the order of 3 hours. The mooring had a 41 inch diameter buoyancy sphere at a depth of 16 m and used an acoustic release (see Figure 1.5). The duration of the mooring deployment was 77.3 hours from 1310 Z January 25 to 1830 Z January 28, 1975.

The current meters were set to record speed and direction continuously at 5 second intervals. Five minute averaged values of direction, speed, east, and north for each of the CM's are shown in Figures A.1,

A.2, and A.3 in order of increasing depth. The instrument designation denotes the top most set of instruments, that is a pair of one CM and one temperature sensor, as BNL1, the next one down as BNL2, etc. Due to the shortness of the records, we used a simple 12.40 hour running average to reduce the power of the semi-diurnal tidal constituent. Time series of the filtered records are shown in the text in Figure 3.15.

The temperature records were digitized by means of an X-Y digitizer from the paper tape output of the Rustrac recorders at approximately half hour intervals. Time series of the four temperature records are shown in Figure A.4. Visible in these series are the deployment and retrieval transients and the effect of the large sensor time constants. In laboratory calibration experiments, we were able to determine the response function for three of the recorders, numbers BNL 1, 2, and 4. From the response function we calculated an inverse convolution filter with which we could speed up the effective response time of the sensors. The results of this process are shown in Figure A.5.

Wind speed and direction were obtained from the ship's deck log where they were recorded at four hour intervals. Direction was recorded to the nearest point of the compass (i.e., within $\pm 6.25^\circ$ at best) and wind was recorded according to the Beaufort scale. Thus the wind record is meant to be used as an indication only of the wind direction and magnitude. A wind stress was calculated from this record using a drag coefficient of 1.22×10^{-3} . A time series of the wind stress is shown in the upper part of Figure 3.15.

A total of 11 Nansen casts (shown in Figure 1.4) and 33 XBT's were made to measure the hydrography. A hiatus in the middle of the hydrographic survey was caused by a rather strong storm. The timing of the

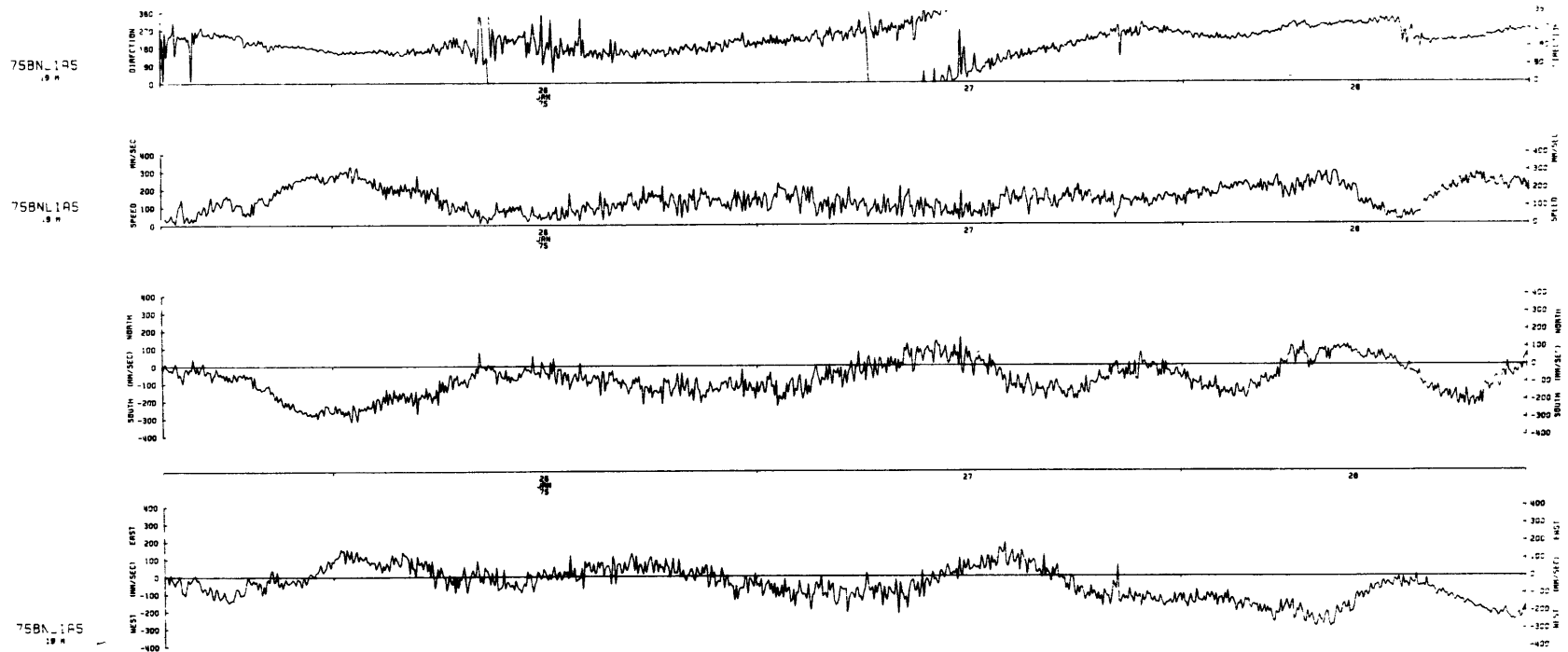


Figure A.1 Five minute averages of speed, direction, east, and north for instrument BNL 1 of the January 1975 shelf edge experiment. Instrument depth was 19m.

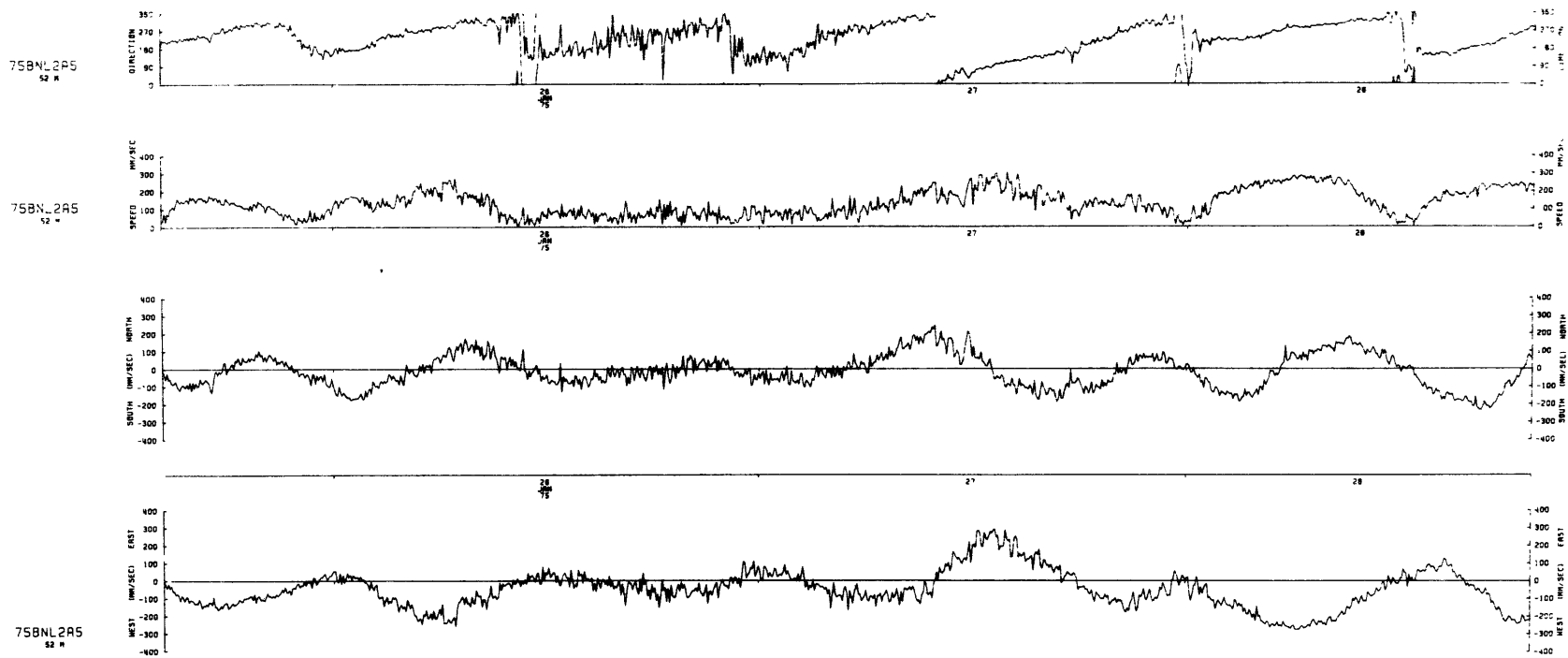


Figure A.2 Five minute averages of speed, direction, east, and north for instrument BNL 2 of the January 1975 shelf edge experiment. Instrument depth was 52m.

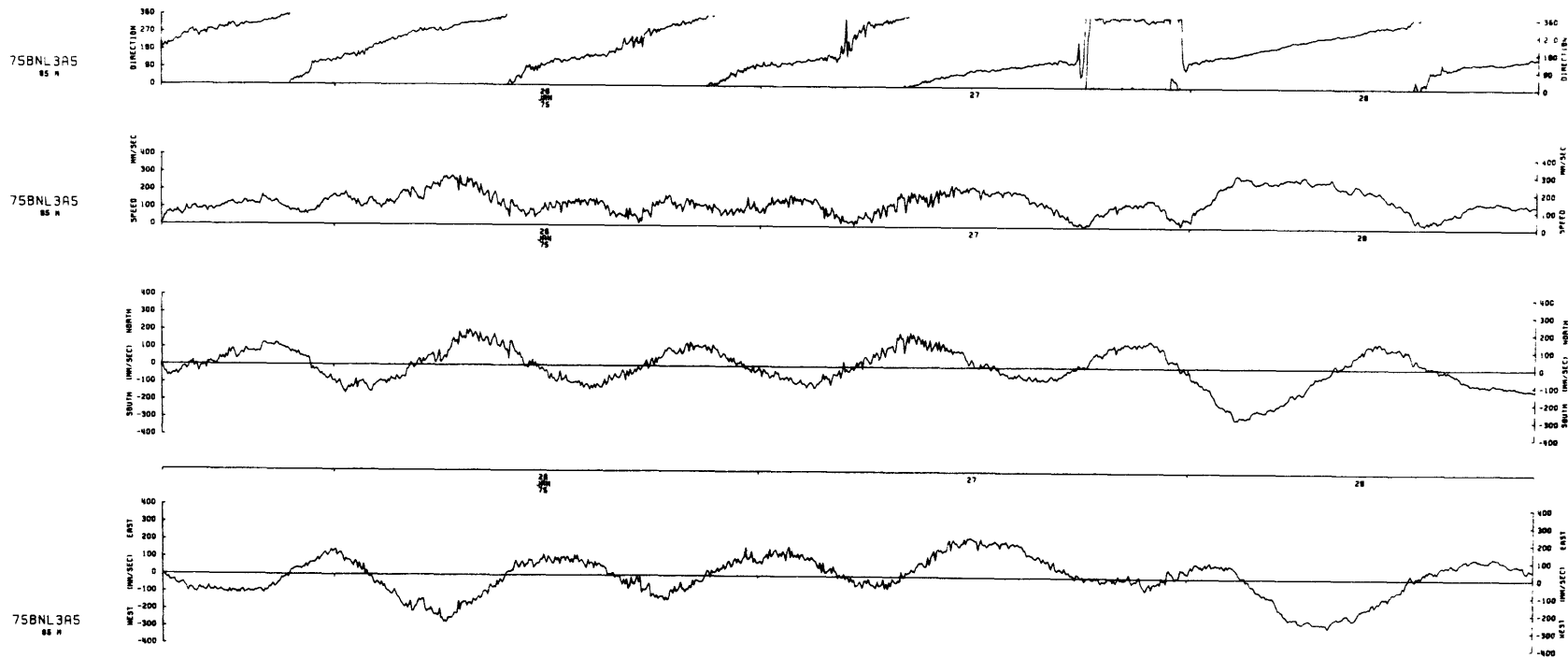


Figure A.3 Five minute averages of speed, direction, east, and north for instrument BNL 3 of the January 1975 shelf edge experiment. Instrument depth was 85m.

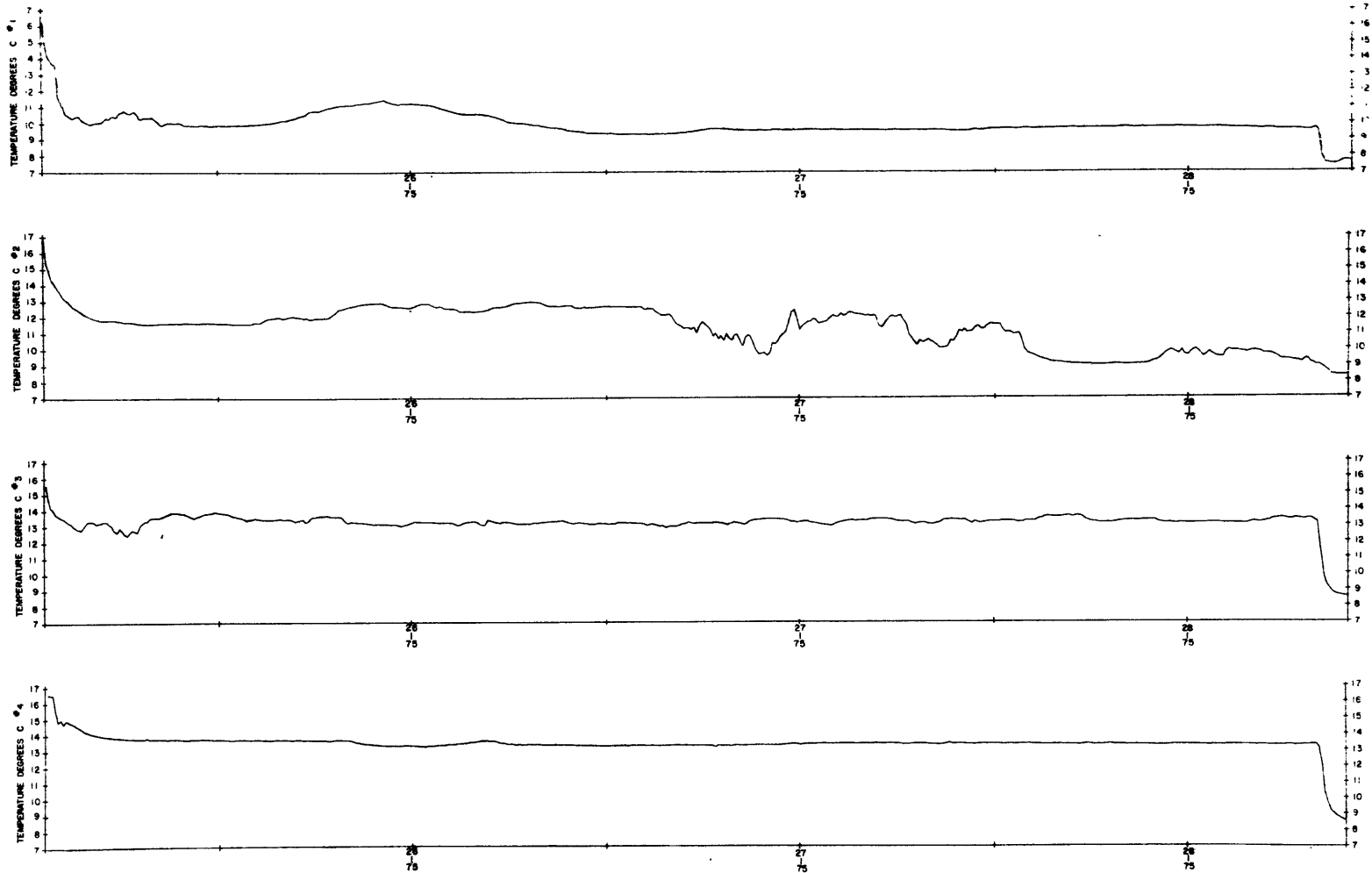


Figure A.4 Digitized temperature at approximately half hour intervals for the temperature recorders BNL 1, 2, 3, and 4 from the January 1975 shelf edge experiment.

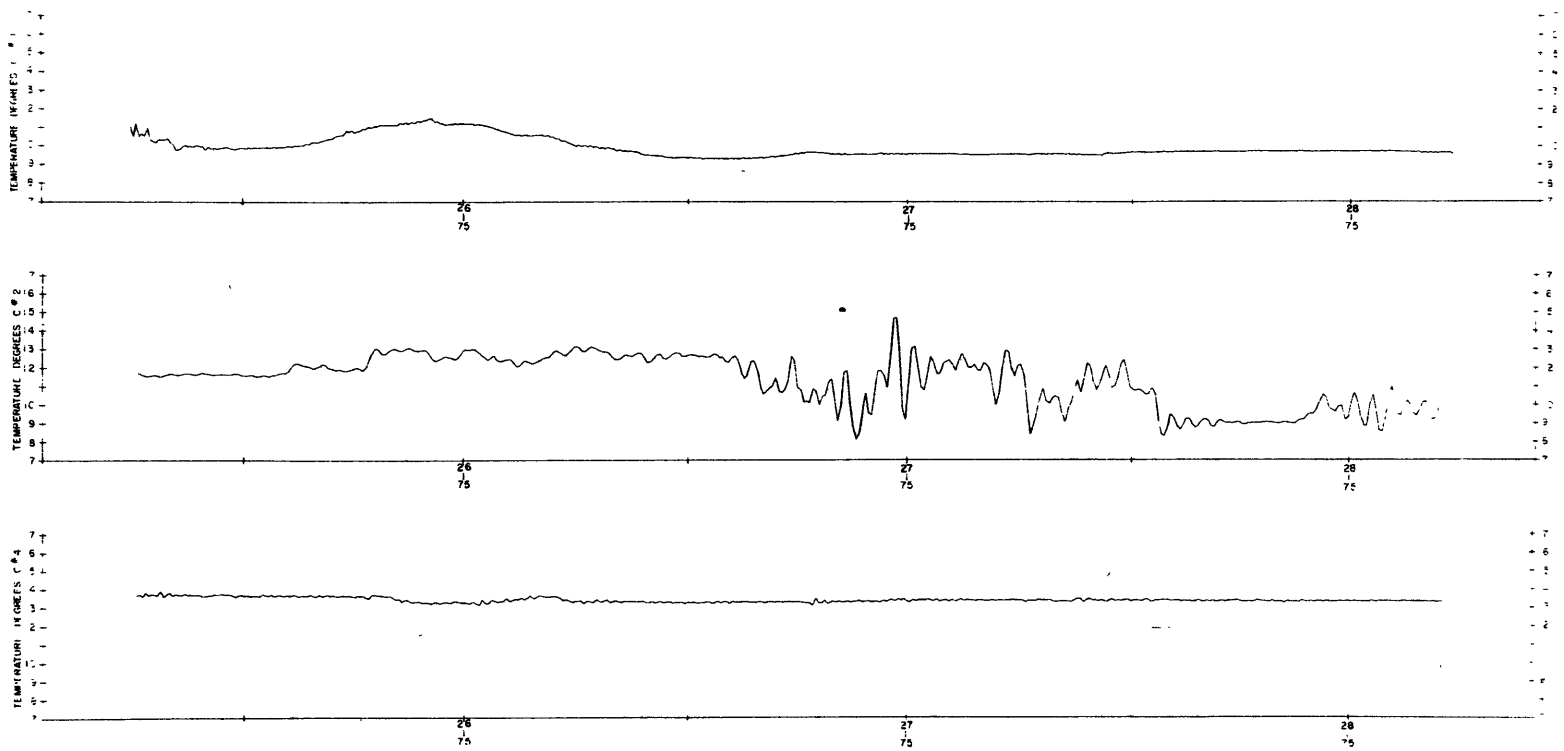


Figure A.5 Temperature records for instruments BNL 1, 2, and 4 which have been corrected for the time lag of the recorders using their response functions determined during calibration for the January 1974 shelf edge experiment.

observations relative to the wind stress and currents is shown in Figure 3.15.

BIOGRAPHICAL NOTE

Charles N. Flagg was born in New York City in October, 1946. He graduated from South Kent School, South Kent Connecticut in 1965. He received a B.S. in mechanical engineering from Cornell University in 1969. Pursuing an interest in hydrodynamics he entered Massachusetts Institute of Technology in the Naval Architecture Department. From this he developed a desire to participate in the discoveries of the dynamics of the ocean rather than being in the role of support engineering for oceanographic research. Thus after receiving an M.S. in naval architecture in 1971 he was admitted to the Massachusetts Institute of Technology - Woods Hole Oceanographic Institution Joint Program in Oceanography.

In the spring of 1970 he married the former Barbara Louise Nord of Cincinnati, Ohio.

Publications:

Flagg, C.N. and J.N. Newman (1971) Sway added-mass coefficients for rectangular profiles in shallow water. J. Ship Res., 15, 4, 257-265.

Flagg, C.N. and R.C. Beardsley (1975) The 1974 Massachusetts Institute of Technology New England Shelf Dynamics Experiment, Data Report, Part I: Hydrography. Department of Meteorology, Massachusetts Institute of Technology, Report 75-1.

Beardsley, R.C. and C.N. Flagg (1975) The water structure, mean currents, and shelf-water/slope-water front of the New England continental shelf. Seventh Liege Colloquium on Ocean Hydrodynamics, 10, 209-226.

Flagg, C.N., J.A. Vermersch, and R.C. Beardsley (1976) The 1974 Massachusetts Institute of Technology New England Shelf Dynamics Experiment, Data Report, Part II: The Moored Array. Department of Meteorology, Massachusetts Institute of Technology, Report 76-1.

Beardsley, R.C., H. Mofjeld, M. Wimbush, C.N. Flagg, and J.A. Vermersch (1977) Ocean tides and weather induced bottom pressure fluctuations in the Middle Atlantic Bight. Submitted to J. Geophys. Res.